Comprehensive Proteomic Analysis and Characterization of Human Bone Marrow Mesenchymal Stem/Stromal derived Extracellular Vesicles

Afnan M N Alam Munshi

Thesis submitted to the
Faculty of Graduate and Postdoctoral Studies
in partial fulfillment of the requirements
for the MSc degree in Biochemistry
March, 2019

Biochemistry Microbiology and Immunology
Faculty of Medicine
University of Ottawa

Contributions:

All the experiments in this study was designed and analyzed by me, the samples for western blot, mass spectrometry and TEM were prepared by for the experiments.

- Western blots - performed by Jelica Mehic (Research Technician; Lab Member)
- Mass Spectrometry - performed by Marybeth Creskey and Dr. Terry Cyr; Mass Spectrometry Laboratory CBE, BGTD, HPFB, Health Canada, Ottawa, ON, Canada
- Statistics - performed Jun Gao (Biostatistician-Methodologist) Health Canada, Ottawa, ON, Canada
- Transmission electron microscopy - performed by Yun Liu; Material Characterization uOttawa Core Facility, University of Ottawa, ON, Canada
- Nanosight (NS300) - NTA performed at the Nanomedicines Laboratory, CBE, BGTD, HPFB, Health Canada, Ottawa, ON. Help and assistance by Dr. Michael Johnston and Christian Luebbert.
- Flow cytometry –Andrew Stalker (Flow Cytometry Manager) CBE, BGTD, HPFB, Health Canada, Ottawa, ON, Canada, assisted in running the samples.

Grant: Genomics Research & Development Initiative (GRDI) Phase VI (2014-2019) obtained by Michael Rosu-Myles and Jessie R. Lavoie.

Thesis Advisory Committee Members:

- Dr. Jessie Lavoie
- Dr. Lisheng Wang
- Dr. William Stanford

Abstract

Extracellular vesicles (EVs) are considered to be a major paracrine effector in therapeutic responses produced by human mesenchymal stromal/stem cells (hMSCs). As the hMSC-EV regenerative capacity is mainly ascribed to the transfer of proteins and RNA composing the EV cargo and to the activity attributed by the protein surface markers, we sought to profile the protein composition of hBM-MSC-EVs using a quantitative proteomics analysis. hBM-MSC-EVs were produced from 5 hBM-MSC donors characterized by Nanoparticle Tracking Analysis showed no differences in the hBM-MSC-EV concentration and size among the 5 donors ($1.83 \times 10^{10} \pm 3.23 \times 10^{9}$/mL), with the mode particle size measuring at 109.3 ± 5.7 nm. Transmission Electron Microscopy confirmed the presence of nanovesicles with bilayer membranes. Flow cytometric analysis identified EVs expressing exosomal tetraspanins (CD63/81/9) and western blot analysis confirmed an enriched expression of MMP-2 and HSP90B1 in hBM-MSC-EVs. Quantitative proteomic analysis performed using Tandem Mass Tag labeling combined to LC-MS/MS identified 5108 proteins in parental hMSCs versus 782 proteins in hBM-MSC-EVs, of which 270 proteins were enriched by at least 2-fold in hBM-MSC-EVs vs hBM-MSCs. Proteomic analysis also confirmed the presence of known exosomal tetraspanins (CD63/151), integrins (alpha 5/CD49e and beta 1/CD29), and adhesions molecules such as Cadherin 5 type 2, as well as novel surface proteins such as NRP1 involved in cellular movement pathways important in migration and invasion of cells, as well as chemotaxis and vasculogenesis. Our hBM-MSC-EV production workflow and proteomics profiling of the protein composition of EVs from multiple hBM-MSC donors has yielded not only commonly reported exosomal and hMSC markers, but also novel mediators of cell-cell interactions which may help to unravel hMSC's mechanism of action.

Table of Content

List of tables

List of Figures

Acknowledgement

First, I would like to express my gratitude to my supervisor Dr. Michael Rosu-Myles and Dr. Jessie Lavoie (Head of the Stem Cell-based Therapeutics Laboratory) for giving me the opportunity to be a part of this laboratory. I am deeply indebted to them for their constant guidance, patience and advice throughout this journey. I owe my deepest and most genuine appreciation to Dr. Jessie Lavoie, for her enthusiastic supervision and continuous support. I am eternally grateful for her steadfast support through out my project.

I would like to thank my co-supervisor Dr. David Allan and thesis advisory committee members Dr. Lisheng Wang, Dr. William Stanford and Dr. Jessie Lavoie for their valuable suggestions and guidance throughout the development of this project.

I would like to express my special appreciation and thanks Carole Westwood for training me, as well ad Gauri Muradia and Jelica Mehic for their cooperation, generous support, indispensable assistance on various aspects of my project. I am thankful to Allolo Aldreiwish, Emma Rigg, Jonathan Gobin and Winston Cheung for the stimulating discussions and for their assistance.

I would also like to show my gratitude to my parents and my husband, without their relentless support and motivation, my completion of this journey would not have been as smooth. I will always be thankful for their belief in me and for their continuous blessings and unflinching support.

Chapter 1: Introduction

1.1 What Are Mesenchymal Stem/Stromal Cells?

Initially referred to as bone marrow (BM) stromal cells, in 1970 *Friedenstein et. al*. first described what is now commonly referred to as mesenchymal stem cells (MSCs), as colony forming fibroblastoid cells in monolayer cultures, isolated from bone marrow and spleen of guinea-pigs [1]. The authors demonstrated MSCs as a rare population of plastic adherent cells (0.01-0.001%) among a population of hematopoietic stem cells (HSCs). These stromal cells demonstrated the ability to self-renew and to differentiate into osteocytes [1]. Though the importance of MSCs playing a key role in controlling the hematopoietic niche was first identified by Friedenstein. MSCs are undeniably known to support hematopoiesis. In 1977, *Dexter et. al.* showed using an in vitro culture system that hematopoiesis or maintenance of HSCs is dependent upon an adherent layer of bone marrow derived stromal cells [2]. As of December 2018, there are about 900 clinical trials using MSCs to treat a wide range of diseases (https://clinicaltrials.gov/). MSCs are a heterogeneous population of non-haematopoietic adult stem cells that supports the hematopoietic stem cell niche [3]. They were first isolated from bone marrow and have now been isolated from a large variety of tissues (bone marrow, cord blood, fat and lungs) and expanded *in vitro* for several passages [3]. They are characterized by their multilineage differentiation potential, namely osteogenic, adipogenic and chondrogenic lineage, as well as their ability to self-renew *in vitro*, although they have a limited lifespan [3]. The precise definition of MSCs is an ongoing debate as there is neither a single definition nor a quantitative assay to help in the identification of MSCs in mixed population of cells [4]. In an effort to address the inconsistencies in the field and

standardize cell preparations to enable reproducibility and exchange of information, in 2006 the International Society for Cellular Therapy (ISCT) set some minimal characterization criteria to define MSCs in culture which include: 1) Plastic adherence, 2) The expression of CD105, CD73 and CD90 (≥95% positive) and lack of expression of CD45, CD34, CD14 or CD11b, CD79a or CD19 and HLA-DR surface markers (≤ 2% positive), 3) In vitro differentiation to adipogenic, chondrogenic and osteogenic lineages [5]. Culture-expanded MSCs have been shown to promote tissue repair, as well as exert angiogenic, anti-apoptotic and anti-inflammatory and immune modulatory properties are mediated by paracrine as well as contact-dependent mechanisms [6]. Equally important from a clinical perspective is the fact that MSCs are immune privileged and are devoid of allogenic reactions because of the low levels of expression of MHC class I and HLA I, as well the lack of expression of MHC class II and HLA-DR [7]. As such, cultured MSCs can be safely transplanted into human subjects without any concerns of allogeneic reactions due to histo-incompatibility [7]. The wide range of therapeutic effects, despite their reported low levels of engraftment *in vivo*, has been mainly attributed to the ability of MSCs to produce a variety of regulatory proteins and bioactive factors at the site of injury. MSCs seem to have the capacity to home to sites of injury, particularly inflamed, apoptotic and hypoxic areas either from the site of transplantation or from their resident tissue to the site of tissue damage via chemokine receptors expressed on their surface [7].

1.2 Long Term *In Vitro* Culture Stability of Mesenchymal Stem Cells

MSCs require extensive *in vitro* expansion to obtain an adequate number of cells prior to therapeutic applications and their high proliferative capacity serves as an advantage.

However, they are restricted by their number of passages or population doublings [8]. Indeed, MSCs tend to lose their potency and undergo senescence and chromosomal alterations at higher passage numbers during in vitro expansion [6]. However, the passage number at which MSCs lose their chromosomal stability is a topic of great controversy. Different studies have attributed loss of potency to senescence, loss of genetic stability, increased p16 expression and telomere shortening after a population doubling between 20-50 [6]. *Binato et. al.* investigated human BM (hBM) MSCs stability between passages 1 to 9 and reported chromosomal variability by karyotypic analysis, reduced proliferation and changes in gene expression from passage 5 onwards [9]. However, the MSCs had a similar proteomic profile and did not present a loss of immunomodulatory and differentiation capacities up to passage 9 [9]. *Stultz et. Al*. conducted a study to investigate chromosomal stability of 10 hMSC donors cultured in DMEM with 15% FBS during passages 3, 5 and 7 in an *in vitro* expansion using spectral karyotyping [10]. Abnormal karyotypes were initially observed at P3 which disappeared subsequently with increasing passages observed at passages 5 and 7 [10]. Several studies have suggested loss of aneuploidy and other karyotypic abnormalities occurs at higher passages due to replicative senescence or apoptosis of abnormal cells. This notion is supported by high level of aneuploidy present in senesced MSCs at late passages analysed using FISH and CGH [11-13]. The consensus in the majority of current literature suggests MSCs are stable and oncogenic transformation of MSCs has not been observed in clinical trial applications [14-17]. Two publications showing spontaneous transformation of MSC lines were retracted as the results were an artifact of cross contamination with immortalized cell lines [18, 19]. A comprehensive meta-analysis of safety of MSCs in clinical trials was unable to find associations between MSCs and malignant transformations or any safety signals other than transient fever upon MSC

administration [20]. However, concerns still remain about the theoretical risks of accumulation of genetic stability if abnormal cells acquired growth advantage.

1.3 Mesenchymal Stem Cell *Donor to Donor Variability*

In vitro BM-MSC preparations are known to be a heterogenic population of plastic adherent cells sharing similar spindle shaped fibroblastoid morphology. Despite the ISCT characteristic criteria, studies have revealed that *in vitro* BM-MSC preparations are composed of poorly defined subpopulations [21]. These studies support the notion of intra and inter individual heterogeneity causing donor-related variations of MSC functions and regenerative properties [21]. Furthermore, variable MSC-mediated efficacies have been reported, depending on the health status, age of donors and other factors. In a study by *Phinney et. al.* 22 distinct h-MSC populations established from 17 donors, ages of 17-45 years showed widely varied growth rates and osteogenic potential *in vitro*. Gene expression analysis revealed differences in the mRNA levels of ALP, BSP, and pTHR following exposure to osteogenic induction media, and marked differences in their expression of ALP enzyme activity after 8 or 22 days of culture in basal media [22]. *Seigel et. al.* [21] and *Olivia et. al.* [23] reported donor age related variability in growth properties of BM-MSCs. *Olivia et. al* further reported impaired chondrogenic and adipogeneic functions, slower population doubling time, increased senescence in old BM-MSCs donors (4–5 years) in comparison to the young BM-MSCs donors (4–6 months) [21, 23]. Though *Seigel et. al.* observed significantly more colonies young donors (<45 years) compared to middle-aged donors (45 to 65 years) and older donors (>65 years), there was no correlation of the donor

age to the potential to suppress T cell proliferation [21]. However, donor to donor variability was observed in the extent of the potential to supress T cell proliferation [21]. *Fan et. al.* [24] and *Zhukareva et. al.* [25] showed differences in donor related hBM-MSC regenerative properties leading to differences in recovery after treatment with MSCs in myocardial ischemia and spinal cord injury using spinal cord extracts following contusion injury respectively. Young (1–5 years old) MSCs significantly showed more plasticity and promoted angiogenesis in a myocardial infarction rodent model, thereby indicating old hMSCs (50–70 years old) lacked the regenerative capacity of younger hMSCs (1–5 years old) [24]. MSCs from different donors also showed variable cytokine, chemokines and growth factor profiles and supported axon growth to a different extent [25].

1.4 Mesenchymal Stem Cells - Paracrine Mode of Action

Paracrine mode of action was initially supported by preclinical studies showing similar therapeutic efficacy by MSCs in comparison to the MSC-conditioned media. This notion was further strengthened when low engraftment after MSC transplantation following systemic administration was observed in various studies [26, 27]. MSCs were trapped in lungs and liver of treated subjects upon intravenously-applied MSCs [26, 27]. Some studies have demonstrated regenerative capacities of MSCs by secreted factors alone in a paracrine rather than a cellular manner [28]. The secreted factors are referred to as secretome which encompasses soluble factors, microvesicles, or exosomes/extracellular vesicles (EVs), and these secreted factors are found in the medium in which the cells are cultured; thus, the medium is called cell-conditioned medium (CCM) [28].

1.4.1 Paracrine Mode of Action - Mesenchymal Stem Cell Immunomodulatory Properties

Immunomodulation is mediated by MSCs through cell-contact-dependent and independent mechanisms through the release of soluble factors or secreted factors [29]. MSCs influence immune function of both innate and adaptive immune cells leading to a tolerogenic environment [29]. hMSCs are immune privileged because of the low level of expression of MHC class I and HLA I as well as the lack of expression of MHC class II, HLA-DR, costimulatory molecules B7, CD80, CD86, CD40, or CD40 ligand [7, 29]. Studies have shown that both allogeneic and autologous MSCs are capable of suppressing the activation of both $CD4^+$ and $CD8^+$ T-lymphocytes, indicating it is not restricted to MHC [30]. MSCs exert their immune modulation effects by secreting several cytokines, growth factors, enzymes and lipid mediators, such as IL-10, HGF, TGF-β1, IDO, PGE2, HLA class I, HLA-G, TSG-6, IL-1 receptor antagonist [30]. TGFβ1, HGF, IDO, NO, and IL-10 secreted by MSCs are involved in T-cell proliferation suppression [31]. MSCs alter effector T cell function by causing a shift from a proinflammatory Th1 cells to an anti-inflammatory Th2 [32], as well as inhibiting the differentiation of naive T cells into Th17 cells and inhibiting secretion of proinflammatory cytokines by those differentiated Th17 cells [30]. MSCs are also able to promote induction of CD4+CD25+ or CD8+ T-regulatory cells both directly and indirectly through immature dendritic cells [32]. Furthermore, TGFβ1 and PGE2 production increases the rate of T-cell reprogramming to T-regulatory cells and a positive feedback amplification loop between IL-10 and HLA-G which leads to induction and expansion of regulatory $CD4^+CD25^{high}$ $Foxp3^+$ T cells [33].

While T cell results are mostly consistent, there are conflicting results of MSC effects on B cell due to the differences in B cell subset purification procedures, such as using a purified CD19+ population [34, 35] or a subpopulation purified by negative selection (CD43 depletion). *In vitro* studies showed that B-cell proliferation inhibition by MSC/T helper cells is dependent upon direct cell-cell contact [31].

Apart from immune modulation of adaptive immune cells activated by MSCs inhibition of dendritic cell maturation and activation by secretion of IL-6 or PGE2 has also been reported [32]. Polarization of pro-inflammatory M1 to anti-inflammatory M2 macrophages are also mediated by MSCs through contact dependent mechanisms though some evidence also showed inhibitory impact of secretome on innate immune cells [32]. HLA-G detected in the secretome of MSC confers protection to MSC lysis by reducing degranulation activities of NK cells [36]. IDO, TGFβ, and PGE2 secreted by MSCs affect NK cell proliferation and function. Overall MSCs promote a tolerogenic environment and suppression of pro-inflammatory immune responses and promote anti-inflammatory immune responses [31].

1.4.2 Paracrine Mode of Action- Mesenchymal Stem Cell in Tissue Regeneration

The use of MSC-CCM has showed improvement for a wide range of diseases conditions (Table 1) [28] "such as, alopecia [37], skin wound [38, 39], myocardial infarct [40, 41], liver injury/failure [42-45], cerebral injury/ischemia/stroke, spinal cord injury, [46-51], kidney injury [52, 53], periodontal defect [54]" and bone defect [28]. The first study to show paracrine mode of action of MSCs was reported by *Gnecchi et. al.* where they showed that injection of CCM obtained from MSC overexpressing *Akt1* reduced acute myocardial

infarction (AMI) size and improved ventricular functions [55, 56]. Fractionation studies showed that only the >1000 kDa (100-220 nm) fraction of the CCM conferred cardioprotection; reduction of infarction sizes, nuclear oxidative stress and apoptosis rates as well as improvements of systolic and diastolic cardiac performance were observed [40]. Nuclear oxidative stress and apoptosis rates were reduced in porcine model for AMI after intravenous and intracoronary injections of MSC-CCM [40]. *Lee et. al.* demonstrated intravenously administered BM-MSCs mainly got trapped in the lungs of a mouse model for AMI [26]. They identified TSG-6 as a candidate cytokine, and showed knockdown of TSG-6 expression by siRNA completely abrogated the therapeutic potential of MSCs used for treating AMI [26].

Supporting further the notion that MSCs mainly act in a paracrine manner in several kidney disease models, *Tögel et. al.* showed in an acute kidney injury (AKI) model that despite the transient engraftment of injected BM-MSCs into damaged renal tissue their beneficial effects on renal function and tubular damage were mediated by anti-apoptotic, pro-mitogenic and vasculotropic factors [57, 58]. Human embryonic stem cell (huESC) and hBM-MSC-CM have also shown improvement in kidney functions in several animal studies [52, 59]. Apart from kidney injury and myocardial infarction, systemically administered BM-MSCs showed the same extent of therapeutic effect in terms of increased survival rates and clinical score of GvHD mice as BM-MSC-CCM which provided further evidence of MSCs paracrine mode of action [60].

Table 1: Studies on various species, conditions, source of conditioned medium, and therapeutic outcome.

Condition/disease	Species	Source of conditioned medium	Outcome	Reference
Alopecia—ID	Human	Hu-AD-MSC	Increased hair growth	[37]
Skin wound direct—SC	Male db/db (diabetic) mice	Hu-UC-MSC	Faster wound closure Increased capillary density	[38]
Skin wound—48 hour after wound—SC	Male NOD-SCID mice	Hu-BM-MSC	Faster wound healing	[39]
MCI—4 hours—IV (jugular vein)	DL pig	Hu-ESC-MSC	Increased capillary density Reduced infarct size Preserved S-D performance	[41]
MCI—5 min before R—IV, -at R—IC	Female DL pig	Hu-ESC derived MSC	(i) Reduced infarct size and apoptosis (ii) Improved S-D performance	[40]
MCI—5 min before R—IV—(tail)	Mouse	Hu-ESC derived MSC	Reduced infarct size (>1000 kD/100–220 nm) = 10–220 nm < 10–100 nm	[40]
RSLT—direct—IV—(penile)	Male SD rat	Rat BM-MSC	Reduced LIB and PIC Increased survival	[42]
Acute hepatic failure—24 hours—intrahepatic (left liver lobe)	CCl4 injured SCID/NOD mice	1-Hu-AF MSC 2-AF-MSC-hepatic progenitor-like cells (HPL)	(i) AST, ALT decreased (ii) Liver phenotype improvement HPL was better than MSC-CM	[43]
Fulminant hepatic failure—24 hours—IV (penile)	Male SD rat	Hu-MSC	Reduced ALT, AST, TNF, IL6, and IL1-rec-A level, and HP, ICI, and apoptosis Increased IL10 level, liver regeneration, and survival	[44]
	Male SD rat	Hu-BM-MSC	Reduced panlobular leucocyte infiltrate, hepatocellular death, and bile duct duplication and increased survival	[45]
Focal cerebral ischemia—72 hours—intranasal	Male SD rat	(i) Hu-SC-EDT (ii) BM-MSC (Lonza)	Increased migration-differentiated endogenous NPC, vasculogenesis, and motor function, and reduced infarct size (Hu SC-EDT = BM-MSC)	[46]
Ischemic stroke—after 8 days—lateral ventricle infusion	Male SD mice	Hu-AD-MSC	Motor function maintained, reduced infarct volume, neural cell apoptosis, and astrogliosis, and increased microvessel	[47]
Cerebral ischemia infarction—1 day—	immunodeficient mice	(i) Hu-BM-MSC (ii) Hu-BM-CD133	Reduced cortical infarct volume (huBM-CD133-CM < huBM-	[48]

IC/intracardiac (LV) injection		(iii) Hu-BM-p75 (iv) Hu-fibro	MSC-CM < hufibroCM < huBM-p75CM)	
Fluid percussion-TBI—direct IV jugular vein	Male SD rat	Hu-BM-MSC	Reduced neuron loss, apoptosis, neuron A, infarction volume, and motor deficit Increased VEGF(+) cells	[49]
Fluid percussion TBI—12 hours after—IV	Male SD rat	Hu-BM-MSC	Decreased brain damage volume, brain damage incidence, and neuron apoptosis (hypoxia < normoxia) Increased motor/cognitive function and neurogenesis (hypoxia > normoxia)	[50]
Contusion spinal cord injury—direct	Female Wistar rat	Rat-BM-MSC	Increased motor recovery	[51]
Chronic kidney disease—week 5—IV (tail)	Male Le rat	Hu embryonic MSC—stable—80 population doublings	Decreased systolic BP, proteinuria, and tubular + glomerular damage Increased inulin and PAH clearance, glomerular endothelium, and DNA repair	[52]
Nephropathy—24 hours—IV (tail)	Mouse BALBc	(i) Hu-UCB-USSC (ii) Mouse BM-MSC	No improvement in serum urea and creatinine, HP, and physical activity score	[53]
Normal—cancer cell line + CM xenograft	BALB mice	Hu-MSC (cell line)	Increased tumor cell proliferation (PCNA) and vascularization	[61]
Intrabony periodontal defect direct—implant	Hybrid dog	Hu-MSC (Lonza)	Increased alveolar bone and cementum regeneration	[54]

(Adapted from *Pawitan et. al.* 2014) [28] AD: adipose tissue derived, AF: amniotic fluid, ALT: alanine amino transferase, AST: aspartate aminotransferase, BM: bone marrow, DL: Dalland Landrace, EDT: exfoliated deciduous tooth, ESC: embryonic stem cell, HP: histopathology, hu: human, IC: intracoronary artery, ICI: immune cell infiltration, ID: intradermal, IL1-rec-A: IL1 receptor antagonist, Imyo: intramyocardial, IV: intravenous, LIB: liver injury biomarker, LV: left ventricular, MCI: myocardial infarct, MSC: mesenchymal stem cells, NOD: nonobese diabetic, NPC: neural progenitor cell, PAH: para amino hippuric acid, PIC: proinflammatory cytokine, RSLT: 50% reduced size liver transplantation, SC:subcutaneous, SD: Sprague-Dawley, SC: stem cell, SCID: severe combined immunodeficient, S-D: systolic-diastolic, TBI: traumatic brain injury, UC: umbilical cord, UCB: UC blood, USSC: unrestricted somatic stem cell,W: Wistar, Le: Lewis.

1.5 Mesenchymal Stem Cell-Derived Extracellular Vesicles

MSC-derived EVs have been found to promote a wide range of therapeutic efficacy mainly by a protein based mechanism of action, that are comparable to MSCs themselves and therefore have great potential as a novel alternative to whole-cell therapies [62]. MSC-EV-mediated therapeutic potential in the treatment of a wide range of diseases including kidney injury, myocardial injury, cerebral injury and lung injury has been reported [40-53]. MSC-EVs contain MSC-associated critical surface markers and signalling molecules characteristic of MSCs thereby potentially mediating the therapeutic effects of MSCs [63]. The broad range of cargo identified in EVs have shown to reduce oxidative stress, stimulate angiogenesis and regulate neurite outgrowth, both *in vitro* and *in vivo* in ischemic injuries such as cardiovascular diseases and ischemic stroke [64]. EVs have also shown tissue repair and immune modulation in kidney, liver and cornea [65]. The most addressed disease models tested for therapeutic impacts of MSC-EVs are kidney, liver, heart and brain in preclinical studies. There are 5 known clinical trials; GvDH (1), ischemic stroke (1), chronic kidney disease (2) and Type I Diabetes Mellitus (1).

Cell free therapies can circumvent many challenges associated with cell-based therapy such as tumorigenic potential, occlusion in microvasculature, possible ectopic ossification and/or calcification, removal of cells after engraftment in the event of an adverse response or upon disease resolution [62]. As EVs lack nuclei they cannot self-replicate and thus in contrast to cells, EVs have the potential to circumvent any endogenous tumorigenic potential. In addition, EVs are easier to handle and, due to their small size, they can be sterilized by filtration and would not occlude microvasculature. Furthermore, MSC-EVs share membrane properties of MSCs, thereby are also thought to be immune privileged [66]. Overall, MSC

exosome/EV-based therapies could potentially be a safer, cheaper and more effective treatment option than cell-based MSC therapeutics [66]. One of the major pitfalls of studying EVs is that there is no gold standard method of isolation, characterization or quantification and this makes reproducibility of results difficult. There is also a major lack of global characterization of MSC-EV molecular profiling and not enough proteomic studies have been conducted to fully understand its molecular composition. As they may potentially be the drivers of therapeutic effects further investigation of molecular profiling is important.

1.6 Extracellular Vesicles - Overview

Initially, EVs were proposed to represent a cellular waste disposal mechanism to eliminate unwanted proteins and other molecules, to now being known as important and novel mediator of cell-to-cell communication [67]. While EVs are involved in maintaining tissue homeostasis they also play important roles in normal physiological as well as pathological functions and can be biomarker for disease [68-70]. EVs were first clearly described by Johnstone in 1983 while trying to understand transformation from a reticulocyte to a mature erythrocyte [71]. Subsequently in 1987 Johnstone coined the term “exosome” because “the process seemed to be akin to reverse endocytosis, with internal vesicular contents released in contrast to external molecules internalized in membrane-bound structures” [72, 73].
Despite the biogenesis of exosomes explained in the literature (but not yet fully understood, mostly due to the limitations in isolation techniques) most exosome preparation contains a heterogeneous population EV subtypes [74].
EVs are released by almost all cell types and are detected in all body fluids (plasma, urine, tears, sweat, milk, seminal fluid, cerebrospinal fluid saliva or urine) [75]. There has been an

exponential interest in MSC-EVs in the last ten years, as they portray similar therapeutic efficacy as MSCs and MSC-CCM [76]. EVs can interact and modulate recipient cell signalling and mediate cell to cell communication either by internalization of EVs by endocytosis or by transfer of bioactive molecules (proteins, mRNA, miRNA) via fusion of membrane [77]. EVs can also stimulate cell signalling pathways of the recipient cells by receptor mediated interaction without transfer of bioactive molecules [77]. Finally, EVs can transfer EV surface receptors or lipids to the recipient cells [77].

One of the major pitfalls of studying EVs is that there is no gold standard method of isolation, characterization or quantification and this makes reproducibility of results difficult. To address these issues and to facilitate exchange of information, the International Society of Extracellular Vesicles (ISEV) in 2014 proposed a minimal set of requirements for studies of extracellular vesicles (MISEV) for characterization. The ISEV has also proposed that fractions containing different EV subtypes (exosomes, MVs, apoptotic bodies and/or other EV types) be appropriately termed as EV fractions [78].

Though the 2014 guidelines still remain valid, in 2018 ISEV released a revised MISEV guideline taking into consideration the evolving EV field. The new guidelines propose that when reporting EV-based studies, the methods of EV isolation and production be described in details as a part of EV characterization [79]. The 2018 guidelines have made it mandatory to report the source of EVs, cell culture conditions (O_2%, size of vessel), number of cells from which EVs were isolated, frequency and interval of CCM harvest, total starting volume or weight of EV biofluid and total number of particle concentration or protein amount, pre-treatment to remove contaminants before EV isolation, temperature and time of biofluid/tissue handling before and during pre-treatment [79]. The 2014 and 2018 guidelines requires mandatory characterization of at least one protein listed in the MISEV guidelines

from 3 categories of: 1) Presence of transmembrane or GPI-anchored proteins associated to plasma membrane and/or endosomes, 2) Presence of cytosolic proteins recovered in EVs, 3) Presence or absence of major components of non-EV co-isolated structures (purity determination). In the 2018 guidelines there are additional criteria when reporting functional studies, namely EV doses used for treatment, negative control (non-conditioned medium), functional activity comparison between total fluid or EV depleted fluid or EVs, and functional activity comparison between different EV subtypes. A new nomenclature based on size has been proposed: 1) small EVs (sEVs): < 100nm or < 200nm [small], 2) medium/large EVs (m/lEVs) > 200nm [large and/or medium]. If EV preparations consist of multiple types of EVs (small/medium/large) at least one protein from the categories of transmembrane, lipid-bound and soluble proteins associated to other intracellular compartments than PM/endosomes and secreted proteins recovered with EVs, is encouraged to be identified [78, 79].

1.7 Extracellular Vesicles - Types

In the last 10 years many different types of EV classifications have been reported, where exosomes and microvesicles are unanimously distinguished. In addition, apoptotic bodies are also commonly described in the literature as the third type of EVs. Exosomes, microvesicles and apoptotic bodies are characterized primarily based on their size, density, markers and composition [80]. Although different origin and different sizes had been proposed for all three EV subtypes (exosomes, microvesicles and apoptotic bodies) they could not be discriminated in an experimental setting as microvesicles and exosomes have overlapping settings.

1.8 Extracellular Vesicles - Biogenesis

An editorial review by *Biancone et. al*. described that EVs are categorized into exosomes which have a size range of 30-180nm formed by the inward budding of late endosomes forming multivesicular body (MVB) and released by exocytosis during fusion the MVB with the plasma membrane [81]. The classical pathway of exosome formation is by far the most extensively studied. Microvesicles are formed by budding from the plasma membrane and have a heterogeneous size ranging from 100-1000nm, whereas apoptotic bodies have a size greater than 1000nm [81]. Exosomes and microvesicles, both have similar molecular content; proteins, lipids, mRNA, microRNA and rarely DNA [81]. Apoptotic bodies only contain fragmented DNA [81]. Table 2 shows the different types of EVs categorized based on sucrose density gradient, origin and composition [82]. Exosomes are commonly characterized by a set of tetraspanin markers CD63, CD81 and CD9 [81]. Two intracellular pathways of MVB sorting exist by which proteins and proteolipids are sorted into the intraluminal vesicles (ILV): 1) The Endosomal Sorting Complex Required for Transport (ESCRT) machinery ubiquitin-dependent pathway - cargo predestined for degradation by fusion with lysosomes, 2) ESCRT ubiquitin-independent pathway of MVB biogenesis directing cargo into intraluminal vesicles which are then released as exosomes upon fusion with the plasma membrane [83, 84]**.** Protein sorting into ILV is facilitated by syntenin (a cytosolic adapter protein) which initiates interaction between heparan sulfate proteoglycan syndecan and ALIX (ESCRT-III-associated protein). This results in ubiquitin-independent ESCRT III-mediated exosome formation. Trimming of the heparan sulphate chains by heparanase triggers syndecan clustering which stimulates syntenin-ALIX-ESCRT-mediated selective cargo sorting results in CD63 incorporated but not CD81, flotillin and CD9

exosome production [83]. CD9 or CD63 are thought to play a role in the sorting of transmembrane proteins toward intraluminal vesicles [83]. ESCRT-independent sorting of the proteolipid protein to ILV depends on sphingolipid ceramide, generated from sphingomyelin hydrolysis by neutral sphingomyelinase 2 (nSMase2) which induces negative membrane curvature leading to ILV budding into MVBs. It is still unclear whether MVBs generated by ubiquitin-dependent mechanisms are mainly destined to lysosomes for cargo degradation or can fuse with the plasma membrane to release exosomes [84].

Table 2: Characteristics of 3 types of EVs

	Size (nm)	**Sucrose density (g/ml)**	**Origin**	**Composition**
Exosomes	40 - 200	1.13 – 1.19	Late endosomal compartment forming MVB; fusion with plasma membrane	proteins, lipids, mRNA, microRNA and rarely DNA
Microvesicles	50 - 1000	1.04 – 1.07	Outward budding of plasma membrane	proteins, lipids, mRNA, microRNA and rarely DNA
Apoptotic Vesicles	1000 - 5000	1.16 – 1.28	Outward budding of plasma membrane	fragmented DNA

Adapted from *Choi et. al. 2017* [80] EV: extracellular vesicles, MVB: multivesicular body

1.9 Mesenchymal Stem Cell Derived Extracellular Vesicle Mediated Therapeutic Effects in Preclinical Studies

1.9.1 Kidney Injury

The effects of MSC-EVs on tissue regeneration have been investigated as a therapeutic in several acute kidney injury (AKI) models [59, 85-88]. *Bruno et al.* found that MSC-MV/EV were able to improve renal function and reduce the extent of kidney damage by preventing apoptosis and increasing renal tubular epithelial cell proliferation in an AKI model in severe combined immunodeficiency mice [88]. In an *in vivo* study MSC-EV/MV conferred renoprotection by horizontal transfer of insulin-like growth factor-1 receptor (IGF-1R) mRNA to tubular cells [89]. Treatment of MSC-EVs has been shown to improve kidney function, alleviate fibrosis, activate proliferation of tubular cells and reduce apoptosis [85, 86, 88, 90]. In vitro studies demonstrated that MSC-EVs enabled tissue repair by inducing expression of anti-apoptotic (Bcl-xL, Bcl-2 and BIRC8) and simultaneously downregulated pro-apoptotic genes (Casp1, Casp8, and LTA) in renal tubular epithelial cells [85, 86]. An *in vivo* study using rats, reported MSC-EVs may inhibit recruitment of kidney macrophage by reducing the expression of CX3CL1 [90].

1.9.2 Cardiac Injury

The beneficial therapeutic impacts of MSC-EVs have been reported in several experimental models of myocardial ischemic/reperfusion (I/R) injury [91-95] where MSC-EVs not only reduced fibrosis and apoptosis but also promoted angiogenesis [95-98]. *Lai et al.* reported human embryonic stem cell-derived MSC significantly reduced infarct size in pig and mouse

models of I/R injury [92, 99]. Furthermore, in a separate study *Lai et. al.* also reported significantly reduced infarct size and improved left ventricular function upon administration of purified MSC exosomes prior to reperfusion. The therapeutic effects were hypothesized to be mediated by membrane proteins and the EV cargo. MSC-EV contain membrane proteins such as integrins and tetraspanins. EV membrane proteins such as integrins could home exosomes to cardiomyocytes that expressed ICAM1 after myocardial I/R injury [100] or to VCAM-1 on endothelial cells [101] whereas the tetraspanin proteins, which function primarily to mediate cellular penetration, invasion and fusion events [102] could also facilitate cellular uptake of exosomes. Using mass spectrometry and antibody array to identify proteins in MSC-EV *Lai et al.* found enzymes such as glycolytic enzymes and proteasomes. The glycolytic enzymes from MSC-EV may be able to replenish the glycolytic deficit and potentially increase glycolytic flux and ATP production in the reperfused myocardium [103]. Additionally, 20s proteasomes degraded intracellular protein damaged by oxidation and removed/degraded the misfolded or oligomerized proteins in reperfused hearts may be reduced [104].

1.9.3 Traumatic Brain Injury (TBI)

Doeppner et al. reported that increase neural plasticity, improve functional recovery and long-term neuroprotection were associated with enhanced angioneurogenesis in ischemic stroke mice that received MSC-EVs [105]. *Kim et al.* [106], *Otero-Ortega et al.* [107] and *Xin et al.* [108] were also able to show MSC-EV mediated neuroprotection in models for ischemic stroke and traumatic brain injury or intracerebral hemorrhage [106-108]. In a study by *Xin et. al.* MSC-EVs could influence brain plasticity and help tissue repair in rat-based middle cerebral occlusion model of stroke [109]. MSC-MV/EVs suppressed neuro-

inflammation immediately after TBI in mice and showed improvement in neurocognitive function even after one month post-TBI [107].

1.9.4 Liver injury

The beneficial effects of MSC-EVs on liver diseases have been studied in models for acute liver injury. *Tan et al.* found that MSC-EVs elicited protective effects and inhibited the acetaminophen- and H_2O_2-induced injury by increasing hepatocyte proliferation and inhibiting apoptosis through upregulation of Bcl-xL and signal transducer and activator of transcription 3 (STAT3) expressions [109]. MSC-EV treatment improved liver functions in a tetrachloride (CCL_4)-induced liver injury model by replenishing serum aspartate aminotransferase activity and inactivating the TGF-β1/Smad signaling pathway by decreasing collagen type I/III and TGF-β1 and the phosphorylation of Smad2 [110].

1.10 Mesenchymal Stem Cell-Derived Extracellular Vesicles - Clinical Studies

Despite the overwhelming therapeutic effects portrayed by MSC-EV/exosomes, there are currently only 5 known clinical studies. A published clinical study demonstrated MSC-EVs were able to suppress the symptoms of a steroid-refractory acute GvHD in a patient. EVs were isolated using polyethylene glycol (PEG) enrichment method and quantified by nanoparticle tracking analysis (NTA). MSC-EVs were first tested *in vitro* in a mixed lymphocyte reaction assay showing a decrease in proinflammatory cytokines, confirming immunomodulatory properties [111, 112]. MSC-EVs were administered in increasing doses

without any side effects observed during the course of treatment. The clinical GvHD symptoms improved significantly within two weeks of treatment and the patient showed decreased levels of pro-inflammatory cytokines IL-6, IL-8 and IL-17A and reduced anti-inflammatory cytokine. The MSC-EV therapy was well tolerated and improvement was stable up to 5 months before the initial gut acute GvHD symptoms reappeared [111, 113]. A phase II/III clinical pilot study using human cord blood MSC (hCB-MSC) derived EVs was performed with 40 patients in Cairo, Egypt, suffering from chronic kidney disease (CDK) [125]. EVs were characterized by TEM (80 nm to 1000 nm) and flow cytometry confirming the presence of EV and MSC markers such as the presence of CD44, CD29, α4- and α5 integrins and CD73 and the lack of expression of HLA-class I and HLA-class II. The trial was divided into two groups, 20 patients each; one group received two doses of MSC-EVs with an interval of one weeks between the doses, one intravenously and one intra-arterial, and the control group, received one saline injection intravenously. One year after therapy CDK symptoms were improved in the MSC-EV treated but not in the control group in a non-significant manner although there was in increasing trend towards recovery. In contrast with the control group the biopsies of the MSC-EV treated patients revealed the presence of activated renal progenitor cells indicating tissue regeneration. Taking immunomodulatory effects of the MSC-EV therapy into account, TGF-β, IL-10 (anti-inflammatory cytokines) levels were significantly increased and TNF-α (inflammatory cytokine) levels were significantly decreased after one year following the MSC-EV treatment [114]. Apart from these two studies, a phase II-III clinical study investigating the effects of MSC-derived exosomes for the improvement of β-cell mass in type 1 diabetes patients entitled “Effect of Microvesicles and Exosomes Therapy on β-cell Mass in Type I Diabetes Mellitus (T1DM)” (NCT02138331) was registered in 2014 . However, results of this study have not been

published, yet. Two other ongoing clinical trials are currently investigating MSC-EV based therapeutics for acute ischemic stroke and macular hole (MH). The first one, a phase I-II clinical study entitled "Allogenic Mesenchymal Stem Cell Derived Exosome in Patients With Acute Ischemic Stroke" has been registered with an estimated enrolment of 5 patients (NCT03384433) investigating functional recovery post ischemic stroke using modified MSC-EV loaded with miR-124 treatment. The second ongoing clinical study is investigating whether MSC-EV (exosome) therapy may promote functional and anatomic recovery from MH caused by aging. An early phase 1 clinical study entitled "MSC Exosomes Promote Healing of Macular Holes" with an estimated enrolment of 44 patients (NCT03437759). MSC-EVs have demonstrated a similar or even superior functional potential to MSCs themselves and the potential to circumvent MSC associated risks [114].

1.11 Mesenchymal Stem Cell Derived Extracellular Vesicles - Proteomics

The first evidence of biological function of EV proteins dates back to 1996 demonstrating clearly that MHC II was present in EVs secreted by B cells [115]. The evidence for the therapeutic effects of MSC-EV proteins was only provided in 2010 by *Chai et. al* in a study demonstrating that MSC-EVs were able to reduce infarct size in a mouse model of myocardial ischemia/reperfusion injury [92]. In a comparative proteomic analysis of MSC and MSC-EVs from porcine adipose tissues, *Eirin et. al.* reported 5469 and 4937 in MSC and MSC-EVs, respectively using mass spectrometry (LC-MS/MS). In silico analysis revealed 128 proteins enriched in MSC-EVs were linked to a wide range of biological function such as angiogenesis, immune-regulation, blood coagulation, apoptosis and

extracellular matrix remodelling [116]. Studies have reported the role of MSCs and MSC-EVs in facilitating angiogenesis, reducing apoptosis and oxidative stress in several ischemic studies. MSC-EV proteins including angiopoietin-1, Notch-1 and Wnt Family Member-5A involved in angiogenesis and vascular development were reported by *Anderson et. al* [117]. The authors further reported that angiogenesis is modulated in a NFkB signalling dependent pathway [117]. Zhang *et al*., reported comparable wound healing *in vivo* using deep second degree burn injury model when treated with human umbilical cord MSC (hucMSC) and hucMSC-EVs. The author demonstrated that MSC-EVs promoted recovery from skin burns by promoting skin cell proliferation by EV-Wnt4-mediated direct promotion of β-catenin nuclear translocation [118]. Treatment of myocardial ischemia followed by reperfusion (I/R injury) *in vivo* with MSC-EV reduced infarct size and activated multiple cardioprotective intracellular signalling pathways [91]. *Arsalan et. al.* indicated that this therapeutic effect is mediated by replenishment of glycolytic enzymes and thereby restoring biogenetics, as ATP and NADH levels increased followed by MSC-EV treatment. Oxidative stress was reduced by peroxiredoxins and glutathione S-transferases in EVs, whereas the pro-apoptotic signals were reduced due to decreased c-JNK phosphorylation and proliferation via pro-survival PI3K/Akt pathway activation [91]. Therapeutic potential of MSC-EV for Alzheimer's disease has shown promising results. Adipose tissue (AD)-MSC-EVs contain enzymatically active neprilysin (also known as CD10), the rate-limiting amyloid beta (Aβ)-degrading enzyme expressed in the brain, and AD-MSC-EV were able to reduce the levels of Aβ in cells overexpressing Aβ [119]. *Chopp and Li* reported that MSC-EVs in stroke model can alter neuroplasticity via EV cargo proteins such as nestin, neuro-D, growth-associated protein 43, synaptophysins, VEGF and FGF which promote regenerative events such as neural development, synaptogenesis and angiogenesis [120]. *Kim et al*. investigated

proteomic profiles of hMSC-EVs and reported 730 proteins packaged in EVs [134]. Among them were unique surface receptors proteins, signaling molecules, cell adhesion molecules. MSC surface markers, proteins involved in pathways related to MSC self-renewal and differentiation was also detected. Proangiogenic proteins (ANGTL, HGF, VEGF) as well as proteins involved in apoptosis (caspase-14) and immune modulation and fibrosis (matrix metalloproteinase-3, TGFβ-1, TGFβ-2, IL-10) were found by mass spectrometric analysis of human embryonic MSC-derived EVs [121]. In an effort to find a proteomic signature of MSC-EVs, *Balkom et. al.* in 2018 reported a comprehensive study using publically available MSC-EV proteomic datasets. Their search results yielded 59 matches ("PubMed; (msc OR (mesenchymal AND (stem OR stromal))) AND (exosom* OR microvesic* OR vesicle*) AND proteom*") [122]. Only 18 publications out of 59 conducted proteomic analysis and finally 10 publications met their inclusion criteria (human source, adequate description of MSC characterization, LC-MS/MS approach of proteomic analysis and exclusion of repeated analysis of already published data). A detailed description of the EV isolation and characterization used for proteomic analysis in these 10 publications is shown in Table 4 [122]. Despite the overwhelming evidence of MSC-EV proteins as the main driver of the therapeutic effects a thorough investigation of the proteins enriched in EVs derived from hBM-MSC has not been reported [122].

Table 3: human MSC-EV isolation and characterization methods for downstream proteomic analysis in various studies

Source	Isolation	Size (nm)	Characterization	Western Blot	No. of proteins	References
ESC	TFF-HPLC-filter	110-130	SG	CD63,CD81, CD59	766	[104]
PL chorionic villi	UC (12K-filter-100K)	40-100	EM	CD9, CD63, CD81	390	[123]
BM	100 kd filter-seq UC	50-200	EM	CD63,Hsp9, Galectin-1	730	[121]
ESC, immortalized	TFF-HPLC-filter	50-150	NTA	CD9, CD81, Alix,Tsg101, CD59	978	[124]
Umb	UC: 10K-100K-filter	40-100	EM	CD9, CD81	157	[125]
AT	TFF-sucrose cushion 100K-optiprep	50-200	EM	CD63,Hsp9, Galectin-1	2334	[126]
BM	UC (10k-filter-100k)	50-200	NTA, EM	CD9, CD63, CD81, Tsg101	538	[127]
BM	UC (filter-10k-100k)	50-200	NTA, EM	CD63, Alix, Tsg101	145	[128]
BM	UC (4K-100k)	158 (mod)	NTA, EM	n/a	797	[129]
BM	UC (filter-1k-17k-120k)	50-200	EM	n/a	2546	[117]

Adapted from *Balkom et. al.* [122] EM: Electron microscopy, ESC: Embryonic Stem Cells, HPLC: High pressure liquid chromatography, mod: modular size, NTA: Nanoparticle tracking SG: sucrose gradient, (seq) UC: (sequential) Ultracentrifugation, analysis, TFF: Tangential Flow Filtration, Umb: Umbilical cord.

1.12 Limitations

Little is known about the different EV subpopulations and whether one specific subpopulation such as exosome mediates the therapeutic effects of MSCs or a combination

of all small EVs. Furthermore, the current technology available does not allow the experimental separation or even discrimination of different EV types of similar sizes. We are still limited by the lack of standardized isolation and storage methods of EVs**.** Table 5 describes the main advantages and disadvantages of the top 10 commonly used methods for EV isolation [130]. Several isolation techniques are available such as differential centrifugation which is the most commonly used method for exosome isolation, but it might not be the best method as it is limited by small sample size and can compromise the membrane integrity [130]. Density gradient centrifugation method of isolation yields the highest purity of EV subsets but at the expense of scalability, yield, cost, time and therapeutic potency [130]. Immunoaffinity methods using exosomal tetraspanins markers seem to be promising as *Mathivanan et. al* [131] and *Kowal et. al.* [132] have reported this method results in relatively pure subpopulation of EVs. However, this method will be limited at large scale production as its expensive [131, 132]. Polyethylene glycol (PEG)-based precipitation of exosomes is becoming a popular method of isolation as its highly scalable and easy to use but can be contaminated with lipoparticles and other vesicles of similar size. Finally, two other EV isolation techniques gaining popularity are size exclusion chromatography (SEC) and EV purification in closed systems such as tangential flow filtration (TFF) [130, 133]. Both SEC and TFF methods enable large scale production, high purity and biologically functional EVs. It is important, however, to keep in mind that, depending on the isolation method, different EV subtypes might be enriched and may differ in their functional properties. There are no gold standards methods for EV characterization and quantification or *in vitro* potency assays. It is important to understand the molecular and physical characteristics of EVs for the clinical translation of EV-based therapeutics regardless of the method of isolation. Furthermore, no quality control assay is in place to

determine safety and efficacy, which requires proper molecular profile including protein characterization to identify signature molecular markers or potency markers.

Table 4: Main advantages and disadvantages of the top 10 commonly used methods for EV isolation [143].

Method	Advantages	Disadvantages	No. of original research papers on EV isolation
Ultracentrifugation, differential centrifugation: 300 ×g, 10000 ×g, 100000–200000 ×g (1.5 h)	Cost (in the case of ultracentrifugation), isolation from large volumes, absence of additional chemicals	Equipment, complexity, nonexosomal impurities, low reproducibility, low RNA yield, damage of exosomes; efficiency is affected by the type of rotor, force ,sample viscosity; only six samples can be concurrently processed in one ultracentrifuge	290
Density gradient ultracentrifugation, sucrose or iodixanol density gradient, differential centrifugation	Pure preparations; no contamination with viral particles after iodixanol centrifugation; absence of additional chemicals	Complexity, loss of sample, ultracentrifugation; fails to separate large vesicles with similar sedimentation rates; contamination with viral particles after sucrose density gradient procedure	30
Ultrafiltration, nanomembrane or filters with a pore diameter of 0.8–0.1 μm	Simple procedure allowing for concurrent processing of many samples; pure preparations; additional chemicals; no limitations on sample volume	Filter plugging, loss of sample, contamination (proteins); deformation of vesicles; small quantity of exosomal proteins	14
Size-exclusive chromatography (SEC), columns filled with polymers with heterogeneous pores	Reproducibility and purity; preserves vesicle integrity; use of the buffers with a high ionic strength enhances elimination of nonspecific impurities; high sensitivity, no losses, scalability, large amount of exosomal proteins; prevents EV aggregation; insensitive to high viscosity of samples; no additional chemicals	Limitations on sample volume and number of separated peaks (necessary difference of the components in molecular weight, ≥10%); specialized equipment; complexity; coisolation of large protein aggregates and lipoproteins; processing no more than one sample in each procedure; cost	8

Method	Advantages	Disadvantages	No. of original research papers on EV isolation
Precipitation with polymers, polyethylene glycol caused EV precipitation	Cost and simplicity of procedure; preservation of EV integrity; no need in additional equipment; pH close to physiological range; high ion concentrations	Contamination and retention of the polymer	68
Commercial kits for polymer precipitation (ExoQuick, TEI, and Norgen), polymer precipitates EVs	Simple procedure; preservation of EV integrity; no need in additional equipment; pH close to physiological range; high ion concentrations	Cost (especially for diluted samples, such as urine); poor reproducibility; impurities and retention of polymer; low content of exosomal proteins	
Precipitation of proteins with organic solvent PROSPR, cold acetone	Cost and simplicity	Aggregation in multivesicles	3
Use of antibodies to EV receptors, in particular, tetraspanins (CD9, CD63, CD81), TSG101, EpCAM	Purity and high selectivity	High selectivity, cost, availability of antibodies; difficulties with detachment of molecules and analysis of intact vesicles (eluting buffers can damage EV functional activity); nonspecific binding	5
Use of lectins	Cost, simplicity, purity	Need in the initial purification and concentration (ultracentrifugation of centrifugation at 20000 ×g)	3
Microfluidic technologies	Rapidness, purity, efficiency	Complexity of devices and need in additional equipment; cost	9

Aadapted from *Konoshenko et. al 2018* [143]

1.13 Objective of the study

Hypothesis: Human bone-marrow derived extracellular vesicles are enriched in proteins that promote angiogenesis, cell survival and a wide range of other therapeutically relevant pathways.

Rationale: Extracellular vesicles (EVs) produced by mesenchymal stem cells (MSCs) have been considered to be a major paracrine effector in MSC therapeutic responses. Several studies have implicated that MSC-EV/exosomes have therapeutic potential and despite the overwhelming evidence of MSC-EV proteins as the main driver of the therapeutic potential there is a lack of EV protein identification and characterization. Thorough identification of proteins packaged in MSC-EVs is required to understand the underlying molecular mechanism of action (MOA) and would thereby ease transition to their safe use as cell free therapy.

Aims: This study aims to characterize the phenotypic properties of MSC-EVs and identify the protein composition and dominant biological processes and pathways modulated by exosomal/EV proteins. This will be achieved by using an untargeted and unbiased quantitative approach by mass spectrometry, and pathway analysis which may lead to development of fingerprinting assays and a better understanding the MOA of various therapeutic effects mediated by MSC-EVs.

Objectives:

Part 1 Objective: Production, isolation, characterization and quantification of the EV population of EVs derived from 5 hBM-MSC donors.

Part 2 Objective: To characterize the protein composition of the hBM-MSC-EV and identify the dominant cellular and molecular functions modulated by EV proteins.

Chapter 2: Materials and Methods

2.1 hBM-MSC culture expansion

Human bone marrow-derived MSCs (hBM-MSCs) were obtained at P1 or P2 from Texas A&M University Health Science Center for this study. MSCs from all 5 hBM-MSC donors were expanded to generate cell banks as per protocol with slight modifications. For expansion all hBM-MSCs in a vial were seeded (~ 1 x 10^6) in T-175 flask overnight as per recommendation. The cells were harvested using 0.25% Trypsin-EDTA (Gibco, Cat#25200-072) in the morning and seeded at a seeding density of 17,500 cells/T-175 (100 cell/cm^2), all hBM-MSCs were used at P3 -P 4. All hBM-MSCs from 5 healthy male donors were cultured in alpha-MEM (Invitrogen, Cat#12561-056) supplemented with 15% MSC-Screened FBS (HyClone, Cat#SH30070.03) in a T-175 flasks. Media was changed on day 4 and cells were harvested and frozen on day 7 to create working cell banks to be used for this study. The cells obtained from Texas A&M University, Health Science Center, were pre-characterized for MSC surface marker, differentiation and growth (Table 5) and reconfirmed for surface markers according to the ISCT's minimal criteria (Table 5 and Figure 1; Results section). The hBM-MSCs and maintenance protocol employed in this work were provided by the Texas A&M Health Science Center College of Medicine Institute for Regenerative Medicine at Scott & White through a grant from ORIP of the NIH, Grant # P40OD011050.

2.2 hBM-MSC-EV production

A 7-day culture timeline for MSC expansion was established and this included a 48 hour EV production time (Figure 2). hBM-MSCs were initially seeded at seeding density of $1.4x10^5$ per T-175 flask on day 1**.** From day 1 to day 3 hBM-MSCs were cultured in 25mL of alpha-MEM supplemented with 15% MSC-Screened FBS or complete media (CM). On day 4, media was aspirated and replaced with 25mL of CM. A second media changed was performed on day 5, where media was aspirated and cells were rinsed twice with 15 mL of PBS prior to replacing the media with 32mL of alpha-MEM supplemented with 15% exo-depleted FBS (Gibco, Cat#A2720801) or exo-depleted complete media (ED-CM). 48 hours after the second media change which was day 7, the CCM was collected. CCM was centrifuged at 2000 x g for 30 minutes to remove cell debris, the supernatant (CCM) was recovered and was frozen at -80^{o}C in 50mL falcon tubes in 15mL aliquots until use. Furthermore, cells were harvested and counted to later normalize EV counts. After cell count the cells were rinsed twice with cold PBS by centrifuging at 300g x 8 mins, after the second rinse the PBS was aspirated and the cell pellet was also stored at -80^{o}C in 15mL falcon tubes until ready for use.

2.3 hBM-MSC-EV isolation

CCM was thawed at room temperature on the day of use, and processed immediately once liquid. Each CCM aliquot was filtered using 0.2µm PALL Acrodisc 25 mm Syringe Filters (PN 4612). Filtered samples were then added to Amicon Ultra-15 centrifugal filters (previously equilibrated with PBS) and centrifuged at 2,000 x g for 20 minutes. Collection

tube was emptied of filtrate, and double filtered PBS was added to the concentrated sample until final volume of 15mL. Samples were centrifuged a second time at 2000xg for 20 minutes. Concentrated samples were added new 50mL falcon tubes, mixed with 0.5 volume of Total Exosome Isolation Reagent (Invitrogen, Cat#4478359) and vortexed. Samples were allowed to incubate overnight at 4^{o}C, and in the morning centrifuged at 10,000 x g for 1 hour at 4^{o}C. Supernatant was removed and pellet was resuspended in double filtered PBS. For NTA and flow cytometric analysis a starting volume of 15mL CCM was used from which EVs were isolated using the procedure mentioned above and eventually resuspended in 0.5mL of double filtered PBS.

2.4 Flow Cytometry

2.4.1 hBM-MSC-EV Surface Marker Analysis

hBM-MSC-EVs were analyzed using flow cytometry to confirm the presence of exosome/EV-specific tetraspanin markers CD63, CD81 and CD9 using CD63 conjugated magnetic beads according to the manufacturer's protocol, (Invitrogen, Cat#10622D) except for the volume of hBM-MSC-EVs used which were further optimized. hBM-MSC-EVs were isolated according to the protocol mentioned above. For this procedure hBM-MSC-EVs were isolated from a starting volume of 15mL and the hBM-MSC-EVs were eventually resuspended in double filtered PBS. The hBM-MSC-EV suspension is referred to as pre-enriched hBM-MSC-EVs. Briefly for flow cytometry, isolation buffer was prepared (dPBS+0.1% BSA) and filtered through a 0.2µm syringe filter. 40µL of magnetic beads were first rinsed with 200µL isolation buffer using DynaMag2 magnet (Invitrogen, Cat#12321D)

and incubated with 300µL pre-enriched hBM-MSC-EVs. The samples were vortexed for 30 seconds each in round bottom 2mL eppendorf tubes. Samples were incubated overnight at 4^{o}C while mixing using Orbitron rotator. After incubation, samples were centrifuged for 30 seconds at 1,000 rpm to gather the bead bound-EV samples at the bottom of the tube. Bead-bound hBM-MSC-EVs were then rinsed twice with 300µL followed by 400µL of isolation buffer (dPBS+0.1% BSA) using the DynaMag2 magnet and removing supernatant. Bead-hBM-MSC-EV conjugates were resuspended in 500µL of isolation buffer from which 100µL was transferred to each 5mL flow tubes and stained separately with CD63, CD81 and CD9 antibodies or isotypes. The concentration of the CD63, CD81 and CD9 antibodies were matched to isotype antibody concentration. Samples were incubated for 45 minutes in the dark while shaking. Stained samples were rinsed two times with isolation buffer and supernatant containing excess antibody was discarded using DynaMag2 magnet. Samples were suspended in 0.5mL isolation buffer and placed on ice until ready for flow cytometric analysis using the LSRII flow cytometer (BD Biosciences).10, 000 events per sample were collected. Raw data was analysed using FlowJo V10 (FlowJo LLC, Ashland, OR, USA) where CD63, CD81, CD9 positive expression was measured against isotype control **IgG1, κ** which served as a negative control. For information on antibodies refer to Table 1 in appendices.

2.4.2 hBM-MSC Surface Marker Analysis

To analyse hBM-MSC surface marker set by ISCT, the Human MSC analysis kit from BD Biosciences (Cat# 562245) was used according to the manufacturer's protocol (Antibodies

for positive surface markers; CD73, CD90, CD105 and antibodies for negative surface markers; CD11b, CD19, CD34, CD45, HLA-DR). Briefly, cells were expanded as per hBM-MSC culture expansion protocol (Section 2.1) and after harvesting, the cells were counted using trypan blue after which the cells were washed PBS+2%FBS (flow buffer). The cells were then resuspended in 1mL flow buffer so that each 100µL had approximately 0.5 x 10^6 for staining followed by cells filtered through 40 µm cell strainer. 100 µl of cell suspension to each flow tube was added (9 as per protocol to which specific antibodies provided in the kit were used) and tubes were incubated in the dark for 30 minutes at 4^0C after which the cells were washed two times with flow buffer. The volume was then brought volume up to 4 ml, and cells were centrifuged at 1,100 rpm for 6 minutes at 4^0C. The supernatant was discarded and the pellet was resuspended in 500µL staining buffer and analysed by flow cytometry using LSRII flow cytometer (BD Biosciences). Raw data was analysed using FlowJo V10 (FlowJo LLC, Ashland, OR, USA).

2.5 NTA analysis of MSC-EV using NanoSight NS300

hBM-MSC-EVs were isolated from 15mL of CCM through centrifugation and ultrafiltration (described in Section 2.3) and resuspended in 0.5mL of double filtered PBS. For NTA analysis using NS300, an appropriate volume was taken from 0.5mL of enriched hBM-MSC-EV samples and diluted 50x in double filtered PBS to a final volume of 3mL for analysis and vortexed prior to filling syringe with 1mL of 50x diluted hBM-MSC-EV sample. The syringe was then clamped and secured in the syringe pump and analyzed at flow mode. Each 1mL sample was ran using the following syringe pump script: 6 captures of one minute, speed 10.

Samples were vortexed prior to be added to syringe to reduce clumping. For capture settings a screen of 2 and camera level 15 was used and for analysis setting a screen gain of 3 and detection threshold of 13 was used. In between each sample, 3mL of double filtered water, 3mL 70% ethanol, and 3mL double filtered water was flushed through the system for cleaning. Analysis of raw data was done using Excel and Graphpad Prism. The total hBM-MSC-EV concentration or concentration at each size distribution generated by NTA was multiplied by 50 first (as the samples were diluted 50x) and followed by times 2 to calculate hBM-MSC-EV concentration in 30mL CCM per flask.

2.6 hBM-MSC and hBM-MSC-EV protein lysate preparation for Western blot and Mass Spectrometry Analysis

Lysis buffer (100mM TEAB with 1% SDS final concentration) was prepared according to the manufacturers protocol using the reagents provided in the TMT labeling kit (TMT10plex Mass Tag Labeling Kits and Reagents Thermo Cat #90113). 250uL of lysis buffer was added to cell or EV pellets (isolated form 30 ml CCM) and gently vortexed. The samples were incubated for 30 minutes at 4^{o}C on end over end shaker (LabQuake Shaker). After incubation the samples were centrifuged down for 30 seconds at 1000rpm. The samples were sonicated at amplitude setting 20%(EV) or 30% (Cell) to lyse membranes for 3x10 seconds with 30 seconds on ice between pulses. After sonication, samples were centrifuged at 14,000 x g for 5 minutes at 4^{o}C. The supernatant was recovered with a pipette and stored in LoBind tubes at -80^{o}C. Prior to freezing an aliquot was taken out for BCA (Pierce BCA Protein assay kit, Cat# 23227) quantification and freeze at -80^{o}C.

2.7 WESTERN BLOTS

hBM-MSC and hBM-MSC-EV protein lysates were extracted from biological samples, 40µg of protein sample were combined with 4X LI-COR Protein Loading Buffer (LI-COR Biosciences, Cat#92840004), and Bolt™ 10X Reducing Agent (Invitrogen, Cat#B0009) to a final concentration of 1X. Samples were boiled for 5 minutes then loaded onto precast Bolt™ Bis-Tris 4%-12% 17 well SDS-PAGE (Invitrogen, NW04127BOX). Gels were run using an MOPS buffer system (Invitrogen, Cat#B0001) for 32 minutes at 200V. Gels were trimmed and transferred to the Millipore Immobilon FL PVDF membrane (Millipore, Cat#IPFL00005) using the Bolt™ Mini Module wet transfer system for one hour at 20V. Following transfer, membranes were washed 3 times in distilled water for 5 minutes on orbital shaker at speed 4 (≈ 300 RMP) then stained with LI-COR REVERT total protein stain (LI-COR Biosciences, Cat#92611010) according to manufacturer's protocol and imaged at 700nm using the LI-COR Odyssey CLx NIR imager. Membranes were blotted using the iBind Flex Western device. REVERT Total Protein Stain was used to ensure proper loading of sample.

2.8 Transmission Electron Microscopy (TEM) of hBM-MSC-EVs

For TEM, hBM-MSC-EVs were isolated as described above from a starting volume of 15mL of CCM and eventually resuspended in 300uL of double filtered PBS. The 300uL hBM-MSC-EV suspension was filtered using vivaspin filters, following a rinse of the filters with 200uL of double filtered PBS centrifuged at 2000xg for 3 minutes. The concentrated hBM-MSC-EVs were resuspended in equal volume 4% PFA for 30 minutes. Next, two 50uL drops of hBM-MSC-EV suspension with PFA were deposited on parafilm and on which carbon

coated electron microscopy grids (Cat# CF300-CU) were inverted and placed for 5 minutes on each 50uL sample followed by a rinse with 50uL drops of PBS on a sheet of parafilm. Blot grids on filter paper to remove excess and let dry for an hour before imaging. The TEM imaging for samples was performed using a FEI Tecnai Spirit TEM with a LaB6 emitter, operating at 120kV. The images were acquired with an Eagle camera with 4k x4k resolution.

2.9 TMT labeling Protocol for Mass Spectrometry Analysis

hBM-MSC and hBM-MSC-EV lysate was prepared according to the lysis protocol above (Section 2.6) and quantified by BCA as 100µg of protein from each sample was used. The TMT protocol was followed according to the manufacturer's protocol, with slight modifications. Please refer to (TMT10plex Mass Tag Labeling Kits and Reagents Thermo Cat #90113) for background information and details.

Preparing Protein Extracts: The proteins were quantified using BCA after which 100µg per donor per replicate (Refer to Table 3 appendices for more information on labelled samples) was transferred into a new microcentrifuge tube and adjusted to a final volume of 100µL with 100mM TEAB. 5µL of the 200mM TCEP was added to 100µg protein in 100µL and incubated at 55°C for 1 hour in a heating block. One tube of iodoacetamide (9mg) was dissolved in 132µL of 100mM TEAB to make 375mM iodoacetamide. 5µL of the 375mM iodoacetamide was added to the 100µg protein sample and incubated for 30 minutes protected from light at room temperature. Next a three stepwise acetone precipitation was performed by adding pre-chilled (-20°C) acetone (4 times the volume of 100µg protein added 3 times every 15 minutes). Samples were kept at -20°C for 90 minutes, vortexing every 15 minutes after which the samples were precipitated overnight at -20°C. The next morning

samples were centrifuged at 14,000 x g for 10 minutes at 4°C to remove acetone, which was done carefully without dislodging the protein pellet. The pellet was then dried for ~10 minutes in the fumehood.

Protein Digestion: Next 100µg of the acetone-precipitated protein pellets was resuspended with 100µL of 100mM TEAB (flick, slow vortex to dissolve). Immediately before use, 20µL of the Trypsin Storage Solution was added to the bottom of the trypsin glass vial and incubated for 5 minutes. 2.5µL of trypsin (i.e., 2.5µg) was added per 100µg of protein and incubated overnight at 37°C in Thermomixer C at 500 rpm.

Peptide Labeling: The next morning protein digest concentration was measured using Thermo Scientific™ Pierce™ Quantitative Colorimetric Peptide Assay kit (Cat#23275) according to manufacturer's protocol. TMT Label Reagents were equilibrated to room temperature immediately before use and 41µL of anhydrous acetonitrile was added to each to each TMT Label (0.8mg) vials which was then allowed to dissolve for 5 minutes with occasional vortexing. 41µL of the TMT Label Reagent was added to each 100µL sample and incubated for 1 hour at room temperature. 8µL of 5% hydroxylamine was added next to the sample and incubated for 15 minutes to quench the reaction. Equal amounts of each sample was combined in a new microcentrifuge tube and given samples to mass spectrometry lab for analysis or store at -80°C until ready for analysis.

2.9.1 Mass Spectrometric analysis

The Orbitrap Fusion Tribrid Mass Spectrometer coupled to an Easy-nLC 1000 (Thermo Scientific) was used to analyse hBM-MSC (n = 5) and hBM-MSC-EV (n = 5) TMT labeled peptides. The instrument was calibrated by infusion prior to analysis with a mixture of

caffeine, MRFA, and Ultramark 1621. For each fraction 6 µl were analyzed by loading onto a NanoViper Acclaim pepmap 100 trap column (75 µm 20 mm with 3 µm beads) and desalting with 0.1% formic acid in water (solvent A), before separating on a NanoViper Acclaim pepmap RSLC C18 reverse-phase analytical column (75 µm 150 mm with 3 µm beads). Chromatographic separation was achieved at a flow rate of 0.300 µl/min over 140 min in seven linear steps as follows (solvent B was 0.1% formic acid in acetonitrile): initial, 5% B; 3 min, 5% B; 5 min, 10% B: 110 min, 25% B; 130 min, 60% B; 135 min, 90% B; 140 min, 90% B. The eluting peptides were analyzed in data-dependent mode for both MS2 and MS3 methods. A MS survey scan of 400−1500 m/z was performed in the Orbitrap at a resolution of 120000 and an AGC target of 4×10^5. The top speed mode was used to select ions for MS2 analysis, requiring charge state 2-7 and dynamic exclusion 40 s with a ±10 ppm window, and monoisotopic precursor selection. During the MS2 analyses, precursors were fragmented by HCD at collision energy of 35% +/- 10%, followed by Turbo IonTrap analysis using automatic m/z normal scan range. Precursors were isolated in the quadrupole using a width of 1.2, accumulated to an AGC target of 1×10^4 or a maximum injection time of 50ms. The 10 most intense fragments in MS2 spectra were selected for MS3 analysis with the filters mass range 400-1200, precursor exclusion +/- 5 m/z, and TMT isobaric tag loss exclusion. MS3 analysis was performed in the Orbitrap at resolution 60000 from 100-500 m/z, precursors isolated using a 2 m/z isolation window, accumulated to an AGC target of 5×10^4 or a maximum injection time of 120 ms. The MS3 precursor population was isolated using the SPS waveform and then fragmented by HCD, with a normalized collision energy set to 65.

2.9.2 Data Processing

The software package Proteome Discoverer 2.2 (Thermo) was used to process the data. The SEQUESTHT algorithm was used to search MS2 spectra against a database containing human proteins (Uniprot-Trembl, downloaded 20171116, 124124 entries) concatenated with a database of common contaminants (cRAP). Database search parameters were 10 ppm precursor ion tolerance, 0.6 Da fragment ion tolerance, and allowing up to two missed cleavages. Fixed modifications were TMT tags on peptide N termini/lysine residues (+229.162932 Da) and carbamidomethylation of cysteine residues (+57.02146 Da) while variable modifications were N-terminal acetylation (+42.011 Da), methionine oxidation (+15.99492 Da). An MS2 spectra assignment false discovery rate (FDR) of less than 1% was achieved by applying Percolator algorithm. For quantification, a 20 ppm integration tolerance with the most confident centroid integration method was used. To account for differences in sample handling samples were normalized on total peptide amount. Missing values were replaced with minimum values, and only MS3 spectra having minimum average signal to noise (S/N) ratio of 10 were accepted for quantification.

2.10 Statistical Analysis for Mass Spectrometry

The mean raw abundance value of all 5 donors for hBM-MSC-EV was compared to the mean raw abundance value of all 5 donors for hBM-MSCs for corresponding proteins. There were 5089 observations (proteins) in hBM-MSC data and 770 observations in the hBM-MSC-EV data. 673 proteins remained, after excluding proteins with 100% missing values in both hBM-MSC and hBM-MSC-EV data. The absolute minimal missing value from the hBM-MSC-EV data was used to impute all missing data in hBM-MSC data (the value is 4.70). The intensity data of both datasets were log2-tranformed after the imputation. The

transformed data from hBM-MSC and hBM-MSC-EV of 673 proteins were compared by using a paired t test procedure. The p-values were adjusted for multiplicity by a false discovery rate (FDR) controlling method based on the linear step-up method suggested by Benjamini and Hochberg (1995). Benjamini, Y. and Hochberg, Y. (1995). Controlling the false discovery rate: a practical and powerful approach to multiple testing. Journal of the Royal Statistical Society, Series B 57, 289–300

Chapter 3: Results

3.1 MSC characterization according to minimal criteria set by ISCT

3.1.1 Growth (population doubling), immunophenotypic profile by flow cytometry confirming MSC surface identity and confirmation of differentiation to osteocyte and adipocytes

The minimal set of criteria to define MSCs in culture set by ISCT are 1) Plastic adherence 2) The expression of CD105, CD73 and CD90 (≥95% positive) and lack of expression of CD45, CD34, CD14 or CD11b, CD79a or CD19 and HLA-DR surface markers (< 2% positive) 3) In vitro differentiation to adipogenic, chondrogenic and osteogenic cells [6]. hBM-MSCs used for this study were obtained pre-characterized for surface markers, differentiation and growth (Table 1) at passages (P)1 and 2. These cells were then expanded to create a working cell bank from 5 healthy hBM-MSC male donors using Alpha-MEM and 15% hMSC screened Fetal Bovine Serum (FBS). The hBM-MSCs were then confirmed for minimal characterization criteria by the ISCT, which showed ≥ 95% for expression of positive (CD73, CD90, CD105) and < 2% expression of the negative (CD11b, CD19, CD34, CD45, HLA-DR) cell surface markers again in the laboratory (Figure 1) at P4-5, as well as growth (population doubling) at P3-P4 (Table: 5). The growth (population doubling) of hBM-MSC following expansion in the laboratory seemed similar to the original growth at P3-P4.

[a]Donor (D) ID	[b]Donor ID/gender/age	[c]P1-P2 Population doublings	[c]P2-P3 Population doublings	[c]P3-P4 Population doublings	[d]P3-P4 growth MSCs plated per cm^2 / cells harvested per cm^2 / days	[e]P3-P4 Population doublings	[d]Differentiation osteocyte / adipocyte / chondrocytes	[g]Surface Marker (P2)	[h]Surface Marker
Donor 1	7078/M/24	6.61	6.29	6.44	99/3143/6	4.99	P1,2,3 testing + / + / NA	≥95% CD105, CD73a and CD90, ≤2% CD34, CD19, CD11b, CD45, CD79a, HLA-II:DRDQDP, CD14	≥95% CD105, CD73 and CD90, ≤2% CD34, CD19, CD11b, CD45, HLA-DR at P4 for D1-5 and P3 for D5 Human MSC analysis kit, BD Biosceinces (Cat# 562245)
Donor 2	8004/M/22	6.37	6.92	6.12	94/6286/7	6.05	P1,2,3 testing + / + / NA	≥95% CD105, CD73a and CD90, ≤2% CD34, CD19, CD11b, CD45, CD79a, HLA-II:DRDQDP, CD14	
Donor 3	7043/M/28	6.70	7.12	6.88	100/5714/7	5.84	P1,2,3 testing + / + / NA	≥95% CD105, CD73a and CD90, ≤2% CD34, CD19, CD11b, CD45, CD79a, CD14	
Donor 4	7083/M/24	6.94	7.41	6.26	100/8917/7	6.48	P1,2,3 testing + / + / NA	≥95% CD105, CD73a and CD90, ≤2% CD34, CD11b, CD45, HLA-II:DRDQDP, CD14	
Donor 5	8013/M/22	6.43	5.87	5.57	98/4698/7	5.58	P1,2,3 testing + / + / NA	≥95% CD105, CD73a and CD90, ≤2% CD34, CD11b, CD45, HLA-II:DRDQDP, CD14	

Table 5: **hBM-MSC characterization according to minimal criteria set by ISCT for surface identity, differentiation to mesodermal lineage and growth (population doubling)**. [a]For simplicity numbers 1, 2, 3, 4 and 5 were assigned to the healthy donors for this thesis. [b]Healthy donors were identified by anonymous identifier/gender/age for the 5 hBM-MSC donors designated by Texas A&M university. [c]P1-P2, P2-P3 and P3-P4 MSC population doubling data was provided in the specification sheet during purchase. [d]P3-P4 growth is defined as MSC cells plated per cm2 / number of cells harvested per cm2 at / days of incubation. Cells were harvested at 70-90% confluence; this was assessed in our laboratory. [e]Cell population doublings were calculated as n = log2 (harvested viable cells / initial seeded viable cells). [f]Differentiation was assayed at P1, P2 and P3 prior to purchase (+ = present), (NA = not applicable). [g]Cell surface profiling by flow cytometry was also performed prior to purchase at P2. [h]Cell surface profiling by flow cytometry was reconfirmed at out laboratory at P3-4 using human MSC analysis kit, BD Biosciences (Cat# 562245).

3.1.2 Immunophenotypic profile by flow cytometry confirming MSC surface identity

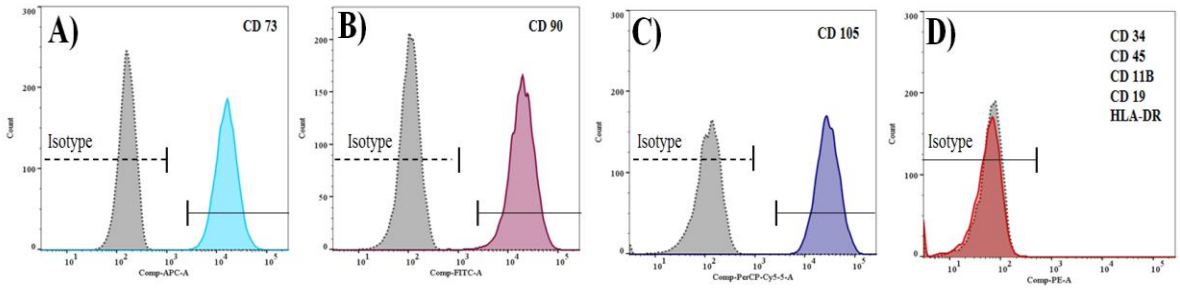

Figure 1: Representative immunophenotypic profile by flow cytometry confirming hBM-MSC surface marker identity at P4-5 for all 5 hBM-MSC donors. 100% positive expression for A) CD73, B) CD90, C) CD105 and D) less than 2% positive for the negative marker cocktail: CD34, CD45, CD11b, CD19, and HLA-DR (red), against isotype control (grey).

3.2.1 Timeline for hBM-MSC-EV production

A 7-day culture timeline for hBM-MSC expansion, which included a 48 hour hBM-MSC-EV production time was developed (Figure 2). The cell conditioned media (CCM) was then collected and the cells were harvested to obtain a live cell count. The CCM was collected and centrifuged at 2000xg for 30mins to remove cell debris, the supernatant was recovered prior to being frozen at -80^{o}C, until ready for downstream analysis. When ready for downstream analysis the CCM was thawed at room temperature on the same day. After thawing the CCM was filtered through 0.2µm filter from which hBM-MSC-EVs were isolated and purified. The CCM which was concentrated twice using 10 kDa filters and hBM-MSC-EVs were isolated from concentrated CCM using a polyethylene glycol (PEG)-based method of purification using a commercial kit. The cells were seeded initially at seeding density of 1.4x10^{5} per T-175 flask on day#1 with two technical replicates. hBM-MSCs from 5 donors which were initially cultured in Alpha-MEM and 15% hMSC screened FBS from day 1-5

followed by media change with α-MEM with 15% exosome depleted FBS 48 hours prior to collection of CCM. Normal culture conditions were maintained throughout the culture timeline ~22% $O_2$and 5% CO_2. This timeline was developed after several seeding density optimizations, as higher seeding densities yielded similar hBM-MSC-EV concentration and a lower seeding density was unable to yield enough hBM-MSC-EVs in a timely fashion (data not shown). This timeline also provided a balance between resources and experimental time, as well as yielded a final overall confluence of ~70% with areas of 80% (Figure 2), which is ideal for EV production and maintaining good cell health.

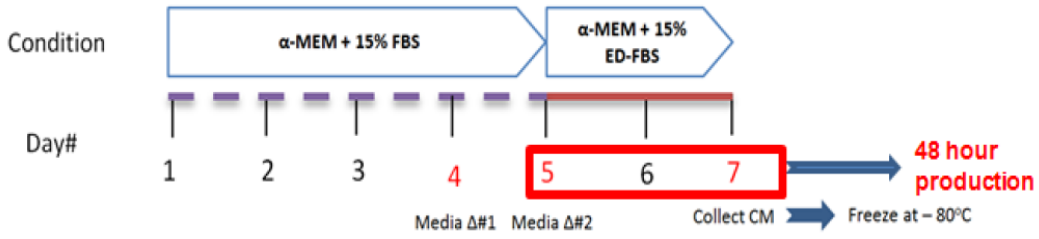

Figure 2: A 7-day culture timeline of hBM-MSCs seeded at $1.4x10^5$ per T-175 flask on day#1 for hBM-MSC-EV production. The hBM-MSC-EVs were harvested from CCM after 48 hours of production at the end of day 7 and the CCM was frozen at -80°C until ready for downstream analysis. (ED: exosome depleted).

3.2.2 Phase contrast images of hBM-MSCs taken at Day 7 during the hBM-MSC-EV production

Phase contrast images of hBM-MSCs at 10x magnification taken on day 7 during the culture timeline for hBM-MSC-EV production. hBM-MSCs from all 5 donors look healthy and shared a typical fibroblastoid appearance.

Donor 1

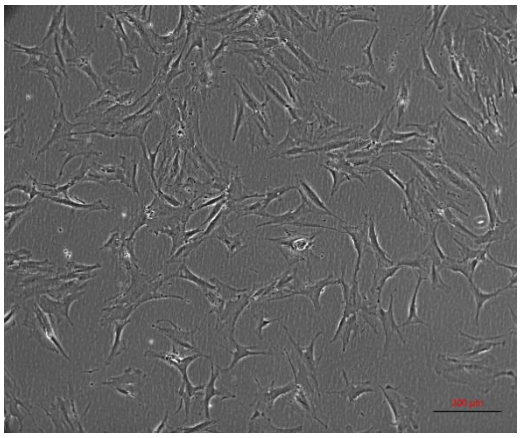

Donor 4

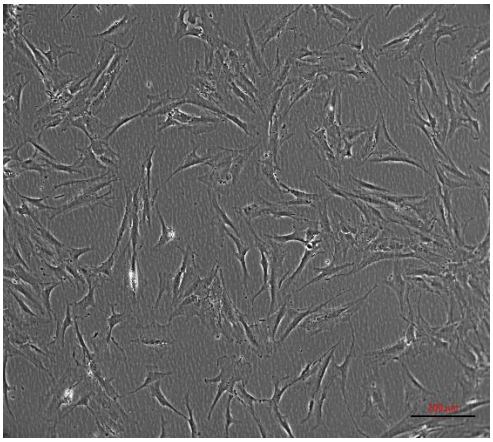

Donor 2

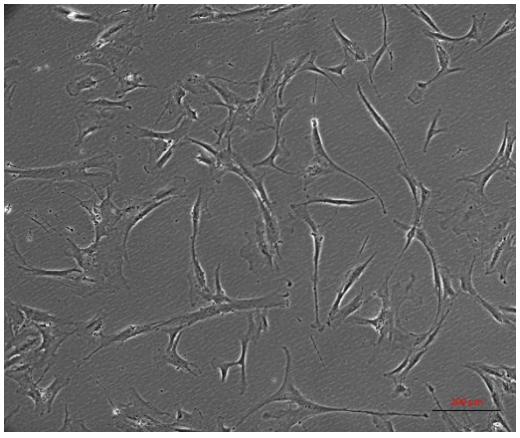

Donor 5

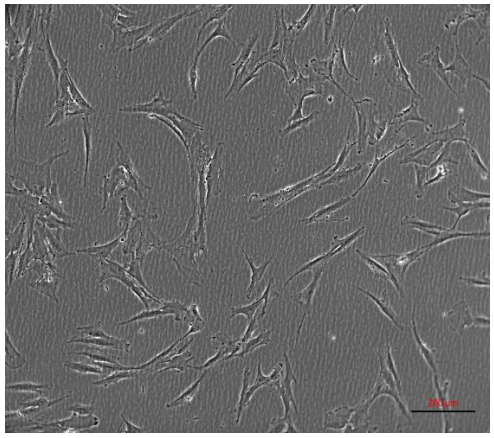

Donor 3

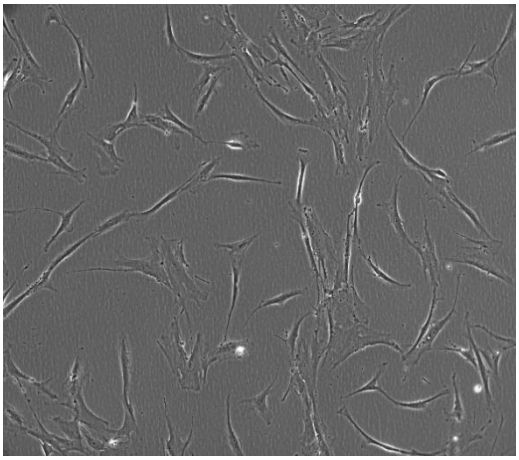

Figure 3: Representative phase contrast images at 10x magnification taken for all 5 hBM-MSC donors taken on day 7 during hBM-MSC-EV production culture timeline. (Scale bar = 200µm).

3.3 Similar enumeration of live hBM-MSC counts after collection of CCM for hBM-MSC-EV isolation from 5 hBM-MSC donors

Viability of cell counts were taken using trypan blue which is a cell stain used to assess viability of cells based on dye exclusion method, at the end of the 7-day culture for hBM-MSC-EV production (Figure 4). Bars represent the cell count for individual MSC donors (D1- 5). According to the MISEV 2018, it is mandatory to report the cell count from which EVs are isolated, as a method of EV characterization [79]. No significant differences were observed among all 5 hBM-MSC donors, showing consistency between all 5 cultures.

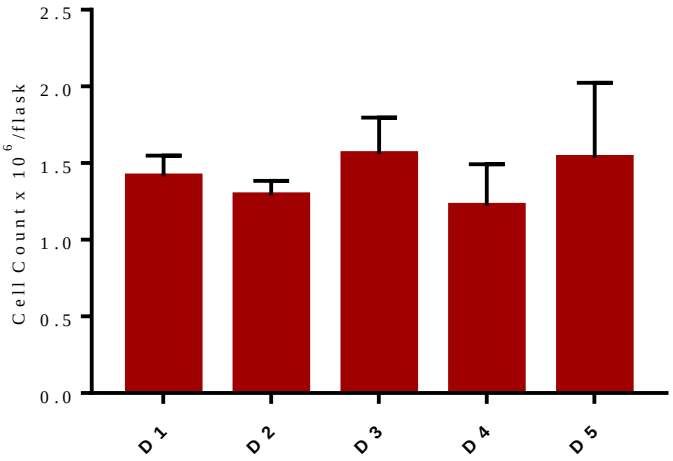

Figure 4: Similar hBM-MSC counts (mean ± SD) of viable cells, where cell counts were taken using trypan blue (exclusion method). This experiment was conducted with five hBM-MSC donors (n=5) in three independent trials with 2 technical replicates per trial.

3.4 Size distribution and quantification of MSC-EV by nanotracking analysis (NTA) using NanoSight NS300

3.4.1 NTA confirmed the desired size distribution of hBM-MSC-EV isolated from 5 hBM-MSC donors

NTA is an important quantification method of EVs and recommended by the MISEV 2018 guidelines as a characterization criteria of EVs [79]. hBM-MSC-EVs were isolated and pre-enriched from a starting volume of 15 ml CCM, by centrifugal ultrafiltration followed by an overnight precipitation of the concentrate with Total exosome isolation reagent from. The concentrate was spun at 10,000 x g for 1 hour at 4^{o}C after the overnight incubation. The pellet was then resuspended in 500µl double filtered PBS and further diluted 50x prior to NTA. The resulting hBM-MSC-EVs were quantified by NTA using Nanosight (NS300) (Figure 5) to determine the concentration and whether the particle size distributions were consistent with that of exosome or small EV size nomenclature according to the MISEV guidelines, 2018. The results confirmed the desired size distribution which fits the criteria of small EV size (50nm – 200 nm) for all 5 hBM-MSC donors.

. **Donor 1**

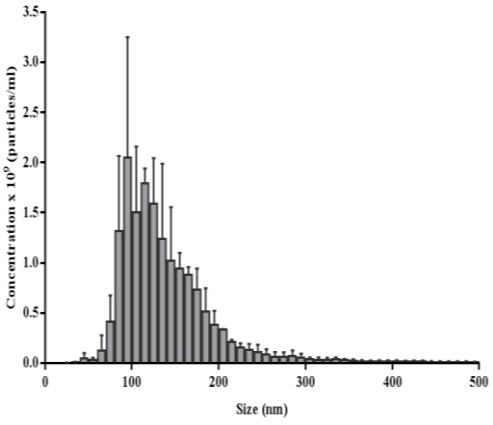

Donor 2

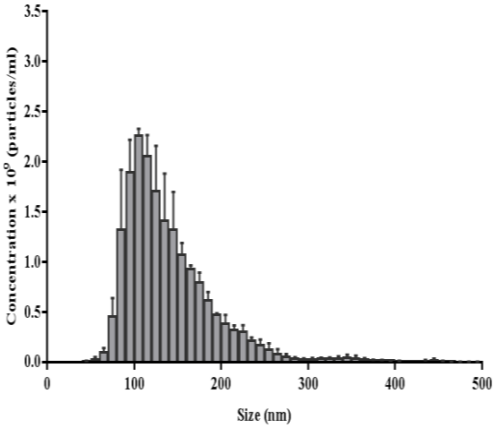

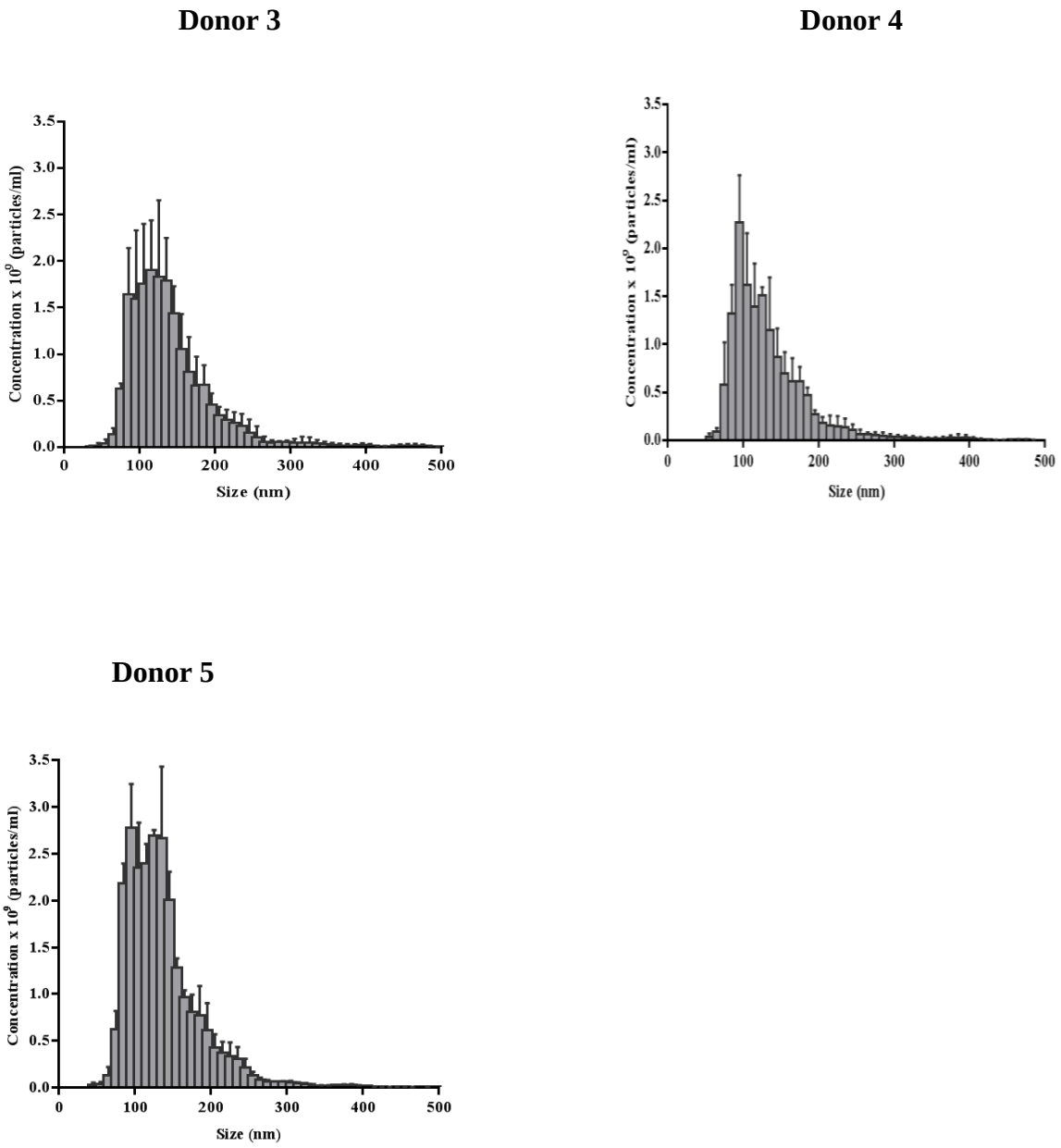

Figure 5: hBM-MSC-EVs were characterized by NTA as a means to quantify hBM-MSC-EV concentration and determine the size distribution. X-axis designates size (nm) and y-axis designates concentration (bars; mean + SD) at different sizes of 5 individual healthy donors (n=5). This experiment was conducted with five hBM-MSC donors (n=5) in three independent trials with 2 technical replicates per trial.

3.4.2 Quantification and size range of hBM-MSC-EVs by NTA of 5 hBM-MSC donors

Apart from size distribution the NTA also generates results for total concentration, mean and mode size of the analyzed sample. The combined concentration of hBM-MSC-EVs was (mean ± SD) $1.83x10^{10}$ + 3.23 x 10^9/mL. Donor to donor variability was observed, where D5 showed the highest production of hBM-MSC-EV, but there were no significant differences in the concentration between the donors (Table 6). There has been a lot of confusion over the nomenclature of late endosomal compartment-derived EVs. However, a new nomenclature based on size has been proposed in the 2018 MISEV guidelines: 1) small EVs (sEVs): < 100nm or < 200nm [small], 2) medium/large EVs (m/lEVs) > 200nm [large and/or medium]. The mean and mode (mean/mode ± SD) particle size measured at 134.1 ± 3.4 and 109.3 ± 5.7 nm, respectively (Table 6). According to the newly established nomenclature by 2018 MISEV guidelines, the hBM-MSC-EVs isolated fall under small EV (< 200nm).

Donor#	[particles/ml] + SD	Mean size + SD	Mode size + SD
Donor 1	**1.63 x 10^{10}** + 5.65 x 10^9	**136.0** + 3.6	**109.6** + 8.1
Donor 2	**1.86 x 10^{10}** + 2.36 x 10^9	**136.1** + 4.6	**106.0** + 3.4
Donor 3	**1.86 x 10^{10}** + 5.78 x 10^9	**135.4** + 4.1	**116.5** + 3.3
Donor 4	**1.48 x 10^{10}** + 3.35 x 10^9	**128.2** + 7.3	**101.7** + 3.5
Donor 5	**2.33 x 10^{10}** + 3.20 x 10^9	**135.4** + 8.1	**112.6** + 7.8

Table 6: Mean concentration, mean and mode size of hBM-MSC-EV + S.D isolated from healthy male hBM-MSC donors (n=5). The mean and mode size are below 200nm which fits the criteria of small EV nomenclature according to MISEV guidelines, 2018. This

experiment was conducted with five hBM-MSC donors (n=5) in three independent trials with 2 technical replicates per trial with 2 technical replicates per trial.

3.4.3 Number of hBM-MSC-EVs produced per hBM-MSC

According to the MISEV 2018, it is mandatory to report the cell count from which EVs are isolated, as well as the number of EVs produced per cell as a method of EV characterization [79]. No significant differences were observed in the cell counts, hBM-MSC-EV concentration or the number of hBM-MSC-EV/ hBM-MSC, showing consistency between all 5 hBM-MSC donors (Table 7).

Donor#	**Total EVs** (mean + SD)	**Live Cell Count** (mean + SD)	**No. of EVs/Cell** (mean + SD)
Donor 1	**1.63 x 10^{10}** + 5.65 x 10^{9}	**1.41 x 10^{6}** + 1.37 x 10^{5}	**11379.77** + 3316.73
Donor 2	**1.86 x 10^{10}** + 2.36 x 10^{9}	**1.29 x 10^{6}** + 0.95 x 10^{5}	**14482.34** + 2456.20
Donor 3	**1.86 x 10^{10}** + 5.78 x 10^{9}	**1.56 x 10^{6}** + 2.36 x 10^{5}	**11812.26** + 2305.44
Donor 4	**1.48 x 10^{10}** + 3.35 x 10^{9}	**1.22 x 10^{6}** + 2.70 x 10^{5}	**12324.56** + 2820.61
Donor 5	**2.33 x 10^{10}** + 3.20 x 10^{9}	**1.53 x 10^{6}** + 4.90 x 10^{5}	**16689.33** + 7351.03

Table 7: Mean concentration of hBM-MSC-EV ± S.D, live cell count of hBM-MSC + S.D from 5 healthy hBM-MSC donors (n=5) and number of hBM-MSC-EVs produced per hBM-MSC as a method of EV characterization. This experiment was conducted with five hBM-MSC donors (n=5) in three independent trials with 2 technical replicates per trial.

3.5 Protein based characterization confirmed the presence of known exosome/small EV tetraspanin markers

3.5.1 Identification and characterization of known EV tetraspanin markers confirmed by flow cytometry analysis

Characterization of EVs requires the detection of proteins such as transmembrane or GPI-anchored proteins associated to plasma membrane and/or endosomes (e.g. tetraspanins; CD63, CD81, CD9). CD63 magnetic beads were used to immuno-precipitate CD63 population and stained for CD63, CD81, and CD9 against isotype control IgG1, κ (grey) which served as a negative control (Figure: 6). High expression of CD63 and CD9 (greater than 95%) were detected and very low or no expression was observed for CD9 (Table: 8).

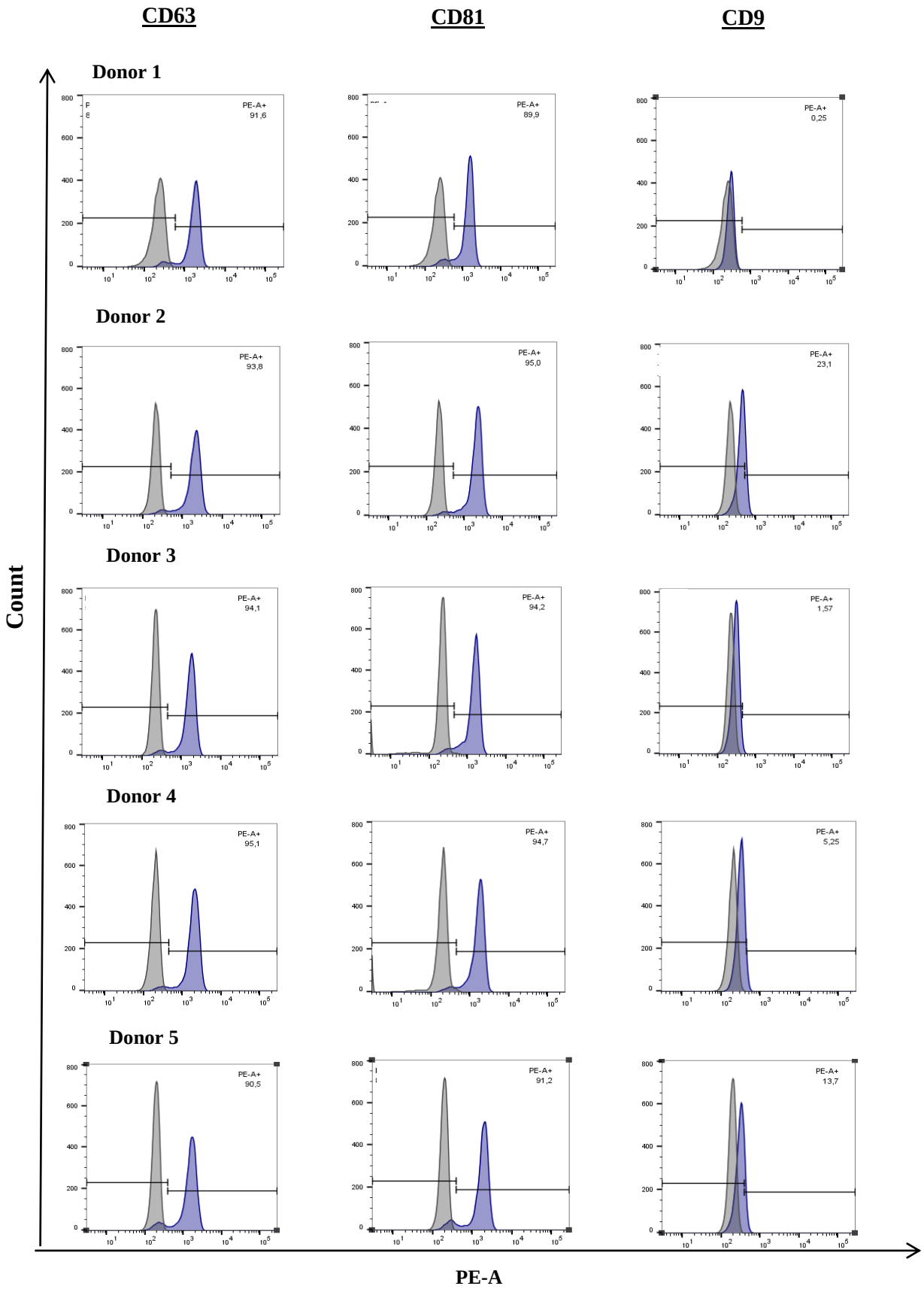
CD63
CD81
CD9
Donor 1
Donor 2
Donor 3
Donor 4
Donor 5
PE-A+ 91,6
PE-A+ 89,9
PE-A+ 0,25
PE-A+ 93,8
PE-A+ 95,0
PE-A+ 23,1
PE-A+ 94,1
PE-A+ 94,2
PE-A+ 1,57
PE-A+ 95,1
PE-A+ 94,7
PE-A+ 5,25
PE-A+ 90,5
PE-A+ 91,2
PE-A+ 13,7
Count
PE-A

Figure 6: Representative flow cytometric plots of CD63 immuno-precipitated population counterstained for CD63, CD81, CD9 against isotype control **IgG1, κ** (grey) which served as a negative control showed high expression of CD63 and CD81 but low or no expression of CD9. This experiment was conducted once with five hBM-MSC donors (n=5).

3.5.1.1 Frequency, median and mean area intensity and count of known hBM-MSC-EV tetraspanin markers confirmed by flow cytometry analysis

Sample Name	Frequency of parent	Median : PE-A	Mean : PE-A	No. of PE-A (+) events
		Donor 1		
Isotope	0.062	205	245	5
Unstained	0	219	195	0
CD63	91.6	1341	1115	5985
CD81	80.3	1308	1276	8034
CD9	55.1	224	185	5514
		Donor 2		
Isotope	0.058	187	199	4
Unstained	0.083	205	201	7
CD63	93.8	1675	1468	6833
CD81	95	2001	2081	8242
CD9	23.1	393	405	1763
		Donor 3		
Isotope	0.036	214	276	3

Unstained	0	201	202	0
CD63	94.1	1507	1358	7595
CD81	94.2	1450	1532	8544
CD9	1.57	290	290	143
Donor 4				
Isotope	0.023	193	206	2
Unstained	0	196	192	0
CD63	95.1	1856	1747	8496
CD81	94.7	1629	1944	8603
CD 9	5.25	309	316	472
Donor 5				
Isotope	0.044	187	264	4
Unstained	0.023	188	183	2
CD63	90.5	1426	1303	7888
CD81	91.2	1723	1663	8221
CD9	13.7	293	386	1142

Table 8: Frequency, median and mean area intensity and counts of known EV tetraspanin markers confirmed by low cytometric analysis. The number of events were set to 10, 000 events per sample. This experiment was conducted once with five hBM-MSC donors (n=5).

3.5.2 Western blot of hBM-MSC-EV characterization for all 5 hBM-MSC donors

According to the MISEV guidelines 2014, HSP90B1 (94kDa) is under represented or absent in exosome/EV but associated with compartments other than plasma membrane or endosomes. The absence of this protein in hBM-MSC-EV and presence in hBM-MSC lysates confirm that our hBM-MSC-EV preparation is not contaminated with proteins from other compartment (Figure 7A). As EVs do not have a consistent house keeping protein, it would be inaccurate use a house keeping protein as a baseline reference, therefore to circumvent this a total protein stain was used (Figure 7B). This also confirms that the samples were loaded properly in the gel.

A)

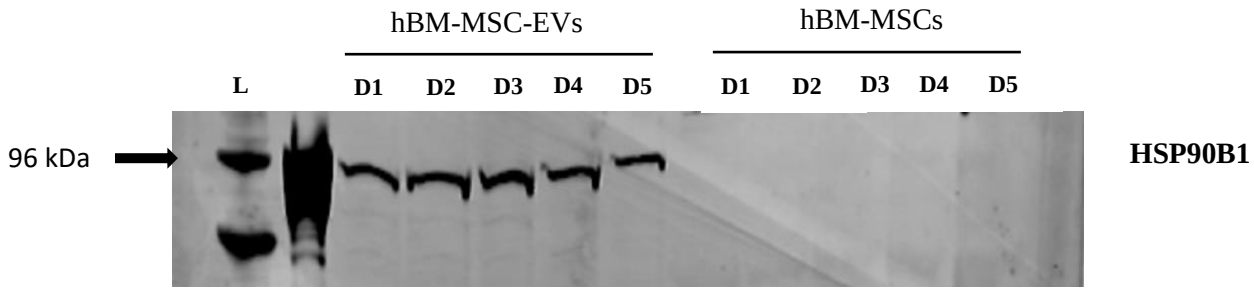

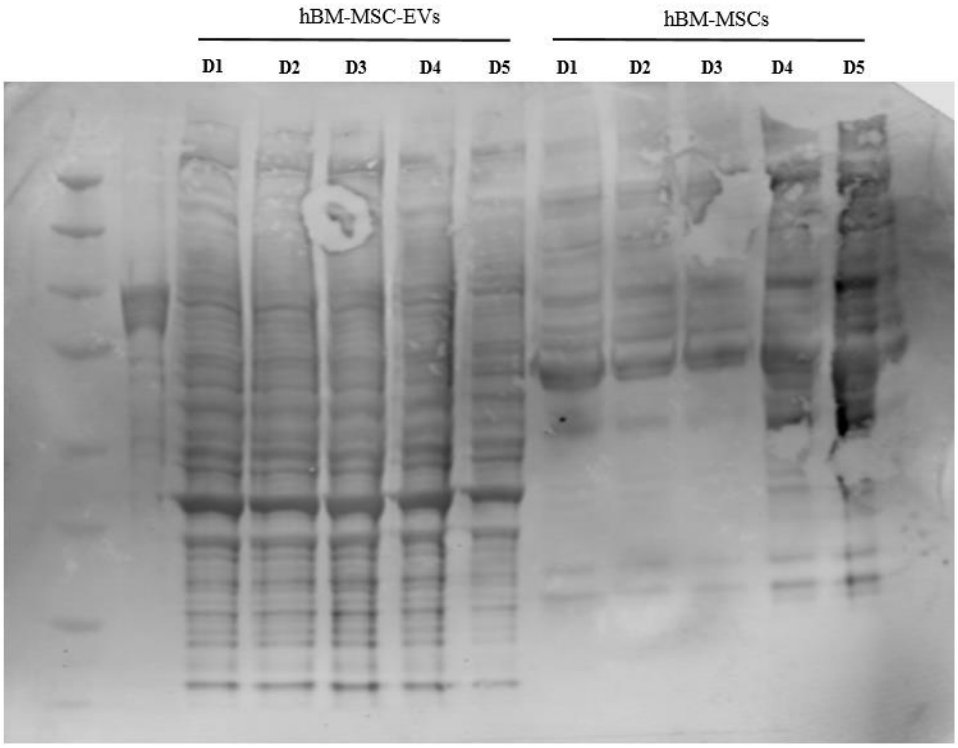

Figure 7A) HSP90B1 (94kDa) expression confirming the presence and absence in hBM-MSC and hBM-MSC-EV respectively. From left to right a ladder (L) was loaded followed by recombinant protein, D1-5: hBM-MSC-EV and D1-5: hBM-MSC. This experiment was conducted with five hBM-MSC donors (n=5) in two independent trials. **B**) Total protein stain of the gel probed for HSP90B1 (94kDa), used for confirmation of proper and equal loading of the samples.

3.6 Morphology and size confirmation of hBM-MSC-EV by Transmission electron microscopy (TEM)

TEM is a qualitative method that allows visualization of nanoparticles. Tem confirmed the presence of hBM-MSC-EV with the expected morphology and size representative of small EV. The bilayer membrane of the vesicles are visible and the size corroborates the NTA data ~ (50nm – 200nm) (Figure 8).

Donor 1

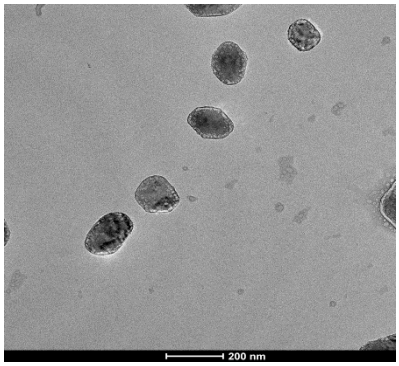

Donor 2

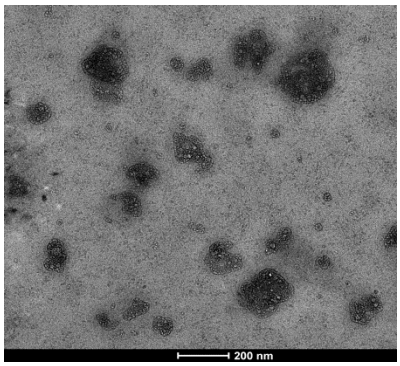

Donor 3

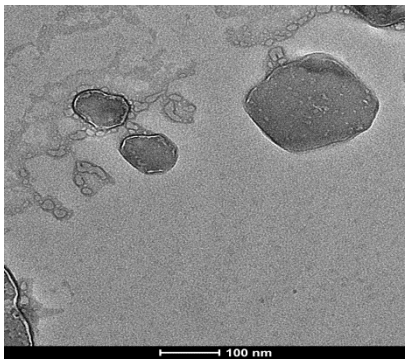

Donor 4

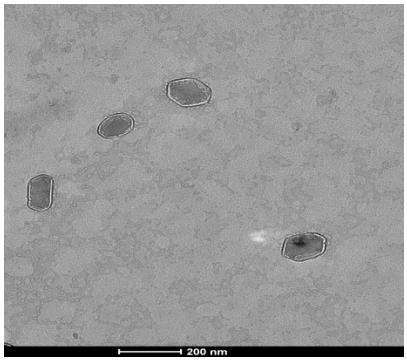

Donor 5

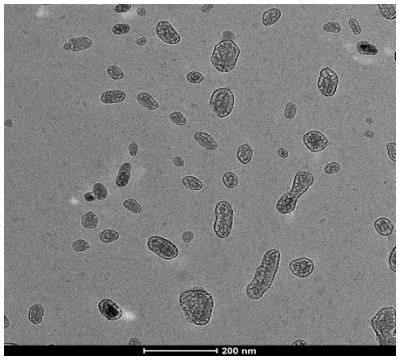

Figure 8: TEM confirmed the presence of hBM-MSC-EV with the expected morphology and size of small EV (< 200nm). Scale bar D1,2,4,5 = 200 nm, D3 = 100 nm. This experiment was conducted once with five hBM-MSC donors (n=5).

3.7 Gene symbol, fold change, protein class and location of greater than 2 fold enriched proteins in hBM-MSC-EVs in comparison to hBM-MSCs

After phenotypical characterization (sections 3.0 – 3.5), the proteomic profile of hBM-MSC-EVs and hBM-MSCs form all 5 donors was investigated using mass spectrometry. A total of 782 proteins were identified for hBM-MSC-EV using mass spectrometry (LC-MS/MS) of which 270 proteins were enriched greater than 2-fold with a cut off p-value of 0.05 in hBM-MSC-EVs compared to hBM-MSCs. Using the bioprofiler tool in ingenuity pathway analysis (IPA), the 270 greater than 2-fold enriched protein dataset were classified into proteins class and location (Figure 9 A, B).

Gene Symbol	Fold Change	Location	Type(s)	Gene Symbol	Fold Change	Location	Type(s)
TUBA1B	163.08	Cytoplasm	other	SERPINC1	23.92	Extracellular Space	Enzyme
EEF1A1	137.078	Cytoplasm	translation regulator	VEGFC	23.6	Extracellular Space	growth factor
QSOX1	109.088	Cytoplasm	enzyme	LAMA2	23.489	Extracellular Space	Other
ACTB	80.837	Cytoplasm	other	MASP1	22.545	Extracellular Space	Peptidase
PKM	74.426	Cytoplasm	kinase	VTN	21.576	Extracellular Space	Other
FERMT3	55.523	Cytoplasm	enzyme	IGFBP2	21.454	Extracellular Space	Other
EXT2	48.271	Cytoplasm	enzyme	FBN1	21.435	Extracellular Space	Other
HBB	46.558	Cytoplasm	transporter	FBN2	19.419	Extracellular Space	Other
ACTA2	44.215	Cytoplasm	other	MST1	19.304	Extracellular Space	growth factor
CAPZB	40.385	Cytoplasm	other	FST	19.072	Extracellular Space	Other

TMOD2	38.558	Cytoplasm	other	C9	18.628	Extracellular Space	Other
ALDH1L1	33.107	Cytoplasm	enzyme	EFEMP2	18.049	Extracellular Space	Other
PGAM1	30.12	Cytoplasm	phosphatase	ABI3BP	17.571	Extracellular Space	Other
MAPRE2	28.607	Cytoplasm	other	FMOD	17.386	Extracellular Space	Other
MYL6	24.647	Cytoplasm	enzyme	F11	17.28	Extracellular Space	Peptidase
HGD	19.286	Cytoplasm	enzyme	COL2A1	16.902	Extracellular Space	Other
UGP2	18.25	Cytoplasm	enzyme	THBS3	16.019	Extracellular Space	Other
PTGES3	16.204	Cytoplasm	enzyme	HBA1/HBA2	15.653	Extracellular Space	Transporter
EML2	15.877	Cytoplasm	other	VWF	14.667	Extracellular Space	Other
PSMB7	15.578	Cytoplasm	peptidase	AMY1C (includes others)	14.184	Extracellular Space	Enzyme
COLEC10	14.923	Cytoplasm	peptidase	OGN	14.05	Extracellular Space	growth factor
S100A1	14.692	Cytoplasm	other	C6	13.878	Extracellular Space	Other
CORO1A	14.62	Cytoplasm	other	ECM1	13.709	Extracellular Space	Transporter
TPM3	12.578	Cytoplasm	other	TIMP1	13.625	Extracellular Space	Cytokine
TPM1	12.256	Cytoplasm	other	LGALS1	13.405	Extracellular Space	Other
GSTA1	12.223	Cytoplasm	enzyme	RNASE4	11.969	Extracellular Space	Enzyme
CKM	11.763	Cytoplasm	kinase	ITIH3	11.848	Extracellular Space	Other
CALD1	11.56	Cytoplasm	other	TIMP2	11.774	Extracellular Space	Other

TKT	10.671	Cytoplasm	enzyme	FBLN5	11.359	Extracellular Space	Other
DCTN2	9.971	Cytoplasm	other	FGL1	11.343	Extracellular Space	Other
ENO3	9.824	Cytoplasm	enzyme	ITGBL1	10.527	Extracellular Space	Other
GSTZ1	9.569	Cytoplasm	enzyme	LCAT	9.973	Extracellular Space	Enzyme
PAH	9.558	Cytoplasm	enzyme	ASPN	9.919	Extracellular Space	Other
XPNPEP1	9.025	Cytoplasm	peptidase	FN1	9.889	Extracellular Space	Enzyme
PPP2R1A	8.995	Cytoplasm	phosphatase	VCAN	8.601	Extracellular Space	Other
ALDH1A1	8.805	Cytoplasm	enzyme	BMP1	8.347	Extracellular Space	Peptidase
CAPRIN2	8.549	Cytoplasm	other	THBS1	7.799	Extracellular Space	Other
HPD	8.401	Cytoplasm	enzyme	ADAMTSL 2	7.544	Extracellular Space	Other
KRT25	7.827	Cytoplasm	other	TGFBI	7.455	Extracellular Space	Other
CALU	7.772	Cytoplasm	other	ADAMTS1 3	7.421	Extracellular Space	Peptidase
FHL1	7.57	Cytoplasm	other	ITIH4	7.199	Extracellular Space	Other
SVEP1	7.139	Cytoplasm	other	KLKB1	6.91	Extracellular Space	Peptidase
GALK1	7.019	Cytoplasm	kinase	IGFBP4	6.876	Extracellular Space	Other
DAPK2	6.765	Cytoplasm	kinase	SPOCK1	6.763	Extracellular Space	Other
CORO1C	6.499	Cytoplasm	other	CPN1	6.627	Extracellular Space	Peptidase
MYOC	6.475	Cytoplasm	other	BGN	6.304	Extracellular Space	Other

GALE	6.459	Cytoplasm	enzyme	CPXM2	5.735	Extracellular Space	Peptidase
AKR1C3	5.924	Cytoplasm	enzyme	FGA	5.636	Extracellular Space	Other
N4BP1	5.756	Cytoplasm	other	MATN3	5.311	Extracellular Space	Other
PACSIN2	5.717	Cytoplasm	transporter	SHBG	5.017	Extracellular Space	Other
PDE5A	5.48	Cytoplasm	enzyme	TGFB1	4.868	Extracellular Space	growth factor
AP1G2	5.426	Cytoplasm	transporter	NID1	4.831	Extracellular Space	Other
SORD	5.366	Cytoplasm	enzyme	SERPINA10	4.805	Extracellular Space	Other
PSMA4	5.131	Cytoplasm	peptidase	PLTP	4.708	Extracellular Space	Enzyme
PPP1CA	5.038	Cytoplasm	phosphatase	PXDN	4.699	Extracellular Space	Enzyme
ASS1	4.996	Cytoplasm	enzyme	COL18A1	4.567	Extracellular Space	Other
MTHFD1	4.97	Cytoplasm	enzyme	COL14A1	4.552	Extracellular Space	Other
PARVB	4.89	Cytoplasm	other	LUM	4.46	Extracellular Space	Other
FAT4	4.852	Cytoplasm	other	COL11A1	4.388	Extracellular Space	Other
SRPX	4.843	Cytoplasm	other	INHBA	4.37	Extracellular Space	growth factor
LPL	4.759	Cytoplasm	enzyme	PPEF1	4.175	Extracellular Space	Phosphatase
CLU	4.131	Cytoplasm	other	SERPINE1	3.987	Extracellular Space	Other
MAT1A	4.003	Cytoplasm	enzyme	LAMA3	3.965	Extracellular Space	Other
NAP1L4	3.741	Cytoplasm	other	PCOLCE	3.754	Extracellular Space	Other

ADSL	3.611	Cytoplasm	enzyme	C2	3.618	Extracellular Space	Peptidase
GSTM3	3.605	Cytoplasm	enzyme	A1BG	3.286	Extracellular Space	Other
TUBA4A	3.544	Cytoplasm	other	TFPI	3.253	Extracellular Space	Other
RRBP1	3.434	Cytoplasm	other	HABP2	3.242	Extracellular Space	Peptidase
TTC38	3.378	Cytoplasm	other	ADAMTS1	3.24	Extracellular Space	Peptidase
DNAH10	3.238	Cytoplasm	other	IGFBP5	3.229	Extracellular Space	Other
DNM1	3.126	Cytoplasm	enzyme	HSPG2	3.195	Extracellular Space	Enzyme
ARPC5	3.083	Cytoplasm	other	SERPIND1	3.152	Extracellular Space	Other
NPEPPS	3.052	Cytoplasm	peptidase	FGG	3.08	Extracellular Space	Other
ARF5	3.041	Cytoplasm	enzyme	SERPINF2	2.964	Extracellular Space	Other
AHCY	2.712	Cytoplasm	enzyme	PRG4	2.852	Extracellular Space	Other
FARP2	2.549	Cytoplasm	other	HAPLN1	2.849	Extracellular Space	Other
MAPK10	2.524	Cytoplasm	kinase	PLA1A	2.809	Extracellular Space	Enzyme
ALAD	2.347	Cytoplasm	enzyme	F10	2.805	Extracellular Space	Peptidase
NME3	2.212	Cytoplasm	kinase	IGF1	2.624	Extracellular Space	growth factor
BHMT	2.146	Cytoplasm	enzyme	ANGPT1	2.614	Extracellular Space	growth factor
EXT1	2.124	Cytoplasm	enzyme	WNT5A	2.587	Extracellular Space	Cytokine
C3	1528.586	Extracellular Space	peptidase	ANGPTL2	2.468	Extracellular Space	Other

FBLN1	363.504	Extracellular Space	other	MMP9	2.361	Extracellular Space	Peptidase
C4A/C4B	333.94	Extracellular Space	peptidase	TGFB2	2.213	Extracellular Space	growth factor
F2	237.221	Extracellular Space	peptidase	LTBP3	2.116	Extracellular Space	Other
GC	193.419	Extracellular Space	transporter	AEBP1	13.481	Nucleus	Peptidase
ITIH2	189.859	Extracellular Space	other	RGN	11.886	Nucleus	Enzyme
TNC	176.423	Extracellular Space	other	CCDC80	8.637	Nucleus	Other
F5	170.72	Extracellular Space	other	HIST2H2BF	8.299	Nucleus	Other
COL4A2	150.198	Extracellular Space	other	MTAP	6.024	Nucleus	Enzyme
COMP	124.448	Extracellular Space	other	SPDL1	4.775	Nucleus	Other
APOA1	112.192	Extracellular Space	transporter	MLX	4.021	Nucleus	transcription regulator
AHSG	98.765	Extracellular Space	other	TEF	3.629	Nucleus	transcription regulator
APOE	98.098	Extracellular Space	transporter	PCBP4	3.468	Nucleus	Other
APOH	96.509	Extracellular Space	transporter	FEN1	2.931	Nucleus	Enzyme
PLG	96.018	Extracellular Space	peptidase	DHRS11	11.114	Other	Other
SERPINE2	93.668	Extracellular Space	other	VNN2	6.203	Other	Enzyme
LTBP2	92.603	Extracellular Space	other	TMEM132C	4.368	Other	Other
CLEC3B	86.422	Extracellular Space	other	PRG1	4.086	Other	Other
LTBP1	85.01	Extracellular Space	other	BRD9	3.841	Other	Other

CTGF	81.167	Extracellular Space	growth factor	PPIAP30	3.564	Other	Other
SERPINF1	74.108	Extracellular Space	other	ARPC4-TTLL3	3.351	Other	Other
C8B	73.411	Extracellular Space	other	ABHD16A	3.11	Other	Other
LOXL2	72.561	Extracellular Space	enzyme	ERICH1	2.912	Other	Other
OLFML3	69.115	Extracellular Space	other	CAP1	73.324	Plasma Membrane	Other
TNXB	67.784	Extracellular Space	other	APP	68.092	Plasma Membrane	Other
C7	63.58	Extracellular Space	other	NEO1	53.653	Plasma Membrane	transcription regulator
DCN	63.067	Extracellular Space	other	NRP2	53.549	Plasma Membrane	Kinase
TF	62.64	Extracellular Space	transporter	VNN1	39.608	Plasma Membrane	Enzyme
LTF	61.401	Extracellular Space	peptidase	PTPRD	31.705	Plasma Membrane	Phosphatase
CFH	60.815	Extracellular Space	other	CNTN1	29.984	Plasma Membrane	Enzyme
AFP	60.646	Extracellular Space	transporter	PTPRF	27.525	Plasma Membrane	Phosphatase
C4BPA	54.563	Extracellular Space	other	PTPRS	27.293	Plasma Membrane	Phosphatase
APOB	53.601	Extracellular Space	transporter	ENPP2	18.185	Plasma Membrane	Enzyme
THBS4	52.537	Extracellular Space	other	AGRN	17.583	Plasma Membrane	Other
LTBP4	48.83	Extracellular Space	growth factor	CDH5	16.381	Plasma Membrane	Other
C1QTNF3	45.288	Extracellular Space	other	TNFRSF11B	13.845	Plasma Membrane	transmembrane receptor
CLEC11A	45.26	Extracellular Space	growth factor	TIE1	13.422	Plasma Membrane	Kinase

C1R	42.97	Extracellular Space	peptidase	FAT1	10.827	Plasma Membrane	Other
APOC3	41.277	Extracellular Space	transporter	MRC2	9.79	Plasma Membrane	transmembrane receptor
MMP2	41.17	Extracellular Space	peptidase	SCARA5	8.79	Plasma Membrane	transmembrane receptor
FGB	40.594	Extracellular Space	other	LGALS3BP	8.629	Plasma Membrane	transmembrane receptor
HTRA1	39.647	Extracellular Space	peptidase	APOM	8.595	Plasma Membrane	Transporter
IGFBP3	39.439	Extracellular Space	other	NOTCH3	7.38	Plasma Membrane	transcription regulator
THBS2	38.741	Extracellular Space	other	SCUBE3	7.061	Plasma Membrane	Other
RELN	35.544	Extracellular Space	peptidase	CLSTN1	5.098	Plasma Membrane	Other
CFI	32.724	Extracellular Space	peptidase	GPC1	4.874	Plasma Membrane	transmembrane receptor
ADIPOQ	30.491	Extracellular Space	other	NRP1	4.709	Plasma Membrane	transmembrane receptor
NID2	29.886	Extracellular Space	other	CDH13	3.249	Plasma Membrane	Other
F13A1	29.06	Extracellular Space	enzyme	ITM2B	2.873	Plasma Membrane	Other
POSTN	29.035	Extracellular Space	other	SPTBN1	2.656	Plasma Membrane	Other
ANGPTL3	27.228	Extracellular Space	growth factor	TNN	2.647	Plasma Membrane	Other
PLAT	25.43	Extracellular Space	peptidase	DMBT1	2.577	Plasma Membrane	transmembrane receptor
EFEMP1	25.215	Extracellular Space	enzyme	ITGA2	2.491	Plasma Membrane	transmembrane receptor
HGFAC	23.945	Extracellular Space	peptidase	NFASC	2.067	Plasma Membrane	Other

Table 9: Classification hBM-MSC-EV enriched protein dataset (designated by gene symbol) greater than 2-fold with p-value 0.05, in comparison to hBM-MSC, into protein class and location of cell using IPA. This experiment was done using all 5 hBM-MSC donors with 2

replicates. The bold line separates two columns of gene symbol, fold change, protein location and types.

3.8 Common EV markers

Our proteomic analysis identified 65 of the top 100 EV markers listed in the Exocarta database (http://www.exocarta.org/).

65 EV proteins of the top 100 Exocarta database					
PDCD6IP	EEF1A1	PPIA	CLIC1	PRDX2	HIST2H4A
HSPA8	YWHAZ	MSN	CCT2	GDI2	THBS1
GAPDH	PGK1	CFL1	CDC42	ACTN4	RAN
ACTB	EEF2	PFN1	YWHAG	EHD4	CCT5
ANXA2	HSP90AB1	RAP1B	A2M	RAB7A	CCT3
CD63	YWHAE	ITGB1	TUBA1B	LDHB	AHCY
ENO1	CLTC	HSPA5	RAC1	EZR	UBA1
HSP90AA1	ALB	HIST1H4A	LGALS3BP	ACLY	RAB1A
PKM	VCP	YWHAQ	GNAI2	TFRC	HIST1H4B
LDHA	TPI1	FLNA	MFGE8	RAB14	YWHAH
TKT	TCP1	STOM	RAB8A	MYH9	

Table 10: 65 EV proteins of the top 100 Exocarta database identified

3.9 IPA of dataset

3.9.1 hBM-MSC-EV 2-fold enriched dataset categorized into cellular compartment and protein class

The 270 enriched proteins were used to carry out all IPA. IPA is a bioinformatics tool that can identify pathways, molecular mechanisms and biological processes most relevant to the data uploaded or list of genes, proteins etc. IPA was used to characterize the 2-fold enriched proteins into subcellular component and protein class. Extracellular space proteins (51.48 %) and cytoplasmic proteins (30 %) consisted of most number of cellular compartment proteins (Figure 9A). The enzymes (peptidase, phosphatase, enzyme, kinase) (35.18 %) dominated the protein class (Figure 9B).

A) Cellular Compartment

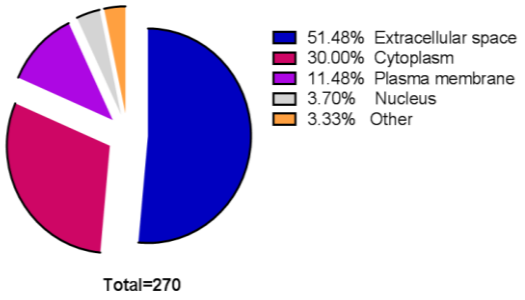

B) Protein Class

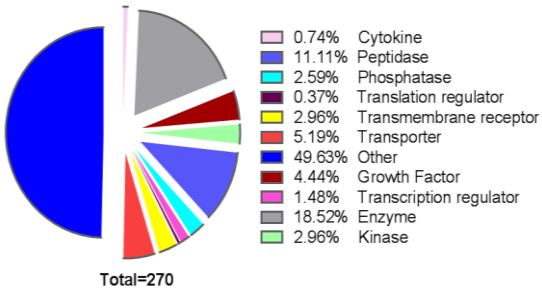

Figure 9: 2-fold Enriched hBM-MSC-EV proteins A) categorized into subcellular compartments B) categorized into protein class using IPA bioprofiler.

3.9.2 Significantly up regulated cellular and molecular functions

IPA generated 16 significantly up regulated cellular and molecular function pathways calculated using a right-tailed fisher's exact test (Figure 10). Each of the pathways consists of several functional annotations in which specific functions are activated or deactivated

based on a cut off of activation Z-score $\geq$ 2 and inactivation Z-score $\leq$ - 2. Tables 11 and 12 show the functions associated with cellular movement and cell-to-cell signalling and interaction. These 2 pathways were chosen instead of top 2 as protein synthesis (2nd most significantly upregulated pathway) pathway only consisted of one function (protein synthesis) with Z-score $\geq$ 2 and cellular compromise (3rd most significantly upregulated pathway) consisted of no functional annotation with significant Z-score.

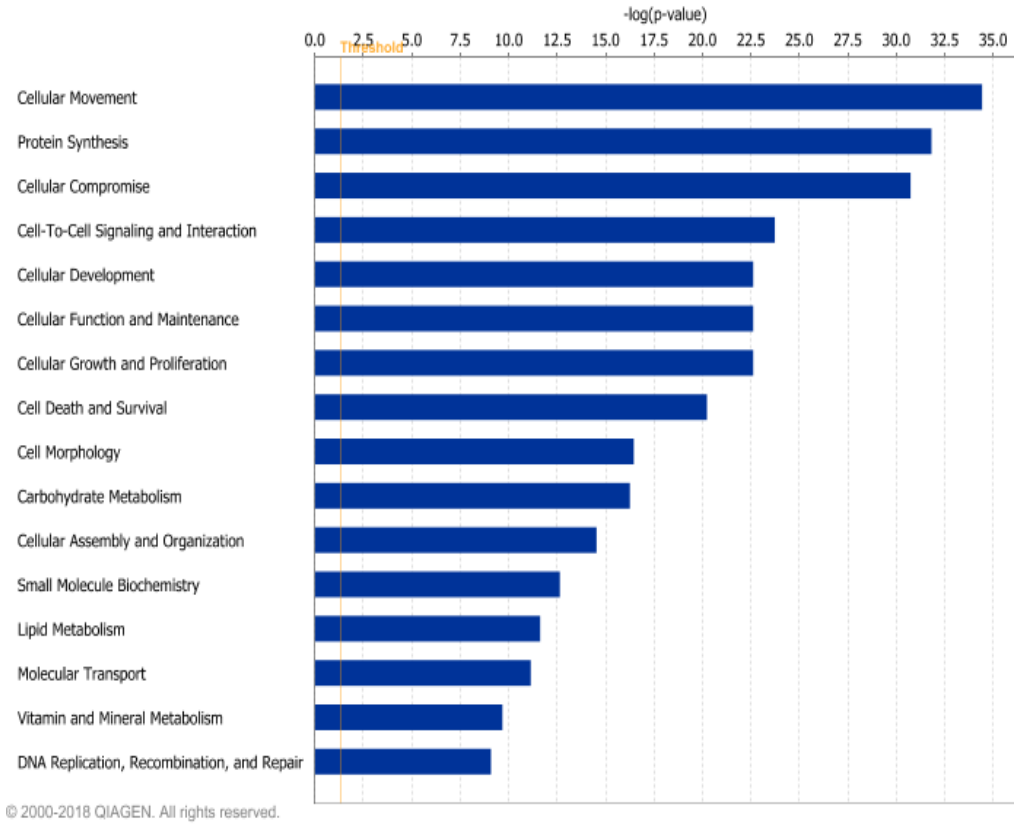

Figure 10: Significantly up regulated cellular and molecular functions of the 2-fold enriched hBM-MSC-EV dataset. 1) Cellular movement 2) Protein synthesis 3) Cellular compromise 4) Cell-to-cell signalling and interaction 5) Cellular development 6) Cellular function and maintenance 7) Cellular growth and proliferation 8) Cell death and survival 9) Cell morphology 10) Carbohydrate metabolism 11) Cellular assembly and organization 12) Small molecule biochemistry 13) Lipid metabolism 14) Molecular transport 15) Vitamin and mineral metabolism 16) DNA replication, recombination and repair. Y-axis shows the

significantly upregulated pathway and the X-axis shows the -log (p value) with a threshold set at 0.05 (p-value). Significantly up regulated pathways calculated using a right-tailed fisher's exact test

3.9.2.1 Functional annotations of cellular movement

30 functional annotations were involved in the cellular movement pathway. Only 11 are shown in the table below as these functions did not overlap with functions in other pathways and were specific to cellular movement. One of the functional annotation under the most significantly upregulated pathway cellular movement (Figure 10) is called cell movement (activation Z-score = 4.74) (Table 11 and Figure 11). The increase in function is based on a cut off of activation Z-score $\geq$ 2.

Functions Annotation	p-Value	Predicted Activation State	Activation z-score	Molecules
Homing of cells	1.58E-13	Increased	4.79	AFP, ANGPT1, ANGPTL2, APOA1, APOE, APP, C3, C4A/C4B, CDH13, CLU, CORO1A, CTGF, DAPK2, DNM1, ENPP2, F10, F2, FBN1, FN1, IGF1, IGFBP3, INHBA, ITGA2, LGALS1, MMP2, MMP9, MST1, NRP1, NRP2, PLAT, PLG, SERPINE1, SERPINF1, TGFB1, TGFB2, THBS1, THBS2, THBS4, VEGFC, VTN, WNT5A
Chemotaxis	5.15E-13	Increased	4.756	AFP, ANGPT1, ANGPTL2, APOA1, APOE, APP, C3, C4A/C4B, CDH13, CLU, CORO1A, CTGF, DAPK2, ENPP2, F10, F2, FBN1, FN1, IGF1, INHBA, ITGA2, LGALS1, MMP2, MMP9, MST1, NRP1, NRP2, PLAT, PLG, SERPINE1, SERPINF1, TGFB1, TGFB2, THBS1, THBS2, THBS4, VEGFC, VTN, WNT5A
Cell movement	3.7E-35	Increased	4.74	ACTA2, ACTB, ADAMTS1, ADAMTS13, ADIPOQ, AFP, AHCY, AHSG, ANGPT1, ANGPTL2, ANGPTL3, APOA1, APOB, APOE, APOH, APP, BGN, C2, C3, C4A/C4B, C6, CALD1, CALU, CAP1, CDH13, CDH5, CFH, CLEC11A, CLU, CNTN1, COL11A1, COL18A1, COL2A1, COL4A2, COMP, CORO1A, CORO1C, CTGF, DAPK2, DCN, DCTN2, DMBT1, DNM1, ECM1, EFEMP1, ENPP2, F10, F13A1, F2, FAT1, FBLN5, FBN1, FERMT3, FGA, FGB, FHL1, FMOD, FN1, FST, GC, GPC1, HABP2, HSPG2, HTRA1, IGF1, IGFBP2, IGFBP3, IGFBP4, IGFBP5, INHBA, ITGA2, ITGBL1, KLKB1, LAMA2, LAMA3, LCAT, LGALS1, LGALS3BP, LOXL2, LTBP2, LTF, LUM, MAPK10, MAPRE2, MAT1A, MMP2, MMP9, MRC2, MST1,

				MTAP, MYOC, NEO1, NOTCH3, NRP1, NRP2, PACSIN2, PARVB, PKM, PLAT, PLG, PLTP, POSTN, PTPRF, RELN, RRBP1, S100A1, SERPINC1, SERPIND1, SERPINE1, SERPINE2, SERPINF1, SORD, TFPI, TGFB1, TGFB2, TGFBI, THBS1, THBS2, THBS4, TIE1, TIMP1, TIMP2, TKT, TNC, TNFRSF11B, TNN, TPM1, TPM3, VCAN, VEGFC, VNN2, VTN, VWF, WNT5A
Migration of cells	2.41E-31	Increased	4.352	ACTA2, ACTB, ADAMTS1, ADAMTS13, ADIPOQ, AHCY, AHSG, ANGPT1, ANGPTL2, ANGPTL3, APOA1, APOB, APOE, APOH, APP, BGN, C2, C3, C4A/C4B, C6, CALD1, CALU, CAP1, CDH13, CDH5, CFH, CLEC11A, CLU, CNTN1, COL11A1, COL18A1, COL4A2, COMP, CORO1A, CORO1C, CTGF, DAPK2, DCN, DCTN2, DMBT1, ECM1, EFEMP1, ENPP2, F10, F13A1, F2, FAT1, FBLN5, FERMT3, FGA, FGB, FHL1, FMOD, FN1, GC, GPC1, HABP2, HTRA1, IGF1, IGFBP2, IGFBP3, IGFBP4, IGFBP5, INHBA, ITGA2, ITGBL1, LAMA2, LAMA3, LCAT, LGALS1, LGALS3BP, LOXL2, LTBP2, LTF, LUM, MAPK10, MAT1A, MMP2, MMP9, MRC2, MST1, MTAP, MYOC, NEO1, NOTCH3, NRP1, NRP2, PACSIN2, PKM, PLAT, PLG, PLTP, POSTN, PTPRF, RELN, SERPINC1, SERPIND1, SERPINE1, SERPINE2, SERPINF1, TFPI, TGFB1, TGFB2, TGFBI, THBS1, THBS2, THBS4, TIE1, TIMP1, TIMP2, TNC, TNFRSF11B, TNN, TPM1, TPM3, VCAN, VEGFC, VNN2, VTN, VWF, WNT5A
Cell movement of myeloid cells	2.09E-19	Increased	3.035	ADAMTS13, ADIPOQ, ANGPT1, ANGPTL2, APOA1, APOE, APP, C2, C3, C4A/C4B, C6, CFH, CLEC11A, CORO1A, CTGF, DAPK2, DCTN2, DMBT1, F10, F2, FERMT3, FN1, IGFBP3, INHBA, LCAT, LGALS1, LTF, LUM, MMP9, MST1, NEO1, PLAT, PLG, PLTP, SERPINC1, SERPINE1, SERPINF1, TGFB1, TGFB2, THBS1, THBS2, THBS4, TIMP1, TIMP2, VCAN, VEGFC, VTN, VWF, WNT5A
Cell movement of dermal cells	1.14E-11	Increased	2.762	ADIPOQ, AHSG, ANGPT1, CTGF, FBN1, IGF1, ITGA2, LAMA3, LTF, MAPRE2, MMP9, POSTN, SERPINE1, TGFB1, THBS2, TIMP1

Invasion of cells	5.59E-22	Increased	2.456	ACTA2, ADAMTS1, ADIPOQ, AHCY, AHSG, APP, CAP1, CDH13, CDH5, CFH, CLU, COL11A1, COL18A1, COL2A1, CTGF, DCN, ECM1, EFEMP1, ENPP2, F2, FAT1, FBLN1, FBLN5, FERMT3, FMOD, FN1, FST, GPC1, HTRA1, IGF1, IGFBP2, INHBA, ITGA2, LAMA3, LGALS1, LOXL2, LTF, MMP2, MMP9, MST1, NEO1, NOTCH3, NRP1, NRP2, PARVB, PKM, PLAT, PLG, POSTN, PTGES3, RELN, RGN, SCUBE3, SERPINE1, SERPINE2, SERPINF1, SERPINF2, TFPI, TGFB1, TGFB2, TGFBI, THBS1, THBS2, TIMP1, TIMP2, TNC, VCAN, VEGFC, VTN, WNT5A
Migration of dermal cells	4.86E-11	Increased	2.408	ADIPOQ, AHSG, ANGPT1, CTGF, IGF1, ITGA2, LAMA3, LTF, MMP9, POSTN, SERPINE1, TGFB1, THBS2, TIMP1
Cell movement of epithelial cells	1.28E-15	Increased	2.4	ADIPOQ, AHSG, ANGPT1, CTGF, FBLN5, FBN1, IGF1, ITGA2, LAMA3, LTF, MAPRE2, MMP2, MMP9, MST1, PLG, POSTN, PTPRF, SERPINE1, SERPINF1, TGFB1, THBS2, TIMP1, VTN
Cell movement of connective tissue cells	8.2E-11	Increased	2.199	ACTB, ADIPOQ, ANGPT1, APOE, CTGF, ENPP2, FBN1, FN1, IGF1, LGALS1, LTF, MRC2, PACSIN2, POSTN, SERPINF1, TGFB1, THBS1, THBS2, TIMP2, TNN, VTN, WNT5A
Migration of epithelial cells	3.73E-16	Increased	2.022	ADIPOQ, AHSG, ANGPT1, CTGF, FBLN5, IGF1, ITGA2, LAMA3, LTF, MMP2, MMP9, MST1, PLG, POSTN, PTPRF, SERPINE1, SERPINF1, TGFB1, THBS2, TIMP1, VTN

Table 11: Functional annotations of cellular movement show increases homing of cells, chemotaxis, migration of cells, invasion of cells, cell movement of myeloid cells, dermal cells, epithelial cells and connective tissue cells. Activation Z-score $\geq$ 2 and inactivation Z-score $\leq$ - 2.

3.9.2.2 IPA predicted proteins involved in cell movement leads to an overall activation

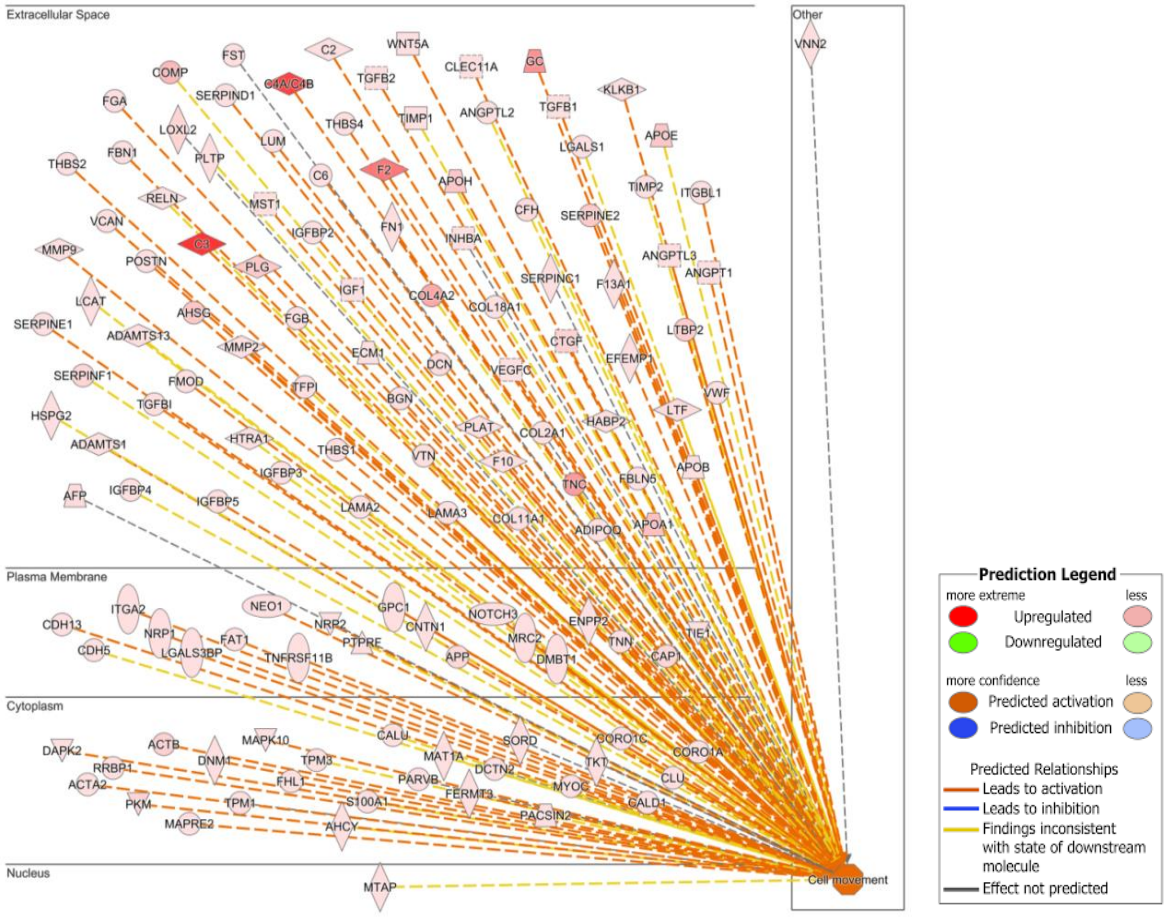

Figure 11: Subcellular network of proteins involved in cell movement

3.9.2.3 Functional annotations of cell-to-cell signalling and interaction

4 functional annotations (Table 12) based on a cut off of activation Z-score ≥ 2 and inactivation Z-score ≤ -2 were involved in the cell-to-cell signalling and interaction pathway (Figure 10). Only 4 are shown in the table below as these functions did not overlap with functions in other pathways and were specific to cellular movement.

Functions Annotation	p-Value	Predicted Activation State	Activation z-score	Molecules
Attachment of cells	2.31E-17	Increased	2.698	ADIPOQ, ANGPT1, CDH13, COMP, CTGF, DCN, FBLN5, FBN1, FN1, HSPG2, ITGA2, MMP2, PKM, PLG, POSTN, TFPI, TGFB1, TGFBI, THBS2, TIMP2, VCAN, VTN, VWF
Activation of cells	7.43E-16	Increased	4.099	ADAMTS13, ADIPOQ, AFP, AGRN, ANGPT1, APOA1, APOB, APOE, APOH, APP, C3, C4A/C4B, C6, CFH, CLEC11A, CORO1A, CTGF, F10, F13A1, F2, F5, FGA, FGG, FMOD, FN1, GC, HSPG2, IGF1, INHBA, KLKB1, LGALS1, LGALS3BP, LOXL2, LTBP1, LTF, MMP2, MMP9, MST1, PKM, PLAT, PLG, PLTP, SERPIND1, SERPINE1, SERPINE2, SERPINF1, SERPINF2, TF, TGFB1, TGFB2, THBS1, THBS4, TIMP1, TNC, TNFRSF11B, VCAN, VNN1, VTN, VWF, WNT5A
Cell-cell contact	2.19E-11	Increased	2.416	AGRN, ANGPT1, APOE, APP, C3, CAPZB, CDH13, CDH5, CLSTN1, CLU, CNTN1, CORO1A, DNM1, F2, FAT1, FAT4, FERMT3, FN1, FST, HSPG2, IGF1, INHBA, LAMA2, LAMA3, LGALS1, MMP2, NEO1, NFASC, PTPRF, RELN, SERPINF1, TGFB1, THBS1, THBS2, TIMP1, TNC, TNFRSF11B, TNXB, VNN1, WNT5A
Recruitment of cells	5.54E-11	Increased	2.192	ADAMTS13, ADIPOQ, ANGPT1, APOA1, APOB, APOE, APP, C3, C4A/C4B, CDH5, CLU, F13A1, FERMT3, FN1, GC, KLKB1, LGALS1, LTF, MMP2, MMP9, PLG, SERPINE1, TFPI, TGFB1, THBS1, THBS2, TNC, VWF

Table 12: Functions annotation of cell-to-cell signalling and interaction shows an increase in

attachment of cells, activation of cells, cell-cell contact and recruitment of cells. activation Z-score ≥ 2 and inactivation Z-score ≤ - 2

3.9.3 Functional annotation of plasma membrane proteins

EV membrane protein are important aspect of EV activity or binding. Out of 75 plasma membrane proteins identified 31 proteins (Table 10) were identified in the 2-fold enriched hBM-MSC-EV dataset, which were associated with processes that matched the activation z-score cut off of ≤ -2 to ≥ 2. These processes are predicted to be associated with an increase in migration of cells, invasion of cells, movement and migration of leukocyte, chemotaxis, vasculogenesis and decrease in organismal death. NRP2, ITGA2, APP, ENPP2 are common proteins involved all the functions (Figure 12) mentioned except organismal death (Figure 13)

Functions Annotation	p-Value	Predicted Activation State	Activation z-score	Molecules
Migration of cells	7.96E-10	Increased	2.646	**APP**, CAP1, CDH13, CDH5, CNTN1, DMBT1, **ENPP2**, FAT1, GPC1, **ITGA2**, LGALS3BP, MRC2, NEO1, NOTCH3, NRP1, **NRP2**, PTPRF, TIE1, TNFRSF11B, TNN
Cell movement of leukocytes	0.000257	Increased	2.557	**APP**, DMBT1, **ENPP2**, **ITGA2**, NEO1, NOTCH3, **NRP2**, TNFRSF11B
Invasion of cells	7.6E-08	Increased	2.555	**APP**, CAP1, CDH13, CDH5, **ENPP2**, FAT1, GPC1, **ITGA2**, NEO1, NOTCH3, NRP1, **NRP2**, SCUBE3
Chemotaxis	0.000951	Increased	2.408	**APP**, CDH13, **ENPP2**, **ITGA2**, NRP1, **NRP2**
Vasculogenesis	5.19E-07	Increased	2.032	**APP**, CDH13, CDH5, **ENPP2**, GPC1, **ITGA2**, NOTCH3, NRP1, **NRP2**, TIE1, TNN
Leukocyte migration	3.01E-05	Increased	2.023	**APP**, CDH5, DMBT1, **ENPP2**, GPC1, **ITGA2**, NEO1, NOTCH3, **NRP2**, TNFRSF11B
Organismal death	0.0000285	Decreased	-3.369	AGRN, APP, CAP1, CDH5, CNTN1, DMBT1, ENPP2, FAT1, NFASC, NRP1, NRP2, PTPRF, PTPRS, SPTBN1, TIE1, TNFRSF11B

Table 13: Functions annotation of plasma membrane proteins show an increase in migration of cells, cell movement of leukocytes, invasion of cells, chemotaxis, vasculogenesis, leukocyte migration and decrease in organismal death. Activation Z-score $\geq$ 2 and inactivation Z-score $\leq$ - 2.

3.9.3.1 Hierarchical network of plasma membrane proteins and its predicted upregulated functions

NRP2, ITGA2, APP, ENPP2 are common proteins involved migration of cells, cell movement of leukocytes, invasion of cells, chemotaxis, vasculogenesis, leukocyte migration (Figure 12).

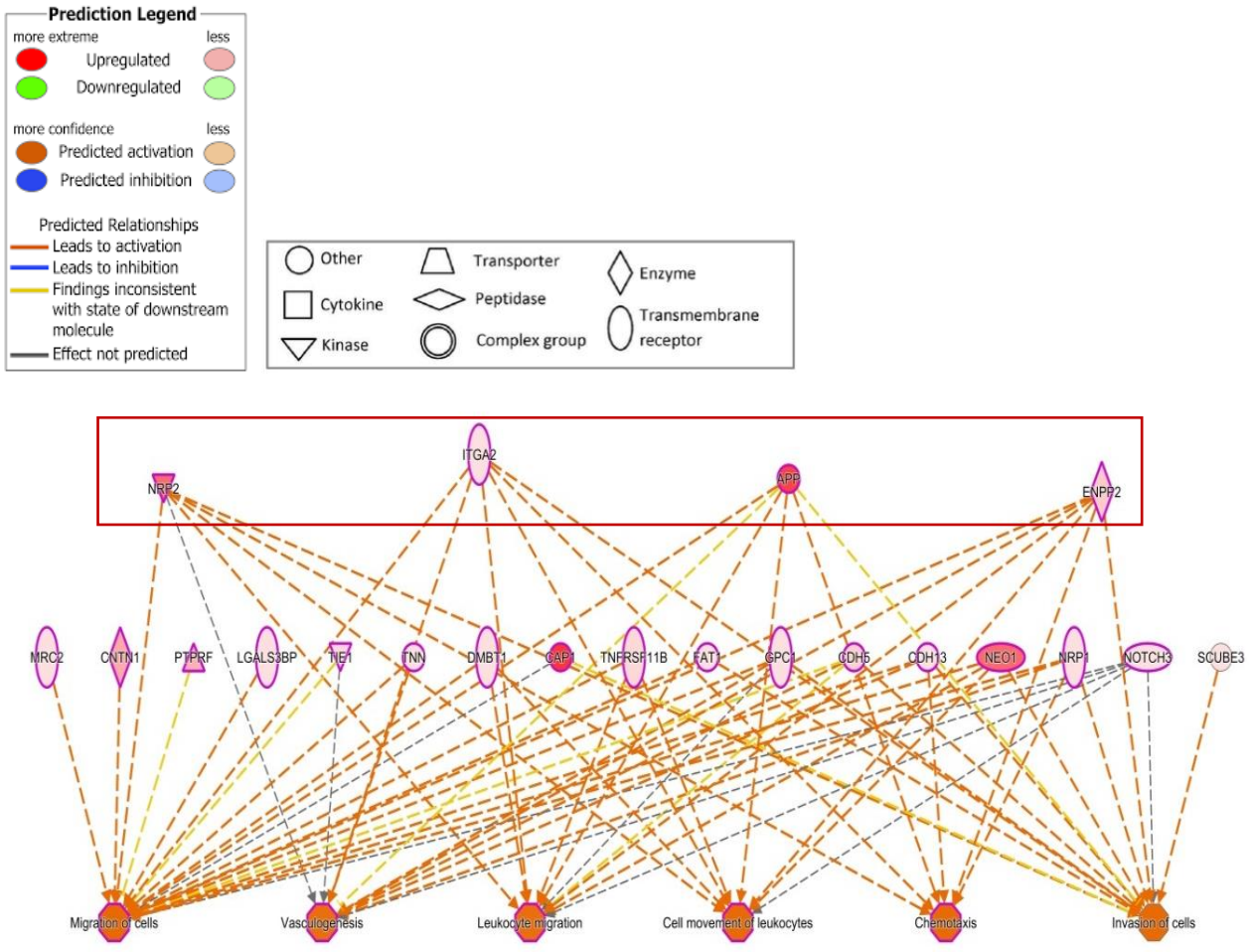

Figure 12: Hierarchical network of plasma membrane proteins and its associated activated functions activation z-score $\geq$ 2, such as migration of cells, cell movement of leukocytes, invasion of cells, chemotaxis, vasculogenesis, leukocyte migration.

3.9.3.2 Plasma membrane proteins leads to a predicted downregulation in organismal death

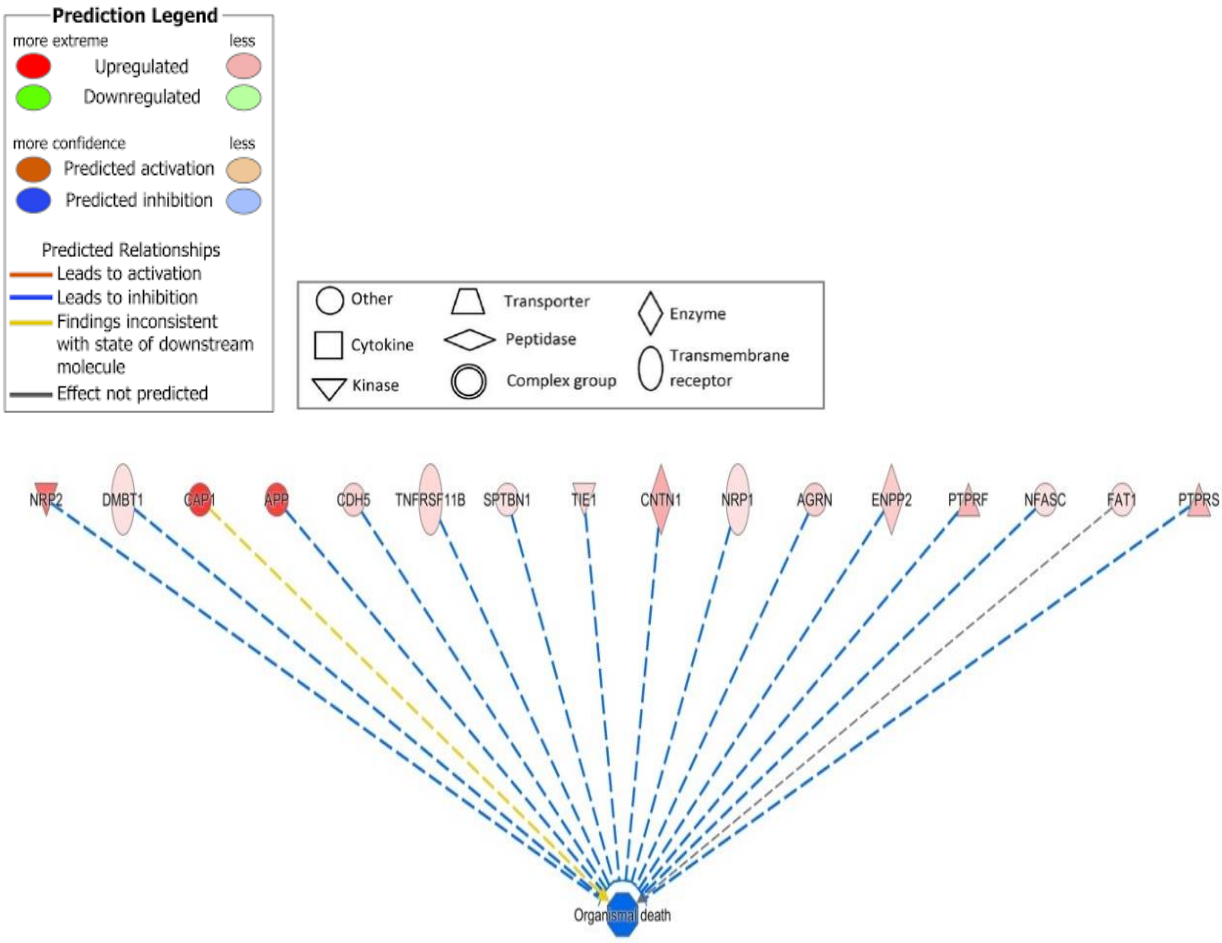

Figure 13: Hierarchical network of plasma membrane proteins predicted to down regulate organismal death activation z-score cut off of < 2. 16 out 30, 2-fold hBM-MSC-EV enriched plasma membrane proteins are involved in decrease in organismal death or pro-survival.

3.9.4 Significantly up regulated physiological development and function

IPA generated 21 significantly up regulated physiological development and function pathways calculated using a right-tailed fisher's exact test (Figure 14). Each of the pathways consists of several functional annotations in which specific functions are activated or

deactivated based on a cut off of activation Z-score ≥ 2 and inactivation Z-score ≤ -2. Tables 14 and 15 shows the functions associated with top 2 most significantly upregulated pathways.

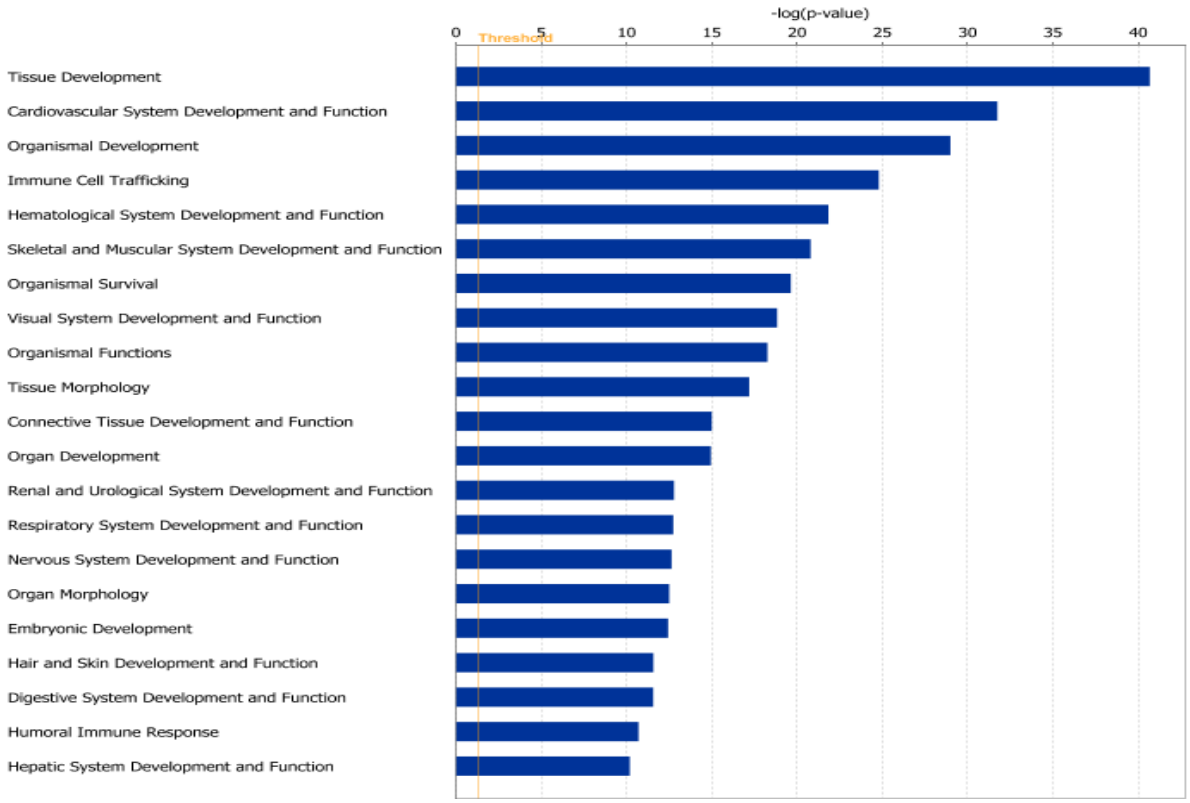

Figure 14: Significantly up regulated physiological development and functions of the 2-fold enriched hBM-MSC-EV dataset. 1) Tissue development 2) Cardiovascular system development and function 3) Organismal development 4) Immune cell trafficking 5) Hematological system development and function 6) Skeletal and muscular system development and function 7) Organismal survival 8) Visual system development and function 9) Organismal functions 10) Tissue morphology 11) Connective tissue development and function 12) Organ development 13) Renal and urological system development and function 14) Respiratory system development and function 15) Nervous system development and function 16) Organ morphology 17) Embryonic development 18) Hair and skin development and function 19) Digestive system development and function 20) Humoral immune response 21) Hepatic system development and function. Y-axis shows the significantly upregulated pathway and the X-axis shows the -log (p value) with a threshold set at 0.05 (p-value). Significantly up regulated pathways calculated using a right-tailed fisher's exact test.

3.9.4.1 Functional annotation of tissue development pathway

11 functions (Table 14) based on a cut off of activation Z-score $\geq$ 2 and inactivation Z-score $\leq$ -2 were involved in the tissue development pathway (Figure 14).

Functions Annotation	p-Value	Predicted Activation State	Activation z-score	Molecules
Proliferation of muscle cells	1.01E-14	Increased	2.023	ADIPOQ, APOE, CDH13, CLU,F2, FBLN5, FHL1, FN1, FST, HABP2, IGF1, IGFBP2, IGFBP3, IGFBP4, IGFBP5, INHBA, ITGA2, MLX, MMP9, NOTCH3, OGN, PLAT, PLG, POSTN, PTPRF, SERPINE1, SERPINF2, TFPI, TGFB1, THBS1, TIMP1, TNC, VCAN, VTN
Adhesion of extracellular matrix	2.91E-14	Decreased	-2.2	ANGPTL3, CTGF, ENPP2, FBLN5, FGA, FGB, FGG, FN1, ITGA2, MYOC, NID1, NID2, POSTN, THBS1, TNN, TNXB, VCAN, VTN
Proliferation of neuronal cells	2.27E-13	Increased	3.304	ACTB, AGRN, ANGPT1, APOE, APP, CAP1, CAPZB, CLU, ENPP2, EXT1, F2, FARP2, FBLN5, FN1, HBA1/HBA2, IGF1, LAMA2, LAMA3, LGALS1, MMP2, MMP9, NRP1, PLAT, PLG, PTPRF, PTPRS, RELN, SERPINE1, SERPINE2, SERPINF2, SPTBN1, TGFB1, THBS1, TMOD2, TNC, TNN, VCAN, VEGFC, VTN, WNT5A
Formation of filaments	5.21E-12	Increased	2.06	ADIPOQ, APOA1, APOE, APP, CALD1, CAPZB, CDH13, COL18A1, CORO1A, CTGF, EML2, F2, FBN1, FHL1, FN1, IGF1, ITM2B, MMP2, MYOC, PLAT, POSTN, RELN, SERPINF1, SERPINF2, TGFB1, TGFBI, TNC, TNN, TPM1, TPM3, TUBA4A, VTN
Growth of neurites	1.67E-11	Increased	3.628	ACTB, ANGPT1, APOE, APP, CAP1, CAPZB, ENPP2, EXT1, F2, FARP2, FN1, HBA1/HBA2, IGF1, LAMA2, LAMA3, LGALS1, MMP2, MMP9, NRP1, PLAT, PLG, PTPRF, PTPRS, RELN, SERPINE1, SERPINE2, SERPINF2, SPTBN1, THBS1, TMOD2, TNC, TNN, VCAN, WNT5A

Differentiation of cardiovascular tissue	7.41E-11	Increased	2.287	ADIPOQ, ANGPT1, CDH5, COL18A1, DCN, F2, FN1, IGF1, IGFBP3, NRP1, PKM, TGFB1, VEGFC, VNN1
Formation of eye	1.65E-10	Increased	2.14	ALDH1A1, ANGPTL3, APOB, APOE, CDH5, CFH, COL18A1, COL2A1, EFEMP1, FMOD, FST, HSPG2, IGF1, LTBP2, LUM, MMP2, NID1, NOTCH3, OGN, PLG, PLTP, PTPRF, PTPRS, SERPINE1, SERPINF1, TGFB2, THBS1, THBS2, TIMP2, TKT, VEGFC
Outgrowth of neurons	2.85E-10	Increased	3.414	ANGPT1, APOE, APP, CLU, ENPP2, EXT1, F2, FN1, HBA1/HBA2, IGF1, LAMA2, LAMA3, LGALS1, MMP9, NRP1, PLAT, PLG, PTPRF, PTPRS, RELN, SERPINE1, SERPINE2, SERPINF2, SPTBN1, THBS1, TNC, TNN, VCAN, WNT5A
Differentiation of endothelial cells	8.09E-10	Increased	2.115	ADIPOQ, ANGPT1, CDH5, COL18A1, DCN, F2, FN1, IGF1, IGFBP3, NRP1, PKM, TGFB1, VEGFC
Outgrowth of neurites	1.05E-09	Increased	3.414	ANGPT1, APOE, APP, ENPP2, EXT1, F2, FN1, HBA1/HBA2, IGF1, LAMA2, LAMA3, LGALS1, MMP9, NRP1, PLAT, PLG, PTPRF, PTPRS, RELN, SERPINE1, SERPINE2, SERPINF2, SPTBN1, THBS1, TNC, TNN, VCAN, WNT5A
Differentiation of bone cells	6.06E-09	Increased	2.3	ADIPOQ, APOE, BGN, C3, FARP2, FBN1, FBN2, FN1, HTRA1, IGF1, IGFBP5, INHBA, LTF, MMP9, MYOC, NRP1, POSTN, PPP1CA, SERPINF1, TF, TGFB1, TGFB2, TNC, TNFRSF11B, TNN, WNT5A

Table 14: The functional annotations under tissue development predicted increase in proliferation of muscle cells and neuronal cells, growth of neurites, outgrowth of neurons and neurites, formation of filaments, differentiation of endothelial, bone cells as well as cardiovascular tissue, formation of eye and decrease in adhesion of extracellular matrix.

3.9.4.2 Subcellular network of proteins involved in neuronal development from tissue development pathway

Out of 11 functions in tissue development pathway (Table 14) 4 functions were associated with neuronal development.

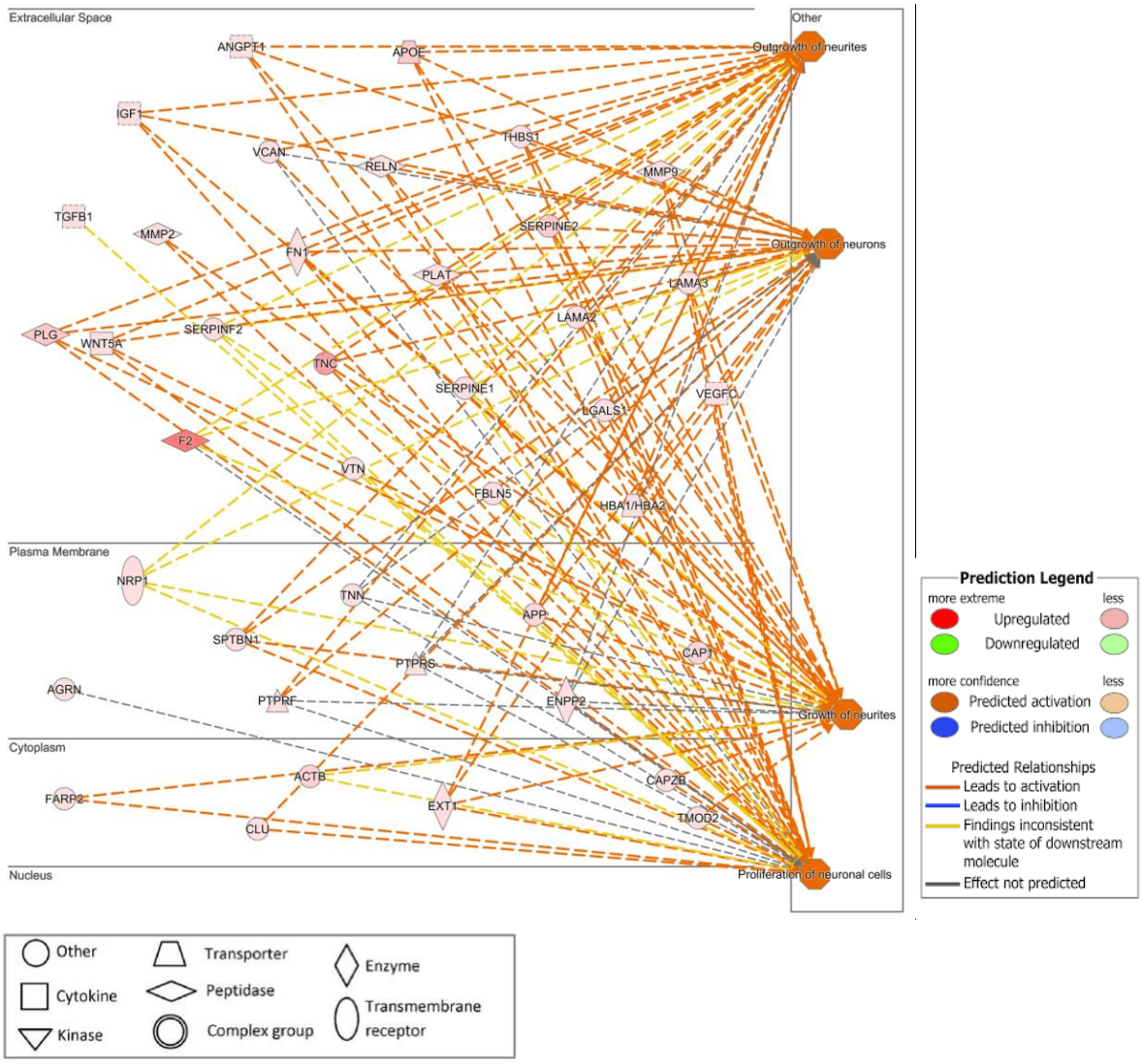

Figure 15: Subcellular network of proteins involved in neuronal development shows predicted increase in growth of neurites, outgrowth of neurites and neurons as well as proliferation of neurons.

3.9.4.3 Functional annotation of cardiovascular system development and function

4 functions (Table 14) based on a cut off of activation Z-score $\geq$ 2 and inactivation Z-score $\leq$ -2 were involved in the cardiovascular system development and function pathway (Table 15 Figure 15).

Functions Annotation	p-Value	Predicted Activation State	Activation z-score	Molecules
Vasculogenesis	1.03E-29	Increased	2.024	ADAMTS1, ADIPOQ, ANGPT1, ANGPTL2, ANGPTL3, APOA1, APOB, APOE, APOH, APP, C3, C6, CDH13, CDH5, COL18A1, COL4A2, COMP, CTGF, DCN, ECM1, EFEMP2, ENPP2, F2, FBLN1, FBLN5, FERMT3, FN1, GPC1, HABP2, HSPG2, HTRA1, IGF1, IGFBP3, IGFBP4, INHBA, ITGA2, LAMA2, LGALS1, LOXL2, LTBP1, MMP2, MMP9, NOTCH3, NRP1, NRP2, PKM, PLAT, PLG, SERPINC1, SERPIND1, SERPINE1, SERPINF1, SERPINF2, TF, TFPI, TGFB1, TGFB2, TGFBI, THBS1, THBS2, THBS4, TIE1, TIMP1, TIMP2, TKT, TNC, TNN, TUBA4A, VEGFC, VTN, VWF, WNT5A
Movement of vascular endothelial cells	5.78E-16	Increased	2.374	ADAMTS1, ADIPOQ, ANGPT1, APOH, CDH13, CDH5, COL18A1, ENPP2, FN1, HSPG2, ITGA2, LGALS1, MMP2, MMP9, NRP1, PKM, PLG, TGFB1, TGFBI, THBS1, THBS2, TIMP1, TIMP2,TNN, VEGFC, VWF
Differentiation of cardiovascular tissue	7.41E-11	Increased	2.287	ADIPOQ, ANGPT1, CDH5, COL18A1, DCN, F2, FN1, IGF1, IGFBP3, NRP1, PKM, TGFB1, VEGFC, VNN1
Differentiation of endothelial cells	8.09E-10	Increased	2.115	ADIPOQ, ANGPT1, CDH5, COL18A1, DCN, F2, FN1, IGF1, IGFBP3, NRP1, PKM, TGFB1, VEGFC

Table 15: Functional annotation of proteins involved in cardiovascular system development and function show an increase in vasculogenesis, movement of vascular endothelial cells, differentiation of cardiovascular tissue, differentiation of endothelial cells.

3.9.4.4 Subcellular network of proteins involved in vasculogenesis from cardiovascular system development and function pathway

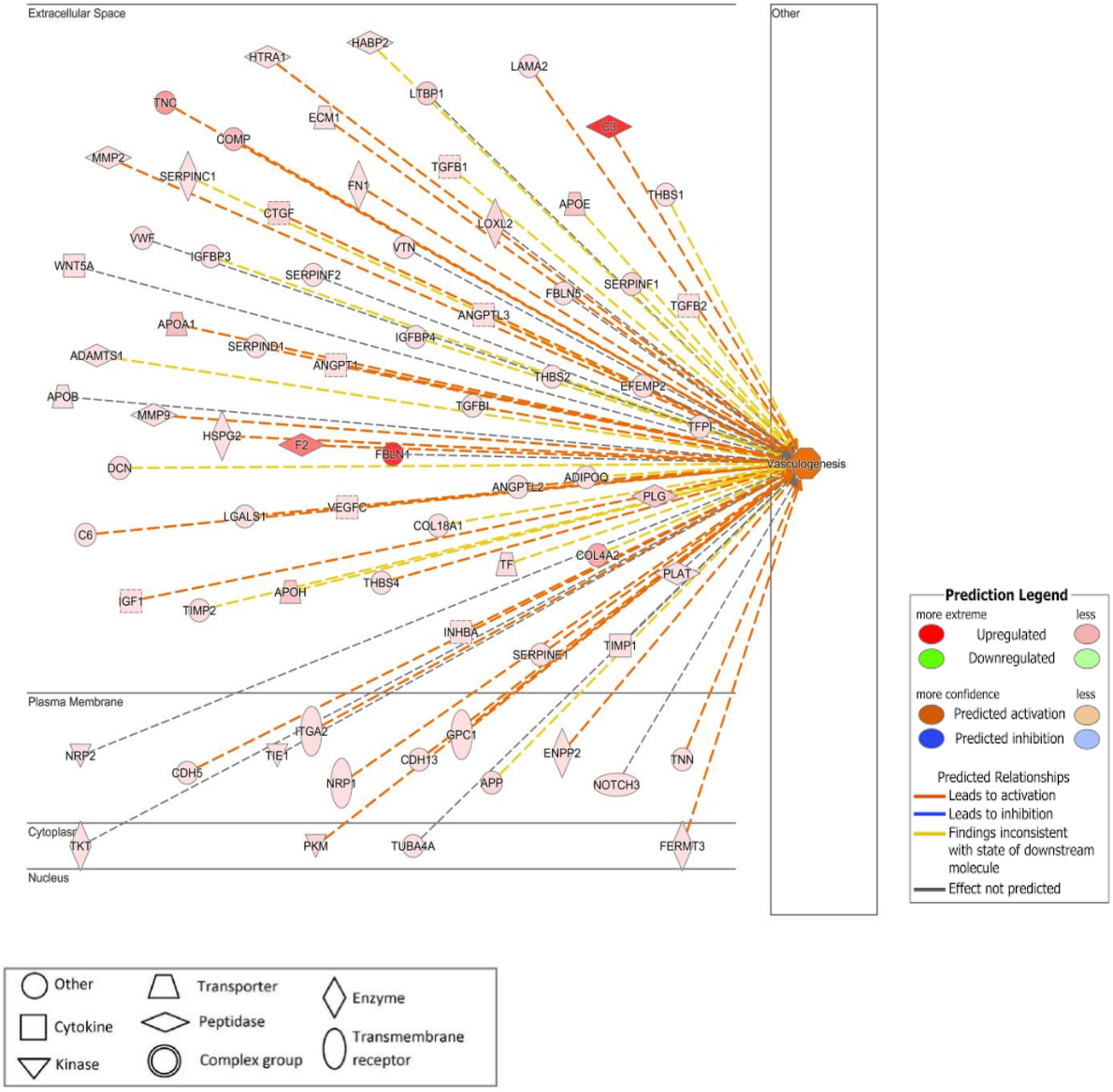

Figure 16: Subcellular network of proteins involved vasculogenesis

3.10 Mass spectrometry detection of MMP-2 (73kDa) and NRP1 (103kDa) in MSC-EV and MSC

	Gene symbol	Sum PEP Score	Coverage %	#Peptides	#PSMs	#Unique Peptides	#AAs	MW [kDa]	Score Sequest HT:
Cells	MMP2	16.772	12	6	7	6	660	73.8	17.9
	NRP1	12.319	4	3	7	4	660	73.8	8.45
EVs	MMP2	122.345	57	28	62	28	923	103	216.2
	NRP1	47.026	18	11	19	11	923	103	68.38

AA: amino acid, PEP: peptide spectrum matches, PEP: posterior error probability

Table 16: Mass spectrometry detection of MMP-2 (73kDa) and NRP1 (103kDa) in hBM-MSC-EV and hBM-MSC.

3.10.1 Validation of proteins identified with mass spectrometry by western blot

MMP-2 and neuropilin 1 (NRP1) were all enriched in hBM-MSC-EVs, these proteins were selected for validation and their expression was measured western blot. The enrichment of MMP-2 (69kDa) (Figure 17A) and NRP1 (89kDa) (Figure 18A) protein in hBM-MSC-EV and absence in hBM-MSC lysates corroborated our mass spectrometry results (Table 16). As EVs do not have a consistent house keeping protein, it would be inaccurate to use the house keeping protein as a baseline reference, therefore to circumvent this a total protein stain was used. This also confirms that the samples were loaded properly in the gel (Figure 18&19B).

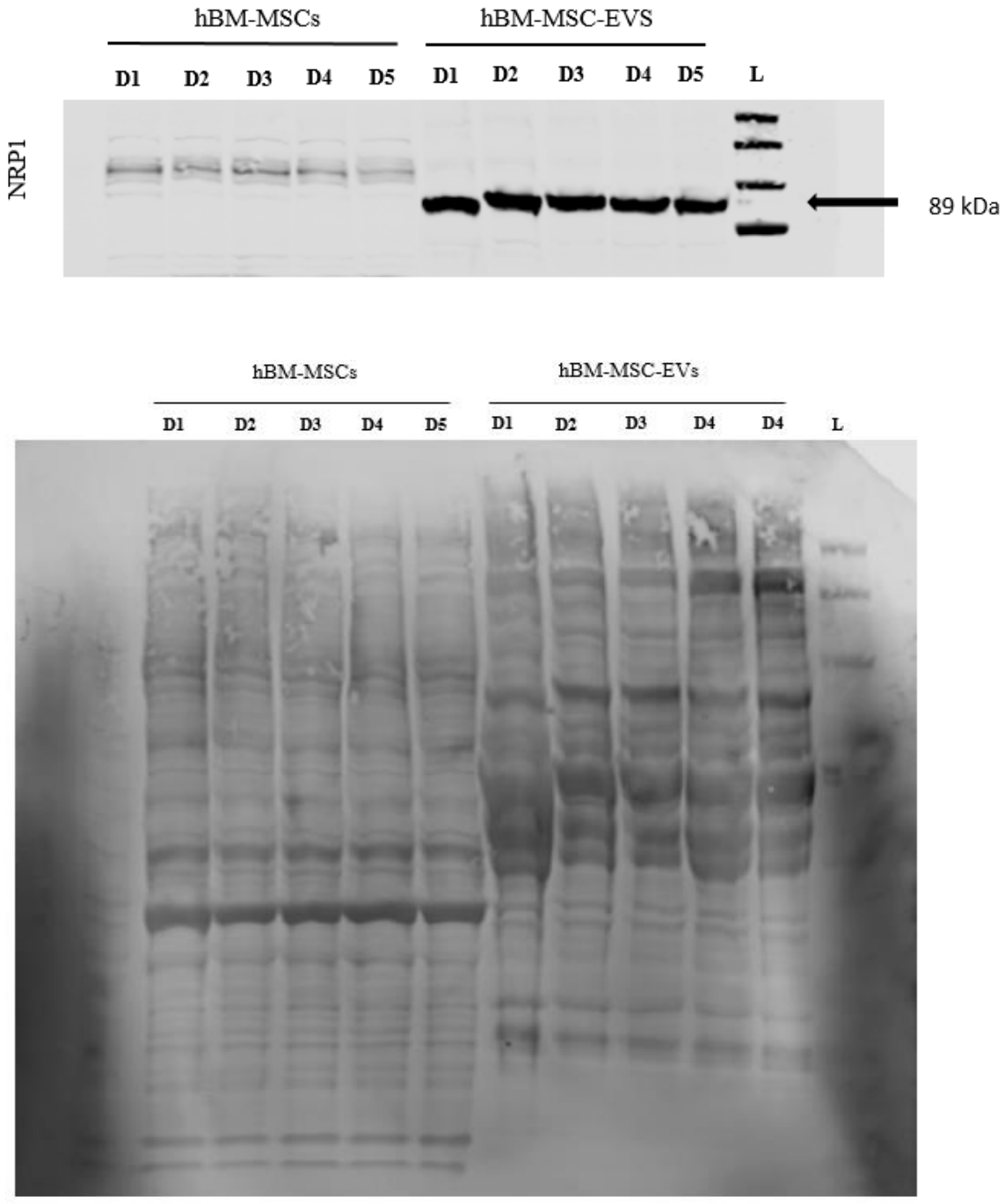

Figure 17: Western blot and total protein stain for NRP1 in hBM-MSC and hBM-MSC-EV. **A)** NRP1 (89kDa) enrichment in hBM-MSC-EV. This experiment was conducted with five hBM-MSC donors (n=5) in two independent trials. **B**) Total protein stain of the gel probed for NRP1 (89kDa), used for confirmation of proper and equal loading of the samples.

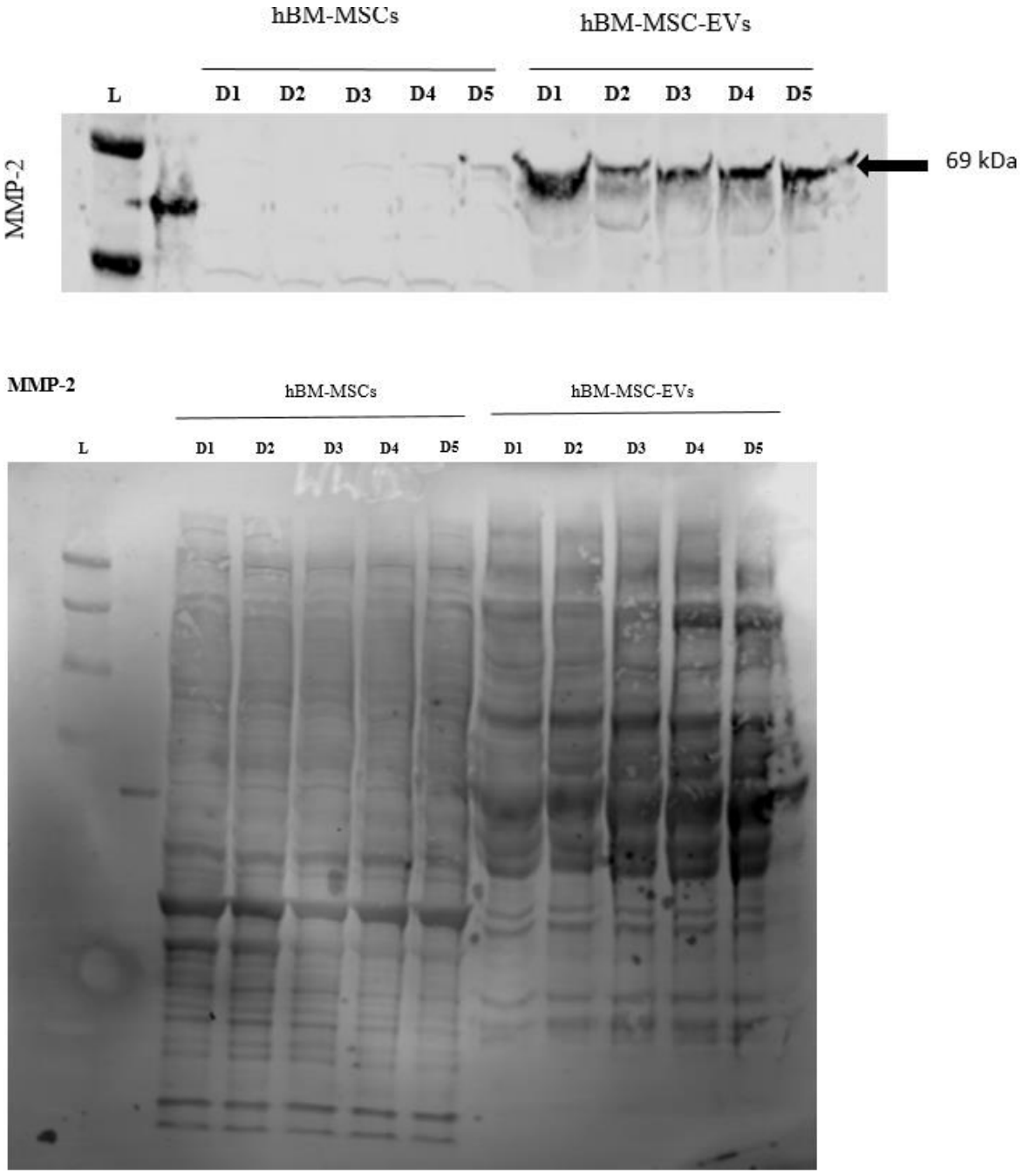

Figure 18: Western blot and total protein stain for MMP-2 in hBM-MSC and hBM-MSC-EV. **A)** MMP-2 (69kDa) enrichment in hBM-MSC-EV. **B**) Total protein stain of the gel probed for MMP-2 (69kDa) used for confirmation of proper and equal loading of the samples. This experiment was conducted with five hBM-MSC donors (n=5) in two independent trials.

Chapter 4: Summary and Discussion

4.1 Summary

MSC-EV clinical and preclinical studies have shown that MSC-EVs promote therapeutic efficacy in several disease settings, however a comprehensive characterization of hBM-MSC-EV protein composition is yet to be reported and is a critical step to further understand the MSC mechanism of action (MOA) through EVs. The aim of this thesis was to first characterize the phenotypic properties of hBM-MSC-EVs from 5 healthy hBM-MSC donors using NTA, flow cytometry, TEM, western blot and second to identify and characterize exosomal/EV protein profile of hBM-MSC-EV from 5 healthy hBM-MSC donors using mass spectrometry and western blot. Furthermore, identification and characterization of proteins enriched in hBM-MSC-EVs could enable identification of proteins that could serve as potential hBM-MSC-EV markers as well as to determine the dominant biological processes involved in the MOA of hBM-MSC-EV. This is the first time a comprehensive comparative quantitative proteomic analysis was performed using hBM-MSCs from multiple donors where the parental cell protein profile was compared to the secreted hBM-MSC-EVs. A total of 782 proteins were identified in hBM-MSC-EVs of which 270 proteins were enriched greater than 2 fold in hBM-MSC-EVs compared to the hBM-MSCs. The 2-fold enriched hBM-MSC-EV dataset (270 proteins) was then used to perform bioinformatics analysis where it showed that the enriched proteins were associated with several biological pathways such as cellular functions important in cell to cell communication as well as metabolic processes, immune modulation, biological adhesion and developmental processes. This research will enable advancement in the use of MSC-EVs as cell-free therapy which could circumvent the safety concerns associated with cell-based therapy.

4.2 Discussion

In this study hBM-MSCs were used and characterized according to the ISCT minimal characteristic criteria, which were obtained from 5 healthy hBM-MSC male donors [5]. A 7-day culture timeline for MSC expansion was established and this included a 48 hour EV production time after which the CCM was collected and cells were harvested to obtain a live cell count. The cell counts were consistent from all 5 donors and according to the MISEV guidelines 2018, it is mandatory to report the cell count from which EVs will be isolated, as method of EV characterization [79]. Herein, hBM-MSC-EVs were purified from CCM from all 5 hBM-MSC donors by polyethylene glycol (PEG)-based method using a commercial kit. PEG-based isolation or purification has been used in many preclinical studies and also has been used in a clinical study for GvHD where it was shown that hBM-MSC-EVs were able to suppress the symptoms of steroid-refractory acute GvHD in a patient [111]. The EVs were further characterized by NTA using both Nanosight and ZetaView and the average particle sizes were measured at 99–123 nm (ZetaView) and 133–138 nm (NanoSight). Presence of Tsg101 and CD81, which are known EV markers were demonstrated by western blot [111]. While this allows large scale isolation in a timely fashion, a drawback is that PEG may co-precipitate poorly soluble proteins and large vesicles. However, this may be circumvented by subsequent wash or filtration steps [130]. In this study the CCM was filtered twice using 10 kDa filters prior to EV purification. hBM-MSC-EVs were characterized using NTA and no significant differences in the hBM-MSC-EV concentration or mean and mode particle size were observed among the different hBM-MSC donors. The average of all 5 donors hBM-MSC-EV mean and mode measuring at 134.1nm and 109.3nm respectively, are categorized under the small EV classification according to the MISEV

guidelines, 2018 [79]. NTA is becoming a widely used method for EV quantification and to analyse size distribution, as this technology can detect particles from about 10 to 2000 nm with an advantage of requiring very little sample volume. However, one of the drawbacks is that the accuracy of the absolute concentration is affected by polydisperse populations and hBM-MSC-EVs are known to be heterogeneous in size population ranging from 50nm – 200 nm, which was confirmed by this study [134]. In order to confirm the known tetraspanin EV markers, flow cytometric analysis identified the presence of hBM-MSC-EVs expressing CD63, CD81, and CD9 exosome associated proteins. Due to size threshold limitation of our flow cytometry (LSR II), 4.2μm CD63 magnetic beads were used to immuno-precipitate CD63 positive hBM-MSC-EV population and stained for CD63, CD81, CD9 against isotype control IgG1, κ (grey) which served as a negative control. The results indicated that CD63 subpopulation of hBM-MSC-EVs also express CD81 and CD9 (to a varying degree). TEM was used for morphological analysis and confirmed the presence of vesicles with bilayer membranes with size within 200nm. However, TEM cannot be used as a quantitative method due to the non-uniform adherence of EVs to the electron microscopy (EM) grid as well as changes in the morphology as a result of the preparation method can also be expected. Western blot was used for the characterization of HSP90B1 (absent in EVs; MISEV guidelines, 2014) and validation (NRP1 and MMP2) of hBM-MSC-EV proteins. While this is a commonly used method for protein identification and characterization and is a good method for mass spectromery results validation, western blot is a semi quantitative method and does not provide an absolute quantification. Quantitative proteomic characterization of hBM-MSC-EV versus hBM-MSC proteins was done using tandem mass tags (TMT) labels by LC-MS/MS. Advantages with TMT or isotope labeling is that multiplexing is possible and has better quantification precision and accuracy in comparison to label-free approaches.

However, the latter has wider proteome coverage and is a more dynamic approach and labelling approaches may mask the low abundant proteins [135].

MSC-EVs are hypothesized to play a major role in MSC-mediated therapeutic function and therefore could serve as a novel alternative to whole-cell therapies [62]. hBM-MSC-EVs contain MSC associated critical surface markers and signalling molecules characteristic of MSCs thereby potentially mediating the therapeutic effects of MSCs [63]. Important from a clinical perspective is the fact that MSCs are hypoimmunogenic and are devoid of allogenic reactions because of their low level of expression of MHC class I and HLA I and the lack of expression of MHC class II and HLA-DR. As such cultured MSC can be safely transplanted into human subjects without any concerns of histocompatibility [7]. MSC-EVs in our study showed similar pattern of low expression of the HLA and MHC complex in mass spectrometry results. In contrast to cell-free therapy, transplanted stem cells such as MSCs immunogenic profile of can change as a result of inflammatory priming, culture condition and cryopreservation [136, 137]. In fact, some groups have shown immune plasticity of MSCs in response to priming by IFN-γ, where MHC I, MHC II, several immune modulatory molecules were upregulated [138-140].

Our proteomic analysis revealed that MSC-EVs express MSC markers such as CD44 and CD105, as well as 65 of the top 100 EV markers identified in the Exocarta database (http://www.exocarta.org/) further confirming the presence of EVs in our preparation. We identified 270 proteins enriched (greater than 2 fold) in hBM-MSC-EVs compared to hBM-MSCs. Functional analysis using IPA of these proteins indicated that the dominant biological pathways are involved in cellular movement, cell-to-cell signalling, metabolic processes, tissue development and immune modulation. These observations may provide new insights

to the molecular mechanism of action of MSC-EV-mediated therapeutic effects in diseases requiring those functions for tissue repair or functional recovery. The most significantly upregulated pathway in the category of cellular and molecular function was cell movement. The functional annotations under cellular movement included increase in homing of cells, chemotaxis, migration of cells, invasion of cells, cell movement of myeloid cells, dermal cells, epithelial cells and connective tissue cells, which are some of the hallmarks of wound healing [141]. Several studies have indeed showed that MSC-EVs are involved in causing cell movement and migration [116, 142, 143].

Our analysis identified 270 enriched MSC-EV proteins, out of which 31 proteins were associated with processes that matched the activation z-score cut off of -2 to +2 (positive; activation and negative; repression). These processes are predicted to be associated with an increase in migration of cells, invasion of cells, movement and migration of leukocyte, chemotaxis, vasculogenesis and decrease in organismal death or pro-survival. NRP1, NRP2, ITGA2, APP, ENPP2 are common proteins involved all the functions mentioned except organismal death. MSCs are known to express NRP1, NRP2, ITGA2, APP and ENPP2 and these proteins were identified and enriched in the hBM-MSC-EV dataset. Interestingly our group had previously reported NRP1 by western blots in hBM-MSCs from 4 healthy donors in an effort to identify proteomic signature that discriminates CD105+ stromal from CD105- non-stromal cells [144].

Many studies have demonstrated MSC-EV-mediated neuroprotection in models for ischemic stroke and traumatic brain injury [106-108]. The primary functions of NRP1, ENPP2, APP are associated with vascular and neural development. NRP1 and NRP2 are membrane associated glycoproteins encoded by genes on two different chromosomes and

share 44% sequence homology only [145, 146]. Though NRP1 and NRP2 are co-receptors for VEGF and semaphorin, they interact selectively with different members of the VEGF and semaphorin families [145]. They are both implicated in potentiating proangiogenic activity and neural development [145]. However, inactivation of the *NRP1* gene in mice is lethal and has more severe consequences than inactivation of *NRP2* gene [145]. NRP1 also regulates platelet-derived growth factor receptors in MSCs and NRP-1/PDGFR cross-talk is essential for vascular remodelling [147].

ENPP2 also commonly known as autotaxin, is an enzyme which catalyzes production of a bioactive lysophospholipid, lysophosphatidic acid (LPA), in extracellular fluids [148]. Neural and vascular developmental defects were observed in LPA receptor knockout mouse models [148]. Lethality at the embryonic stage in mice is observed upon cellular ENPP2 silencing indicating the critical role of the protein for normal development [149]. ENPP2 is involved in multiple roles which are not yet fully understood, apart from neural and vascular development, ENPP2 is also involved in migration, invasion, chemotaxis, differentiation and proliferation [149]. *Aghajanova et. al.* [150] and *Shahdadfar et al.* [151] reported high expression of *ENPP2* mRNA levels in hBM-MSC. *ENPP2* was identified as h-MSC marker by *Shahdadfar et al.* and *Aghajanova et. al.* suggesting that *ENPP2* in MSC is involved in anti-apoptotic pathways [150, 151] ENPP2 has never been reported in MSC-EVs.

CD44 and MMP-2 were detected in our hBM-MSC-EV dataset suggesting CD44 and MMP-2 may also be important for MSC-EVs homing to site of injury. *Herrera et al.* reported that migration of transplanted MSC is influenced by an interaction between CD44 and hyaluronic acid (HA) *in vitro* and *in vivo*. Furthermore, *in vitro* studies showed that the interaction

between HA and CD44 expressing MSCs plays an important role in the migration of MSCs in a dose dependent manner, as HA acts as a chemotactic factor which led to the inhibition of migration when MSCs were incubated with CD44 blocking antibody. To corroborate these results, *in vivo* studies also showed migration of MSCs to inflamed tissue in a mouse model of acute renal failure (ARF). HA was highly expressed in the kidneys of ARF in comparison to the control. In addition, MSCs isolated from CD44 knockout mice, or MSCs isolated from wild type mice pre-incubated with CD44 blocking antibody had reduced capacity to reach the damaged kidneys in comparison to the control indicating CD44-hyaluronic acid interactions is important for MSC mediated therapeutic effect [152]. MMPs and their implications on MSC migration have also been studied. *De Becker et al.* showed that blocking of MMP-2 by an antibody or siRNA showed impaired *in vitro* transendothelial migration and an increased expression of tissue inhibitor metalloproteinase-3 (TIMP-3) [153].

Several glycolytic enzymes, heat shock proteins and glutathione S-transferases were identified in our hBM-MSC-EV dataset and among these proteins PKM isoform 1/2, ENO3, GSTA1, GSTZ1, GSTM3, 20S proteasome subunit beta-2, 20S proteasome subunit alpha-3 were found. *Lai et al.* identified enzymes such as glycolytic enzymes and proteasomes in MSC-EV where the glycolytic enzymes from MSC-EV may be able to replenish the glycolytic deficit and potentially increase glycolytic flux and ATP production in the reperfused myocardium [103]. Furthermore, in the reperfused heart ~90% of all intracellular protein damaged by oxidation and misfolded or oligomerized proteins are degraded or may be reduced by 20S proteasomes, a protein complex found in MSC-EV [104]. Proteomic analysis by *Lai et al., 2012* revealed that ischemic injury in a mouse heart resulted in a depletion of metabolic processes such as fatty acid oxidation, glycolysis, tricarboxylic

acid cycle, redox-homeostasis as well as depletion in gluthatione S-transferase (GST) and heat shock proteins and an increase in apoptotic and electron transport chain proteins were also observed - key features of cell death after myocardial I/R injury. The depletion and accumulation of proteins involved in the mentioned pathways predicted to lead to reduced ATP production, increased oxidative stress and apoptosis. After MSC-EV treatment, an increase in tissue level of ATP and NADH in the heart was observed. The glycolytic enzymes from MSC-EV may be able to replenish the glycolytic and antioxidant deficit and potentially increases the glycolytic flux and ATP production as well as reduce the oxidative stress in the reperfused myocardium. MSC-EVs contained all five enzymes in the ATP generating stage of glycolysis (GAPD, PGK, PGM, ENO, PKM2) as well as phosphorylated PFKFB3. Furthermore, peroxiredoxins and glutathione S-transferases in MSC-derived exosomes reduced oxidative stress [103]. Several glycolytic enzymes and proteasome were identified in our hBM-MSC-EV dataset and among them PKM isoform 1/2, ENO3, GSTA1, GSTZ1, GSTM3, 20S proteasome subunit beta-2, 20S proteasome subunit alpha-3 were found in the enriched hBM-MSC-EV dataset.

Proteins involved in immune cell trafficking and recruitment as well as several inflammatory mediators were also identified, particularly members of the complement system in our MSC-EV proteins. Few studies have reported the importance of the complement system in wound healing, where it regulates tissue regeneration and inflammation as well as aids in the removal of apoptotic and necrotic cells and control infection [154].

Bossi et al. reported beneficial effects of complement C1q in rats, where topically applied C1q showed an increase in angiogenic activity by an augmentation of vessel formation permeability, proliferation, and chemotaxis of endothelial cells, which altogether promoted

wound healing [154]. Topical application of C3 has also been shown to promote wound healing in mice along with an increase in the migration of inflammatory cells, fibroblasts and collagen deposition in the wounds [155]. The complements C3a and C5a are also critical for tissue regeneration in the mouse liver injury model (partial hepatectomy) as reported by *Strey et al*. [156]. Interestingly, C3a and C5a have been identified as chemotactic factors for MSC and also confer protection to MSC from oxidative damage. Migration of MSCs to sites of inflammation and tissue injury is also mediated by the complement system [157]. SDF-1 is a chemokine known to be released at sites of tissue injury [157]. SDF-1/CXCR4 axis has been well characterized as a pathway for cell trafficking, and has been shown to mediate the *in vitro* migration of MSC [157], and CXCR4 is only expressed on the cell surface of a small subpopulation of MSCs and it remains controversial whether SDF-1 is a chemotactic factor for MSCs [158]. Furthermore, C3a and C5a have been identified as chemotactic factors for MSC and also protects MSCs from oxidative damage. This could be physiologically relevant as at the site of injury MSCs are exposed to high level of oxidants due to neutrophil recruitment and reperfusion injury [158]. Although C1q and C3 have shown beneficial effects on wound healing, complement components can also have a detrimental effect in the case of chronic wound, where elevated levels of C3, C3a, C3d, and MAC were reported [158-162].

Additionally, MMP-9 and TGF- β1 (found in our enriched hBM-MSC-EV dataset) are involved in MSC-mediated immune suppressive activity [116]. TGF-β proteins are known to supress inflammatory response and induce CD4+/CD25+ regulatory T-cells thereby promoting tissue regenerative environment [116]. However, TGF-β is also involved in proapoptotic activity where *Jang et. al.* showed TGF-β treatment dependent apoptosis of

Hep3B hepatoma cells [116, 163]. Apart from extracellular matrix (ECM) remodelling, MMP-9 is also involved in suppressing natural killer cell mediated cytotoxicity [116].

Several proteins associated with ECM remodelling process have been identified in our 2-fold enriched hBM-MSC-EV dataset such as fibronectin 1, Collagen type 1, 2, 4, 11, 14, 18, lumican, laminin, decorin, COMP, SPARC, HSPG2 and other proteins (adhesion molecules, MMP-2 and MMP-9). MSC-mediated wound healing is dependent upon angiogenesis or neoangiogenesis and ECM remodelling stimulated by MSCs in a paracrine manner [164]. ECM remodelling is integral for angiogenesis. It is a dynamic process and can have both pro and anti-angiogenic effects [164]. Angiogenesis is a complex process that involves proliferation and migration of endothelial cells and proteolytic degradation of blood vessel basement membrane and associated ECM. Proteolytic cleavage of matrix molecules forms antiangiogenic fragments [164]. Using MALDI/TOF-TOF mass spectrometry analysis of CCM from three hBM-MSC donors, *Walter et. al.* identified several ECM components such as Fibronectin, Type I Collagen, Type VI Collagen, Laminin, COMP, Lumican, Decorin, HSPG, SPARC, IGFBP-1 [165]. Fibronectin and collagen contain protein motifs known to mediate angiogenesis by integrin receptor signalling, laminins are known to promote angiogenesis [165]. However, decorin and lumican inhibit angiogenesis by blocking endothelial cell migration, tubule formation and interfering with $\alpha 2\beta 1$ receptor activity respectively. Furthermore, angiogenesis depends on endothelial cell migration and effects of endothelial cell chemotactic factors and this process was demonstrated to be enhanced by MSC-CM [165]. The ECM is composed of a network of fibrous proteins (collagen and elastin) and glycosaminoglycans (GAGs) - polymer of proteoglycans and these proteins also play a key role in the modulation of angiogenesis. Heparan sulfate glycosaminoglycans

(HSGAGs) are a diverse family of GAGs and have the ability to either inhibit or promote neovascularization by mediating signalling through VEGF receptors or bFGF [166-168].

Important growth factor involved in MSC and MSC-EV mediated tissue repair and migration are IGFs [169, 170]. Several members of the IGF family were identified in our enriched hBM-MSC-EV dataset such as IGF-1, IGFBP-2, -3, -4, and -5 as well as IGF-2R which was also identified in the dataset. IGFs signal mainly via IGF-1 receptor (IGF-1R) which binds to IGF-1 [169-170]. While IGF-1 binds to both IGF-1R and IGF-2R, IGF-2 binds specifically to IGF-2R and different receptor and ligand combinations can cause variable signalling outcomes. IGF-1 and IGF-2 share more than 60% sequence homology at the molecular level [169-170]. IGF-1 and -2 act on a variety of cells similarly by exhibiting proliferative, metabolic and differentiative effects [171-173]. Few studies have reported that IGF-1 exhibits growth, differentiation, and migratory effects on MSCs [171-173]. IGF-1 and IGF-2 are thought to play an especially important role in the proliferation and differentiation of many organs and tissues in developing embryos and during adult life [174, 175]. IGF-1 is more important in postnatal growth, while IGF-2 is important for prenatal fetoplacental growth. IGFs are differentially modulated by six soluble (~30 kDa) IGF-binding proteins (IGFBPs, 1–6) *via* non-covalent binding [176]. IGFBPs confer protection to IGFs from degradation by increasing their half-life [177] and facilitates delivery to specific tissues thereby play an important role in IGF-regulated cell metabolism, development, and growth [178]. IGFBP2 is expressed in fetal tissues that are highly proliferative, and its expression significantly decreases after birth. Apart from binding to IGFs, IGFBP also bind to the ECM or cell surface via glycoproteins, collagens, and integrins, and this causes a decrease in binding affinity to IGF when bound to cell surface or ECM. IGFBP plays an important role

in skeletal muscle development, specifically IGFBP2 has been associated with skeletal muscle cell proliferation and differentiation [179, 180].

Paracrine factors secreted by MSCs, including IGFs, are shown to play a major role in treating organ-failure-causing diseases, MSC mediated therapeutic effects via IGF-1 has been shown to enhance proliferation, differentiation, and repair in several disease models such as kidney, heart, pancreas and liver [180, 181]. IGF-1 secreted by BM-MSCs showed proliferative, antiapoptotic properties and proximal tubular cell regeneration after acute kidney injury [183]. Furthermore, *Tomasoni et. al*. reported murine BM-MSC-derived EVs are selectively enriched with *IGF1R* mRNA, and also demonstrated renoprotection in AKI model [89].

In conclusion we have developed and optimized an in house protocol for isolation of EV derived from hBM-MSCs, as well as their characterization. EV concentration, size distribution and identity were characterized by NTA, TEM, western blot, and flow cytometry, which showed similarity in phenotypic properties among all 5 hBM-MSC donors. Proteomics analysis of hBM-MSC-EV showed pro-angiogenic factors, proteins involved in cellular migrations, chemotaxis, immune modulation and tissue development associated with neurons, heart, muscle, bone and endothelial cells and important functions that may be linked to MSC-mediated therapy. This study will provide new insight into the underlying molecular mechanism of action of hBM-MSC via hBM-MSC-EVs and potential novel markers involved in tissue regenerative processes, surface markers for potency assays and signature markers for hBM-MSC-EVs or EVs in general.

Appendices

Table 1: List of antibodies used for flow cytometry for CD63 bead bound assay

Product Name	**Company**	**Catalog No.**	**Clone**
Exosome-Human CD63 Isolation/Detection Reagent (from cell culture media)	Invitrogen	10622D	Primary monoclonal antibody
PE Mouse Anti-Human CD63	BD Biosciences	557305	H5C6 monoclonal antibody
PE Mouse Anti-Human CD81	BD Biosciences	555676	JS-81 monoclonal antibody
PE Mouse Anti-Human CD9	BD Biosciences	555372	M-L13 monoclonal antibody
PE Mouse IgG1, κ Isotype Control	BD Biosciences	555749	MOPC-21 immunoglobulin

PE: Phycoerythrin

Table 2: Primary and secondary antibodies used for western blot protocol

PROTEIN	**PRIMARY ANTIBODY**	**SECONDARY ANTIBODY**
GRP94	Rabbit mAb anti-GRP94(EPR3988) Abcam: ab108606 1:500 dilution	IRDye 800CW Goat anti-Rabbit IgG LI-COR: 925-32211 1:20000 dilution

MMP2	Rabbit mAb anti-MMP2 (EPR 184) Abcam: ab92536 1:500 dilution	IRDye 800CW Goat anti-Rabbit IgG LI-COR: 925-32211 1:20000 dilution
NRP1	Rabbit mAb anti-NRP1 Abcam: ab81321 1:500 dilution	IRDye 800CW Goat anti-Rabbit IgG LI-COR: 925-32211 1:20000 dilution

Table 3: TMT labels used for hBM-MSC and hBM-MSC-EV samples

	Replicate 1	Replicate 2
Samples	TMT10 Labels	TMT10 Labels
Donor#1 Cell	126	129N
Donor#2 Cell	127N	129C
Donor#3 Cell	127C	130N
Donor#4 Cell	128N	130C
Donor#5 Cell	128C	131
Donor#1 EV	129N	126
Donor#2 EV	129C	127N
Donor#3 EV	130N	127C
Donor#4 EV	130C	128N
Donor#5 EV	131	128C

Ingenuity pathway Analysis

Molecules from the data set that are associated with Ingenuity's Knowledge Base are considered for the analysis. IPA (Ingenuity IPA-46901286, Version 01-07, Content Version: 46901286, Copyright 2019 QIAGEN) calculates two distinct statistics as part of a core analysis:

P-value: Fisher's exact test is used to calculate a p-value determining the probability that the association between the molecules in the data set and the pathway of interest can be explained by chance alone (p-value). The smaller the p-value the less likely that the association is random. The p-value does not consider the directional effect of one molecule on another, or the direction of change of molecules in the data set.

Z-score: Z-score is calculated based on gene expression from Knowledge base (literature) versus Gene expression in the uploaded dataset. Z-score calculation takes into account the directional effect of one molecule on another molecule or on a process, and the direction of change of molecules in the data set. +1 scored for the consistent and -1 scored for the inconsistent relationships. the number of standard deviations from the mean of a normal distribution of activity edges. Z-score > 2 or < -2 is considered significant

Advanced IPA analytics such as bioprofiler was used for categorizations of the proteins into protein class and cellular compartment. Disease and function analysis was used to determine the significantly upregulated physiological development and function pathways as well as cellular and molecular function pathways.

References

1. Friedenstein, A.J., R.K. Chailakhjan, and K.S. Lalykina, *The development of fibroblast colonies in monolayer cultures of guinea-pig bone marrow and spleen cells.* Cell Tissue Kinet, 1970. **3**(4): p. 393-403.
2. Dexter, T.M., et al., *Regulation of haemopoietic stem cell proliferation in long term bone marrow cultures.* Biomedicine, 1977. **27**(9-10): p. 344-9.
3. Lavoie, J.R. and M. Rosu-Myles, *Uncovering the secretes of mesenchymal stem cells.* Biochimie, 2013. **95**(12): p. 2212-21.
4. Shibata, K.R., et al., *Expression of the p16INK4A gene is associated closely with senescence of human mesenchymal stem cells and is potentially silenced by DNA methylation during in vitro expansion.* Stem Cells, 2007. **25**(9): p. 2371-82.
5. Dominici, M., et al., *Minimal criteria for defining multipotent mesenchymal stromal cells. The International Society for Cellular Therapy position statement.* Cytotherapy, 2006. **8**(4): p. 315-7.
6. Ullah, I., R.B. Subbarao, and G.J. Rho, *Human mesenchymal stem cells - current trends and future prospective.* Biosci Rep, 2015. **35**(2).
7. Ma, S., et al., *Immunobiology of mesenchymal stem cells.* Cell Death Differ, 2014. **21**(2): p. 216-25.
8. Gu, Y., et al., *Changes in mesenchymal stem cells following long-term culture in vitro.* Mol Med Rep, 2016. **13**(6): p. 5207-15.
9. Binato, R., et al., *Stability of human mesenchymal stem cells during in vitro culture: considerations for cell therapy.* Cell Prolif, 2013. **46**(1): p. 10-22.
10. Stultz, B.G., et al., *Chromosomal stability of mesenchymal stromal cells during in vitro culture.* Cytotherapy, 2016. **18**(3): p. 336-43.
11. Wang, Y., et al., *Long-term cultured mesenchymal stem cells frequently develop genomic mutations but do not undergo malignant transformation.* Cell Death Dis, 2013. **4**: p. e950.
12. Tarte, K., et al., *Clinical-grade production of human mesenchymal stromal cells: occurrence of aneuploidy without transformation.* Blood, 2010. **115**(8): p. 1549-53.
13. Estrada, J.C., et al., *Human mesenchymal stem cell-replicative senescence and oxidative stress are closely linked to aneuploidy.* Cell Death Dis, 2013. **4**: p. e691.
14. Ben-David, U., Y. Mayshar, and N. Benvenisty, *Large-scale analysis reveals acquisition of lineage-specific chromosomal aberrations in human adult stem cells.* Cell Stem Cell, 2011. **9**(2): p. 97-102.
15. Meza-Zepeda, L.A., et al., *High-resolution analysis of genetic stability of human adipose tissue stem cells cultured to senescence.* J Cell Mol Med, 2008. **12**(2): p. 553-63.
16. Sensebe, L., et al., *Limited acquisition of chromosomal aberrations in human adult mesenchymal stromal cells.* Cell Stem Cell, 2012. **10**(1): p. 9-10; author reply 10-1.
17. Wagner, W., *Implications of long-term culture for mesenchymal stem cells: genetic defects or epigenetic regulation?* Stem Cell Res Ther, 2012. **3**(6): p. 54.
18. Garcia, S., et al., *Pitfalls in spontaneous in vitro transformation of human mesenchymal stem cells.* Exp Cell Res, 2010. **316**(9): p. 1648-50.

19. Torsvik, A., et al., *Spontaneous malignant transformation of human mesenchymal stem cells reflects cross-contamination: putting the research field on track - letter.* Cancer Res, 2010. **70**(15): p. 6393-6.
20. Lalu, M.M., et al., *Safety of cell therapy with mesenchymal stromal cells (SafeCell): a systematic review and meta-analysis of clinical trials.* PLoS One, 2012. **7**(10): p. e47559.
21. Siegel, G., et al., *Phenotype, donor age and gender affect function of human bone marrow-derived mesenchymal stromal cells.* BMC Med, 2013. **11**: p. 146.
22. Phinney, D.G., et al., *Donor variation in the growth properties and osteogenic potential of human marrow stromal cells.* J Cell Biochem, 1999. **75**(3): p. 424-36.
23. Beane, O.S., et al., *Impact of aging on the regenerative properties of bone marrow-, muscle-, and adipose-derived mesenchymal stem/stromal cells.* PLoS One, 2014. **9**(12): p. e115963.
24. Fan, M., et al., *The effect of age on the efficacy of human mesenchymal stem cell transplantation after a myocardial infarction.* Rejuvenation Res, 2010. **13**(4): p. 429-38.
25. Zhukareva, V., et al., *Secretion profile of human bone marrow stromal cells: donor variability and response to inflammatory stimuli.* Cytokine, 2010. **50**(3): p. 317-21.
26. Lee, R.H., et al., *Intravenous hMSCs improve myocardial infarction in mice because cells embolized in lung are activated to secrete the anti-inflammatory protein TSG-6.* Cell Stem Cell, 2009. **5**(1): p. 54-63.
27. Caplan, A.I. and D. Correa, *The MSC: an injury drugstore.* Cell Stem Cell, 2011. **9**(1): p. 11-5.
28. Pawitan, J.A., *Prospect of stem cell conditioned medium in regenerative medicine.* Biomed Res Int, 2014. **2014**: p. 965849.
29. Williams, A.R. and J.M. Hare, *Mesenchymal stem cells: biology, pathophysiology, translational findings, and therapeutic implications for cardiac disease.* Circ Res, 2011. **109**(8): p. 923-40.
30. Matthay, M.A., S. Pati, and J.W. Lee, *Concise Review: Mesenchymal Stem (Stromal) Cells: Biology and Preclinical Evidence for Therapeutic Potential for Organ Dysfunction Following Trauma or Sepsis.* Stem Cells, 2017. **35**(2): p. 316-324.
31. Mardpour, S., et al., *Interaction between mesenchymal stromal cell-derived extracellular vesicles and immune cells by distinct protein content.* J Cell Physiol, 2018.
32. Ghannam, S., et al., *Immunosuppression by mesenchymal stem cells: mechanisms and clinical applications.* Stem Cell Res Ther, 2010. **1**(1): p. 2.
33. Selmani, Z., et al., *Human leukocyte antigen-G5 secretion by human mesenchymal stem cells is required to suppress T lymphocyte and natural killer function and to induce CD4+CD25highFOXP3+ regulatory T cells.* Stem Cells, 2008. **26**(1): p. 212-22.
34. Corcione, A., et al., *Human mesenchymal stem cells modulate B-cell functions.* Blood, 2006. **107**(1): p. 367-72.
35. Tabera, S., et al., *The effect of mesenchymal stem cells on the viability, proliferation and differentiation of B-lymphocytes.* Haematologica, 2008. **93**(9): p. 1301-9.
36. Galland, S., et al., *Tumor-Derived Mesenchymal Stem Cells Use Distinct Mechanisms to Block the Activity of Natural Killer Cell Subsets.* Cell Rep, 2017. **20**(12): p. 2891-2905.

37. Fukuoka, H., K. Narita, and H. Suga, *Hair Regeneration Therapy: Application of Adipose-Derived Stem Cells.* Curr Stem Cell Res Ther, 2017. **12**(7): p. 531-534.
38. Shrestha, C., et al., *Enhanced Healing of Diabetic Wounds by Subcutaneous Administration of Human Umbilical Cord Derived Stem Cells and Their Conditioned Media.* International Journal of Endocrinology, 2013.
39. Mishra, P.J., P.J. Mishra, and D. Banerjee, *Cell-free derivatives from mesenchymal stem cells are effective in wound therapy.* World J Stem Cells, 2012. **4**(5): p. 35-43.
40. Timmers, L., et al., *Reduction of myocardial infarct size by human mesenchymal stem cell conditioned medium.* Stem Cell Res, 2007. **1**(2): p. 129-37.
41. Timmers, L., et al., *Human mesenchymal stem cell-conditioned medium improves cardiac function following myocardial infarction.* Stem Cell Res, 2011. **6**(3): p. 206-14.
42. Du, Z., et al., *Mesenchymal stem cell-conditioned medium reduces liver injury and enhances regeneration in reduced-size rat liver transplantation.* J Surg Res, 2013. **183**(2): p. 907-15.
43. Zagoura, D.S., et al., *Therapeutic potential of a distinct population of human amniotic fluid mesenchymal stem cells and their secreted molecules in mice with acute hepatic failure.* Gut, 2012. **61**(6): p. 894-906.
44. van Poll, D., et al., *Mesenchymal stem cell-derived molecules directly modulate hepatocellular death and regeneration in vitro and in vivo.* Hepatology, 2008. **47**(5): p. 1634-43.
45. Parekkadan, B., et al., *Mesenchymal stem cell-derived molecules reverse fulminant hepatic failure.* PLoS One, 2007. **2**(9): p. e941.
46. Inoue, T., et al., *Stem cells from human exfoliated deciduous tooth-derived conditioned medium enhance recovery of focal cerebral ischemia in rats.* Tissue Eng Part A, 2013. **19**(1-2): p. 24-9.
47. Cho, Y.J., et al., *Therapeutic effects of human adipose stem cell-conditioned medium on stroke.* J Neurosci Res, 2012. **90**(9): p. 1794-802.
48. Bakondi, B., et al., *CD133 identifies a human bone marrow stem/progenitor cell sub-population with a repertoire of secreted factors that protect against stroke.* Mol Ther, 2009. **17**(11): p. 1938-47.
49. Chuang, T.J., et al., *Effects of secretome obtained from normoxia-preconditioned human mesenchymal stem cells in traumatic brain injury rats.* J Trauma Acute Care Surg, 2012. **73**(5): p. 1161-7.
50. Chang, C.P., et al., *Hypoxic preconditioning enhances the therapeutic potential of the secretome from cultured human mesenchymal stem cells in experimental traumatic brain injury.* Clin Sci (Lond), 2013. **124**(3): p. 165-76.
51. Cantinieaux, D., et al., *Conditioned medium from bone marrow-derived mesenchymal stem cells improves recovery after spinal cord injury in rats: an original strategy to avoid cell transplantation.* PLoS One, 2013. **8**(8): p. e69515.
52. van Koppen, A., et al., *Human embryonic mesenchymal stem cell-derived conditioned medium rescues kidney function in rats with established chronic kidney disease.* PLoS One, 2012. **7**(6): p. e38746.
53. Gheisari, Y., et al., *Stem cell-conditioned medium does not protect against kidney failure.* Cell Biol Int, 2011. **35**(3): p. 209-13.
54. Inukai, T., et al., *Novel application of stem cell-derived factors for periodontal regeneration.* Biochem Biophys Res Commun, 2013. **430**(2): p. 763-8.

55. Gnecchi, M., et al., *Paracrine action accounts for marked protection of ischemic heart by Akt-modified mesenchymal stem cells.* Nat Med, 2005. **11**(4): p. 367-8.
56. Gnecchi, M., et al., *Evidence supporting paracrine hypothesis for Akt-modified mesenchymal stem cell-mediated cardiac protection and functional improvement.* FASEB J, 2006. **20**(6): p. 661-9.
57. Togel, F., et al., *Administered mesenchymal stem cells protect against ischemic acute renal failure through differentiation-independent mechanisms.* Am J Physiol Renal Physiol, 2005. **289**(1): p. F31-42.
58. Togel, F., et al., *Vasculotropic, paracrine actions of infused mesenchymal stem cells are important to the recovery from acute kidney injury.* Am J Physiol Renal Physiol, 2007. **292**(5): p. F1626-35.
59. Reis, L.A., et al., *Bone marrow-derived mesenchymal stem cells repaired but did not prevent gentamicin-induced acute kidney injury through paracrine effects in rats.* PLoS One, 2012. **7**(9): p. e44092.
60. Zanotti, L., et al., *Encapsulated mesenchymal stem cells for in vivo immunomodulation.* Leukemia, 2013. **27**(2): p. 500-3.
61. Zhu, W., et al., *Mesenchymal stem cell-secreted soluble signaling molecules potentiate tumor growth.* Cell Cycle, 2011. **10**(18): p. 3198-207.
62. Toh, W.S., et al., *MSC exosome works through a protein-based mechanism of action.* Biochem Soc Trans, 2018.
63. Mouiseddine, M., et al., *Human mesenchymal stem cells home specifically to radiation-injured tissues in a non-obese diabetes/severe combined immunodeficiency mouse model.* Br J Radiol, 2007. **80 Spec No 1**: p. S49-55.
64. Willis, G.R., S. Kourembanas, and S.A. Mitsialis, *Toward Exosome-Based Therapeutics: Isolation, Heterogeneity, and Fit-for-Purpose Potency.* Front Cardiovasc Med, 2017. **4**: p. 63.
65. Cheng, L., et al., *Focus on Mesenchymal Stem Cell-Derived Exosomes: Opportunities and Challenges in Cell-Free Therapy.* Stem Cells Int, 2017. **2017**: p. 6305295.
66. Lener, T., et al., *Applying extracellular vesicles based therapeutics in clinical trials - an ISEV position paper.* J Extracell Vesicles, 2015. **4**: p. 30087.
67. Simpson, R.J., S.S. Jensen, and J.W. Lim, *Proteomic profiling of exosomes: current perspectives.* Proteomics, 2008. **8**(19): p. 4083-99.
68. Skog, J., et al., *Glioblastoma microvesicles transport RNA and proteins that promote tumour growth and provide diagnostic biomarkers.* Nat Cell Biol, 2008. **10**(12): p. 1470-6.
69. Taylor, D.D. and C. Gercel-Taylor, *MicroRNA signatures of tumor-derived exosomes as diagnostic biomarkers of ovarian cancer.* Gynecol Oncol, 2008. **110**(1): p. 13-21.
70. Miranda, K.C., et al., *Nucleic acids within urinary exosomes/microvesicles are potential biomarkers for renal disease.* Kidney Int, 2010. **78**(2): p. 191-9.
71. Pan, B.T. and R.M. Johnstone, *Fate of the transferrin receptor during maturation of sheep reticulocytes in vitro: selective externalization of the receptor.* Cell, 1983. **33**(3): p. 967-78.
72. Alsaker, R.D., *The formation, emergence, and maturation of the reticulocyte: a review.* Vet Clin Pathol, 1977. **6**(3): p. 7-12.
73. Johnstone, R.M., *Revisiting the road to the discovery of exosomes.* Blood Cells Mol Dis, 2005. **34**(3): p. 214-9.

74. Roy, S., F.H. Hochberg, and P.S. Jones, *Extracellular vesicles: the growth as diagnostics and therapeutics; a survey.* J Extracell Vesicles, 2018. **7**(1): p. 1438720.
75. Lawson, C., et al., *Extracellular Vesicles: Evolutionarily Conserved Mediators of Intercellular Communication.* Yale J Biol Med, 2017. **90**(3): p. 481-491.
76. Doeppner, T.R., et al., *Concise Review: Extracellular Vesicles Overcoming Limitations of Cell Therapies in Ischemic Stroke.* Stem Cells Transl Med, 2017. **6**(11): p. 2044-2052.
77. Li, Y., et al., *Extracellular vesicles in mesenchymal stromal cells: A novel therapeutic strategy for stroke.* Exp Ther Med, 2018. **15**(5): p. 4067-4079.
78. Lotvall, J., et al., *Minimal experimental requirements for definition of extracellular vesicles and their functions: a position statement from the International Society for Extracellular Vesicles.* J Extracell Vesicles, 2014. **3**: p. 26913.
79. Thery, C., et al., *Minimal information for studies of extracellular vesicles 2018 (MISEV2018): a position statement of the International Society for Extracellular Vesicles and update of the MISEV2014 guidelines.* J Extracell Vesicles, 2018. **7**(1): p. 1535750.
80. Choi, J.Y., et al., *Extracellular Vesicles as a Source of Urological Biomarkers: Lessons Learned From Advances and Challenges in Clinical Applications to Major Diseases.* Int Neurourol J, 2017. **21**(2): p. 83-96.
81. Biancone, L., et al., *Therapeutic potential of mesenchymal stem cell-derived microvesicles.* Nephrol Dial Transplant, 2012. **27**(8): p. 3037-42.
82. Zhang, B., et al., *Focus on Extracellular Vesicles: Therapeutic Potential of Stem Cell-Derived Extracellular Vesicles.* Int J Mol Sci, 2016. **17**(2): p. 174.
83. Henne, W.M., N.J. Buchkovich, and S.D. Emr, *The ESCRT pathway.* Dev Cell, 2011. **21**(1): p. 77-91.
84. Trajkovic, K., et al., *Ceramide triggers budding of exosome vesicles into multivesicular endosomes.* Science, 2008. **319**(5867): p. 1244-7.
85. Bruno, S., et al., *Microvesicles derived from mesenchymal stem cells enhance survival in a lethal model of acute kidney injury.* PLoS One, 2012. **7**(3): p. e33115.
86. Zhou, Y., et al., *Exosomes released by human umbilical cord mesenchymal stem cells protect against cisplatin-induced renal oxidative stress and apoptosis in vivo and in vitro.* Stem Cell Res Ther, 2013. **4**(2): p. 34.
87. He, J., et al., *Bone marrow stem cells-derived microvesicles protect against renal injury in the mouse remnant kidney model.* Nephrology (Carlton), 2012. **17**(5): p. 493-500.
88. Bruno, S., et al., *Mesenchymal stem cell-derived microvesicles protect against acute tubular injury.* J Am Soc Nephrol, 2009. **20**(5): p. 1053-67.
89. Tomasoni, S., et al., *Transfer of growth factor receptor mRNA via exosomes unravels the regenerative effect of mesenchymal stem cells.* Stem Cells Dev, 2013. **22**(5): p. 772-80.
90. Zou, X., et al., *Microvesicles derived from human Wharton's Jelly mesenchymal stromal cells ameliorate renal ischemia-reperfusion injury in rats by suppressing CX3CL1.* Stem Cell Res Ther, 2014. **5**(2): p. 40.
91. Arslan, F., et al., *Mesenchymal stem cell-derived exosomes increase ATP levels, decrease oxidative stress and activate PI3K/Akt pathway to enhance myocardial viability and prevent adverse remodeling after myocardial ischemia/reperfusion injury.* Stem Cell Res, 2013. **10**(3): p. 301-12.

92. Lai, R.C., et al., *Exosome secreted by MSC reduces myocardial ischemia/reperfusion injury.* Stem Cell Res, 2010. **4**(3): p. 214-22.
93. Lai, R.C., et al., *Derivation and characterization of human fetal MSCs: an alternative cell source for large-scale production of cardioprotective microparticles.* J Mol Cell Cardiol, 2010. **48**(6): p. 1215-24.
94. Chen, T.S., et al., *Mesenchymal stem cell secretes microparticles enriched in pre-microRNAs.* Nucleic Acids Res, 2010. **38**(1): p. 215-24.
95. Bian, S., et al., *Extracellular vesicles derived from human bone marrow mesenchymal stem cells promote angiogenesis in a rat myocardial infarction model.* J Mol Med (Berl), 2014. **92**(4): p. 387-97.
96. Ma, J., et al., *Exosomes Derived from Akt-Modified Human Umbilical Cord Mesenchymal Stem Cells Improve Cardiac Regeneration and Promote Angiogenesis via Activating Platelet-Derived Growth Factor D.* Stem Cells Transl Med, 2017. **6**(1): p. 51-59.
97. Teng, X., et al., *Mesenchymal Stem Cell-Derived Exosomes Improve the Microenvironment of Infarcted Myocardium Contributing to Angiogenesis and Anti-Inflammation.* Cell Physiol Biochem, 2015. **37**(6): p. 2415-24.
98. Zhao, Y., et al., *Exosomes Derived from Human Umbilical Cord Mesenchymal Stem Cells Relieve Acute Myocardial Ischemic Injury.* Stem Cells Int, 2015. **2015**: p. 761643.
99. Lai, R.C., T.S. Chen, and S.K. Lim, *Mesenchymal stem cell exosome: a novel stem cell-based therapy for cardiovascular disease.* Regen Med, 2011. **6**(4): p. 481-92.
100. Kukielka, G.L., et al., *Regulation of intercellular adhesion molecule-1 (ICAM-1) in ischemic and reperfused canine myocardium.* J Clin Invest, 1993. **92**(3): p. 1504-16.
101. Rieu, S., et al., *Exosomes released during reticulocyte maturation bind to fibronectin via integrin alpha4beta1.* Eur J Biochem, 2000. **267**(2): p. 583-90.
102. Hemler, M.E., *Tetraspanin proteins mediate cellular penetration, invasion, and fusion events and define a novel type of membrane microdomain.* Annu Rev Cell Dev Biol, 2003. **19**: p. 397-422.
103. Lai, R.C., et al., *Mesenchymal stem cell exosome ameliorates reperfusion injury through proteomic complementation.* Regen Med, 2013. **8**(2): p. 197-209.
104. Lai, R.C., et al., *Proteolytic Potential of the MSC Exosome Proteome: Implications for an Exosome-Mediated Delivery of Therapeutic Proteasome.* Int J Proteomics, 2012. **2012**: p. 971907.
105. Doeppner, T.R., et al., *Extracellular Vesicles Improve Post-Stroke Neuroregeneration and Prevent Postischemic Immunosuppression.* Stem Cells Transl Med, 2015. **4**(10): p. 1131-43.
106. Kim, D.K., et al., *Chromatographically isolated CD63+CD81+ extracellular vesicles from mesenchymal stromal cells rescue cognitive impairments after TBI.* Proc Natl Acad Sci U S A, 2016. **113**(1): p. 170-5.
107. Otero-Ortega, L., et al., *Exosomes promote restoration after an experimental animal model of intracerebral hemorrhage.* J Cereb Blood Flow Metab, 2018. **38**(5): p. 767-779.
108. Xin, H., et al., *MiR-133b promotes neural plasticity and functional recovery after treatment of stroke with multipotent mesenchymal stromal cells in rats via transfer of exosome-enriched extracellular particles.* Stem Cells, 2013. **31**(12): p. 2737-46.

109. Tan, C.Y., et al., *Mesenchymal stem cell-derived exosomes promote hepatic regeneration in drug-induced liver injury models.* Stem Cell Res Ther, 2014. **5**(3): p. 76.
110. Li, T., et al., *Exosomes derived from human umbilical cord mesenchymal stem cells alleviate liver fibrosis.* Stem Cells Dev, 2013. **22**(6): p. 845-54.
111. Kordelas, L., et al., *MSC-derived exosomes: a novel tool to treat therapy-refractory graft-versus-host disease.* Leukemia, 2014. **28**(4): p. 970-3.
112. Sokolova, V., et al., *Characterisation of exosomes derived from human cells by nanoparticle tracking analysis and scanning electron microscopy.* Colloids Surf B Biointerfaces, 2011. **87**(1): p. 146-50.
113. Giebel, B., L. Kordelas, and V. Borger, *Clinical potential of mesenchymal stem/stromal cell-derived extracellular vesicles.* Stem Cell Investig, 2017. **4**: p. 84.
114. Nassar, W., et al., *Umbilical cord mesenchymal stem cells derived extracellular vesicles can safely ameliorate the progression of chronic kidney diseases.* Biomater Res, 2016. **20**: p. 21.
115. Raposo, G., et al., *B lymphocytes secrete antigen-presenting vesicles.* J Exp Med, 1996. **183**(3): p. 1161-72.
116. Eirin, A., et al., *Comparative proteomic analysis of extracellular vesicles isolated from porcine adipose tissue-derived mesenchymal stem/stromal cells.* Sci Rep, 2016. **6**: p. 36120.
117. Anderson, J.D., et al., *Comprehensive Proteomic Analysis of Mesenchymal Stem Cell Exosomes Reveals Modulation of Angiogenesis via Nuclear Factor-KappaB Signaling.* Stem Cells, 2016. **34**(3): p. 601-13.
118. Zhang, B., et al., *Human umbilical cord mesenchymal stem cell exosomes enhance angiogenesis through the Wnt4/beta-catenin pathway.* Stem Cells Transl Med, 2015. **4**(5): p. 513-22.
119. Katsuda, T., et al., *Human adipose tissue-derived mesenchymal stem cells secrete functional neprilysin-bound exosomes.* Sci Rep, 2013. **3**: p. 1197.
120. Chopp, M. and Y. Li, *Treatment of neural injury with marrow stromal cells.* Lancet Neurol, 2002. **1**(2): p. 92-100.
121. Kim, H.S., et al., *Proteomic analysis of microvesicles derived from human mesenchymal stem cells.* J Proteome Res, 2012. **11**(2): p. 839-49.
122. van Balkom, B.W.M., et al., *Proteomic Signature of Mesenchymal Stromal Cell-Derived Small Extracellular Vesicles.* Proteomics, 2019. **19**(1-2): p. e1800163.
123. Salomon, C., et al., *Exosomal signaling during hypoxia mediates microvascular endothelial cell migration and vasculogenesis.* PLoS One, 2013. **8**(7): p. e68451.
124. Lai, R.C., et al., *MSC secretes at least 3 EV types each with a unique permutation of membrane lipid, protein and RNA.* J Extracell Vesicles, 2016. **5**: p. 29828.
125. Zhang, B., et al., *HucMSC Exosome-Delivered 14-3-3zeta Orchestrates Self-Control of the Wnt Response via Modulation of YAP During Cutaneous Regeneration.* Stem Cells, 2016. **34**(10): p. 2485-2500.
126. Lee, J.Y., et al., *Microvesicles from brain-extract-treated mesenchymal stem cells improve neurological functions in a rat model of ischemic stroke.* Sci Rep, 2016. **6**: p. 33038.
127. Haraszti, R.A., et al., *High-resolution proteomic and lipidomic analysis of exosomes and microvesicles from different cell sources.* J Extracell Vesicles, 2016. **5**: p. 32570.

128. Barile, L., et al., *Cardioprotection by cardiac progenitor cell-secreted exosomes: role of pregnancy-associated plasma protein-A.* Cardiovasc Res, 2018. **114**(7): p. 992-1005.
129. Angulski, A.B., et al., *The Protein Content of Extracellular Vesicles Derived from Expanded Human Umbilical Cord Blood-Derived CD133(+) and Human Bone Marrow-Derived Mesenchymal Stem Cells Partially Explains Why both Sources are Advantageous for Regenerative Medicine.* Stem Cell Rev, 2017. **13**(2): p. 244-257.
130. Konoshenko, M.Y., et al., *Isolation of Extracellular Vesicles: General Methodologies and Latest Trends.* Biomed Res Int, 2018. **2018**: p. 8545347.
131. Mathivanan, S., et al., *Proteomics analysis of A33 immunoaffinity-purified exosomes released from the human colon tumor cell line LIM1215 reveals a tissue-specific protein signature.* Mol Cell Proteomics, 2010. **9**(2): p. 197-208.
132. Kowal, J., et al., *Proteomic comparison defines novel markers to characterize heterogeneous populations of extracellular vesicle subtypes.* Proc Natl Acad Sci U S A, 2016. **113**(8): p. E968-77.
133. Heinemann, M.L., et al., *Benchtop isolation and characterization of functional exosomes by sequential filtration.* J Chromatogr A, 2014. **1371**: p. 125-35.
134. Erdbrugger, U. and J. Lannigan, *Analytical challenges of extracellular vesicle detection: A comparison of different techniques.* Cytometry A, 2016. **89**(2): p. 123-34.
135. Xie, F., et al., *Liquid chromatography-mass spectrometry-based quantitative proteomics.* J Biol Chem, 2011. **286**(29): p. 25443-9.
136. Krampera, M., *Mesenchymal stromal cell 'licensing': a multistep process.* Leukemia, 2011. **25**(9): p. 1408-14.
137. Sensebe, L., P. Bourin, and K. Tarte, *Good manufacturing practices production of mesenchymal stem/stromal cells.* Hum Gene Ther, 2011. **22**(1): p. 19-26.
138. Uccelli, A., L. Moretta, and V. Pistoia, *Mesenchymal stem cells in health and disease.* Nat Rev Immunol, 2008. **8**(9): p. 726-36.
139. Nauta, A.J. and W.E. Fibbe, *Immunomodulatory properties of mesenchymal stromal cells.* Blood, 2007. **110**(10): p. 3499-506.
140. Waterman, R.S., et al., *A new mesenchymal stem cell (MSC) paradigm: polarization into a pro-inflammatory MSC1 or an Immunosuppressive MSC2 phenotype.* PLoS One, 2010. **5**(4): p. e10088.
141. Lee, Y.S., et al., *Wound healing in development.* Birth Defects Res C Embryo Today, 2012. **96**(3): p. 213-22.
142. Chen, J.S., V.W. Wong, and G.C. Gurtner, *Therapeutic potential of bone marrow-derived mesenchymal stem cells for cutaneous wound healing.* Front Immunol, 2012. **3**: p. 192.
143. Rajendran, R.L., et al., *Extracellular vesicles derived from MSCs activates dermal papilla cell in vitro and promotes hair follicle conversion from telogen to anagen in mice.* Sci Rep, 2017. **7**(1): p. 15560.
144. Rosu-Myles, M., et al., *Identification of a candidate proteomic signature to discriminate multipotent and non-multipotent stromal cells.* PLoS One, 2012. **7**(6): p. e38954.
145. Sulpice, E., et al., *Neuropilin-1 and neuropilin-2 act as coreceptors, potentiating proangiogenic activity.* Blood, 2008. **111**(4): p. 2036-45.

146. Wild, J.R., et al., *Neuropilins: expression and roles in the epithelium.* Int J Exp Pathol, 2012. **93**(2): p. 81-103.
147. Ball, S.G., et al., *Neuropilin-1 regulates platelet-derived growth factor receptor signalling in mesenchymal stem cells.* Biochem J, 2010. **427**(1): p. 29-40.
148. Frisca, F., et al., *Role of ectonucleotide pyrophosphatase/phosphodiesterase 2 in the midline axis formation of zebrafish.* Sci Rep, 2016. **6**: p. 37678.
149. Cholia, R.P., et al., *Understanding the Multifaceted Role of Ectonucleotide Pyrophosphatase/Phosphodiesterase 2 (ENPP2) and its Altered Behaviour in Human Diseases.* Curr Mol Med, 2015. **15**(10): p. 932-43.
150. Aghajanova, L., et al., *The bone marrow-derived human mesenchymal stem cell: potential progenitor of the endometrial stromal fibroblast.* Biol Reprod, 2010. **82**(6): p. 1076-87.
151. Shahdadfar, A., et al., *In vitro expansion of human mesenchymal stem cells: choice of serum is a determinant of cell proliferation, differentiation, gene expression, and transcriptome stability.* Stem Cells, 2005. **23**(9): p. 1357-66.
152. Herrera, M.B., et al., *Exogenous mesenchymal stem cells localize to the kidney by means of CD44 following acute tubular injury.* Kidney Int, 2007. **72**(4): p. 430-41.
153. De Becker, A., et al., *Migration of culture-expanded human mesenchymal stem cells through bone marrow endothelium is regulated by matrix metalloproteinase-2 and tissue inhibitor of metalloproteinase-3.* Haematologica, 2007. **92**(4): p. 440-9.
154. Bossi, F., et al., *C1q as a unique player in angiogenesis with therapeutic implication in wound healing.* Proc Natl Acad Sci U S A, 2014. **111**(11): p. 4209-14.
155. Sinno, H., et al., *Topical application of complement C3 in collagen formulation increases early wound healing.* J Dermatolog Treat, 2013. **24**(2): p. 141-7.
156. Strey, C.W., et al., *The proinflammatory mediators C3a and C5a are essential for liver regeneration.* J Exp Med, 2003. **198**(6): p. 913-23.
157. Qiu, Y., L.A. Marquez-Curtis, and A. Janowska-Wieczorek, *Mesenchymal stromal cells derived from umbilical cord blood migrate in response to complement C1q.* Cytotherapy, 2012. **14**(3): p. 285-95.
158. Schraufstatter, I.U., et al., *C3a and C5a are chemotactic factors for human mesenchymal stem cells, which cause prolonged ERK1/2 phosphorylation.* J Immunol, 2009. **182**(6): p. 3827-36.
159. Jacobsen, J.N., et al., *Investigating the humoral immune response in chronic venous leg ulcer patients colonised with Pseudomonas aeruginosa.* Int Wound J, 2011. **8**(1): p. 33-43.
160. van de Goot, F., et al., *Acute inflammation is persistent locally in burn wounds: a pivotal role for complement and C-reactive protein.* J Burn Care Res, 2009. **30**(2): p. 274-80.
161. Machens, H.G., et al., *C3a levels and occurrence of subdermal vascular thrombosis are age-related in deep second-degree burn wounds.* Surgery, 2006. **139**(4): p. 550-5.
162. Wan, K.C., et al., *A longitudinal study of C3, C3d and factor Ba in burn patients in Hong Kong Chinese.* Burns, 1998. **24**(3): p. 241-4.
163. Jang, C.W., et al., *TGF-beta induces apoptosis through Smad-mediated expression of DAP-kinase.* Nat Cell Biol, 2002. **4**(1): p. 51-8.
164. Campbell, N.E., et al., *Extracellular matrix proteins and tumor angiogenesis.* J Oncol, 2010. **2010**: p. 586905.

165. Walter, M.N., et al., *Human mesenchymal stem cells stimulate EaHy926 endothelial cell migration: combined proteomic and in vitro analysis of the influence of donor-donor variability.* J Stem Cells Regen Med, 2015. **11**(1): p. 18-24.
166. Iozzo, R.V. and J.D. San Antonio, *Heparan sulfate proteoglycans: heavy hitters in the angiogenesis arena.* J Clin Invest, 2001. **108**(3): p. 349-55.
167. Sasisekharan, R., et al., *Heparinase inhibits neovascularization.* Proc Natl Acad Sci U S A, 1994. **91**(4): p. 1524-8.
168. Walker, A., J.E. Turnbull, and J.T. Gallagher, *Specific heparan sulfate saccharides mediate the activity of basic fibroblast growth factor.* J Biol Chem, 1994. **269**(2): p. 931-5.
169. Butler, A.A., et al., *Insulin-like growth factor-I receptor signal transduction: at the interface between physiology and cell biology.* Comp Biochem Physiol B Biochem Mol Biol, 1998. **121**(1): p. 19-26.
170. Rinderknecht, E. and R.E. Humbel, *The amino acid sequence of human insulin-like growth factor I and its structural homology with proinsulin.* J Biol Chem, 1978. **253**(8): p. 2769-76.
171. Feng, X., et al., *Insulin-like growth factor 1 can promote proliferation and osteogenic differentiation of human dental pulp stem cells via mTOR pathway.* Dev Growth Differ, 2014. **56**(9): p. 615-24.
172. Zhou, Q., et al., *IGF-I induces adipose derived mesenchymal cell chondrogenic differentiation in vitro and enhances chondrogenesis in vivo.* In Vitro Cell Dev Biol Anim, 2016. **52**(3): p. 356-64.
173. Xinaris, C., et al., *A novel strategy to enhance mesenchymal stem cell migration capacity and promote tissue repair in an injury specific fashion.* Cell Transplant, 2013. **22**(3): p. 423-36.
174. de Pablo, F., et al., *IGF-I and the IGF-I receptor in development of nonmammalian vertebrates.* Mol Reprod Dev, 1993. **35**(4): p. 427-32; discussion 432-3.
175. Heyner, S., et al., *Functions of the IGFs in early mammalian development.* Mol Reprod Dev, 1993. **35**(4): p. 421-5; discussion 425-6.
176. McQueeney, K. and C.N. Dealy, *Roles of insulin-like growth factor-I (IGF-I) and IGF-I binding protein-2 (IGFBP2) and -5 (IGFBP5) in developing chick limbs.* Growth Horm IGF Res, 2001. **11**(6): p. 346-63.
177. Agrogiannis, G.D., et al., *Insulin-like growth factors in embryonic and fetal growth and skeletal development (Review).* Mol Med Rep, 2014. **10**(2): p. 579-84.
178. Baserga, R., et al., *The IGF-I receptor in cell growth, transformation and apoptosis.* Biochim Biophys Acta, 1997. **1332**(3): p. F105-26.
179. Ernst, C.W., R.H. McCusker, and M.E. White, *Gene expression and secretion of insulin-like growth factor-binding proteins during myoblast differentiation.* Endocrinology, 1992. **130**(2): p. 607-15.
180. Yamahara, K., et al., *Comparison of angiogenic, cytoprotective, and immunosuppressive properties of human amnion- and chorion-derived mesenchymal stem cells.* PLoS One, 2014. **9**(2): p. e88319.
181. Sadat, S., et al., *The cardioprotective effect of mesenchymal stem cells is mediated by IGF-I and VEGF.* Biochem Biophys Res Commun, 2007. **363**(3): p. 674-9.